TÉCNICO LISBOA

Fabrication of Transparent and Electroconductive Scaffolds for Neural Stem Cell Culture Combining 3D Printing and Conjugated Polymers

Alexandre Duarte Ribeiro

Dissertation to obtain the Master of Science Degree in

Biomedical Engineering

Supervisors: Prof. Jorge Manuel Ferreira Morgado

Prof. Frederico Castelo Alves Ferreira

Examination Committee

Chairperson: Prof. Luís Humberto Viseu Melo

Supervisor: Prof. Jorge Manuel Ferreira Morgado

Member of the Committee: Dr. Tiago Paulo Gonçalves Fernandes

December 2015

Acknowledgments

First, I would like to thank my supervisors, Prof. Jorge Morgado and Prof. Frederico Ferreira, for the opportunity of working on such promising interdisciplinary field, where I found a latent passion for Materials research and confirmed the already enthusiastic one on Tissue Engineering, for all the ideas and great availability to help and, of course, for all the patience.

I would like to thank Filipa Pires for being the first person that received me in the Organic Electronics group, for the help with the electrical setup and whose work established a strong basis for the development of this thesis.

I would like to give a special thanks to Carla Moura for all the amazing aid she has provided me throughout this work, starting from the work on the 3D printer, measuring contact angles and finishing on the huge support with measuring compressive moduli on hydrogels.

I would like to give a special thanks to Carlos Rodrigues. Without his coaching and availability throughout Stem Cell studies, great part of this work wouldn't have been possible in such a short time.

Also, I would like to say thank everyone in the Organic Electronics Group (Instituto de Telecomunicações) for the cooperative and uplifting environment around the lab, in particular to Dr. Ana Luísa Mendonça, for all the help and support given throughout this work. I would also like to give a special thank you to Prof. Ana Charas for helping me with the Inkjet-printer and availability.

I would like to thank as well to the SCBL team, in particular to Prof. Joaquim Cabral, for the opportunity of working at the lab, to Prof. Margarida Diogo for the support that she has given me since I started my Master's degree and from whom I gained a special passion for Stem Cell Research, and to all my colleagues for the support and comradery.

I would like to thank all my friends for the friendship and laughs throughout this years. Finally, I would like to thank my family, especially for my parents for the support and patience throughout countless times. And I would like to apologize to you Sara, for all the summer time we didn't get to enjoy so I could finish this thesis. With your company and support, I feel I can achieve everything.

Abstract

The emergence of Cell-based therapeutic strategies to treat neurodegeneration has led to developments in scaffolds for Neural Stem Cell (NSC) culture, aiming at mimicking cell microenvironment by providing proper cues for *ex vivo* NSC expansion and differentiation and to promote functional integration and neuroregenerative action upon transplantation. One important cue is electricity, which has shown to enhance NSC growth and neural differentiation. However, further studies on NSC behaviour when subjected to an electric field are needed in order to benefit from electrical cues on the scaffold development.

Transparent, electroconductive scaffolds were developed to establish platforms to study the effect of electric field on neural stem cells (NSC) expansion and differentiation: the first fabricated through the extrusion of commercial filaments; the second from poly(ethylene glycol) diacrylate (PEGDA) hydrogel and inkjet printing of the conjugated polymer poly(3,4-ethylenedioxythiophene):poly(styrene sulfonate) (PEDOT:PSS). Both scaffolds present adequate conductivity to work in the current range explored in literature. While PEGDA hydrogel-based scaffolds present suitable transparency for optical microscopy, optimization of the transparency of 3D extruded scaffolds is needed. NSCs expanded on scaffolds under electrical stimulation showed increased elongation and alignment according to electric field. PEDOT:PSS conductivity is successfully increased 3 orders of magnitude. Tailoring PEGDA mechanical properties with addition of high concentration of plasticizers led to hydrogels with compressive moduli ranging between 100 kPa to 100 MPa, still too high to reproduce physiological brain tissue (0.1 to 1 kPa). PEGDA hydrogel transparency was further enhanced by addition of sorbitol.

Keywords: Neural Stem Cells, Scaffolds, PEGDA, PEDOT:PSS, Electric Field

Resumo

O aparecimento de terapias celulares para o tratamento de doenças neurodegenerativas e lesão neural tem levado ao desenvolvimento de *scaffolds* para cultura de Células Estaminais Neurais (NSCs) com o objectivo de reproduzir o microambiente celular ao fornecer estímulos adequados à expansão e diferenciação *ex vivo* de NSCs e assegurar a integração funcional e acção neuroregenerativa após transplantação. A electricidade é um importante estímulo, tendo mostrado capacidade para promover desenvolvimento e diferenciação neural de NSCs. Contudo, mais estudos acerca do comportamento de NSCs quando sujeitas à acção de um campo eléctrico são precisos para se poder benificiar de estímulos eléctricos no desenvolvimento de *scaffolds*.

Scaffolds transparentes e electroconductores foram desenvolvidos de modo a estabelecer plataformas para estudar o efeito do campo eléctrico na expansão e diferenciação de NSCs: o primeiro fabricado através de impressão 3D de filamentos comerciais para extrusão; o segundo a partir de hidrogel de poli(etileno glicol) diacrilato (PEGDA) e do polímero conjugado poli(3,4-etilenodioxitiofeno):poli(estireno sulfonato) (PEDOT:PSS). Ambas as estratégias apresentam conductividade adequada para trabalhar dentro do espectro de valores de corrente testados na literatura. O PEGDA apresenta transparência adequada para microscopia óptica, enquanto que a transparência dos scaffolds extrudados necessita de optimização. A conductividade do PEDOT:PSS foi aumentada com sucesso para mais de mil vezes. Adição de elevadas concentrações de plastificantes ao PEGDA levou à formação de hidrogéis com módulos de compressão entre 100 kPa e 100 MPa, demasiado elevados para reproduzir tecido cerebral (0.1 a 1 kPa). A transparência do PEGDA foi aumentada após adição de sorbitol.

Palavras-Chave: Células Estaminais Neurais, *Scaffolds*, PEGDA, PEDOT:PSS, Campo Eléctrico

Table of Contents

List of Figures

List of Tables

List of Abbreviations

2D – Two-Dimensional

3D – Three-Dimensional

3DP – 3D Printing

ABS – Acrylonitrile butadiene styrene

AFM – Atomic Force Microscopy

AM – Additive Manufacturing

BDNF – Brain-derived Growth Factor

CNS – Central Nervous System

cPLA – Conductive PLA

DAPI – 4',6-Diamidino-2-phenylindole

DMP – Dimatix Materials Printer

DMPA – 2,2-Dimethoxy-2-phenylacetophenone

DMSO – Dimethyl sulfoxide

ECM – Extracellular Matrix

EDOT – Ethylenedioxythiophene

EG – Ethylene glycol

FDM – Fused Deposition Modelling

FM – Fluorescence Microscopy

FTIR – Fourier Transform Infrared Spectroscopy

GFAP – Glial Fibrillary Acidic Protein

GOPS – (3-Glycidyloxypropyl)trimethoxysilane

HBS – HEPES-Buffered Saline

HEPES – N-(2-Hydroxyethyl)piperazine-N'-(2-ethanesulfonic acid)

IJP – Inkjet Printing

IKVAV – Isoleucine-Lysine-Valine-Alanine-Valine Peptide

ITO – Indium-tin oxide

NGF – Nerve Growth Factor

EGF – Epidermal Growth Factor

FGF-2 – Fibroblast Growth Factor-2

MeOH – Methanol

MMP – Matrix Metalloproteinase

NT-3 – Neurotrophin-3

PA – Polyacrylamide

PBS – Phosphate-Buffered Saline

PCL – Poly(ε-caprolactone)

PDMS – Poly(dimethylsiloxane)

PEDOT – Poly(3,4-ethylenedioxythiophene)

PEDOT:PSS – Poly(3,4-ethylenedioxythiophene): Poly(styrene sulfonate)

PEG – Poly (ethylene glycol)

PEGDA – Poly (ethylene glycol) Diacrylate

PET – Poly(ethylene terephthalate)

PFA – Paraformaldehyde

PLA – Poly(L-lactic acid) or Poly(lactic acid)

PLGA – Poly(lactic-co-glycolic acid)

PLLA – Poly(L-lactic acid)

PMMA – Poly(methyl methacrylate)

PSS – Poly(styrene sulfonate)

RGD – Arginine-Glycine-Aspartic Acid Peptide

RT – Room Temperature

SEM – Scanning Electron Microscopy

SWCNT – Single-Walled Carbon Nanotubes

MAPK – Mitogen-Activated Protein Kinases

NGS – Normal Goat Serum

NSC – Neural Stem Cell

SGZ – Subgranular Zone

SVZ – Subventricular Zone

T_g – Glass Transition Temperature

TCAA – Trichloroacetic Acid

TEM – Transmission Electron Microscopy

TuJ1 - β-Tubulin III Neuronal Marker

UV – Ultraviolet

VEGF – Vascular Endothelial Growth Factor

Aim of the Studies

Advances in Stem Cell Research and Biomaterials have allowed the development of efficient Tissue Engineering therapeutic strategies to address loss of neural tissue resulting from neurodegenerative diseases or neural injury. Due to their intrinsic properties, Neural Stem Cells play a promising role in the development of such applications, as they are highly migratory to regions of neurodegeneration, where they can promote repair and regeneration. The golden standard involves the creation of grafts to be implanted by isolating and culturing Neural Stem Cells on Scaffolds – artificial structures that mimics cell microenvironment, supporting and influencing the growth, proliferation and formation of new tissue. To be able to tailor culture conditions on the development of these grafts, one must, however, study the complex cell microenvironment, whose biochemical and physical cues strongly influence cell behaviour.

One of the important physical cues for neural tissue, particularly for neural stem cells, is electricity, as these cells are subjected and influenced by several electrochemical cues during neurodevelopment on physiological conditions. Several studies have addressed the effect of electric fields on neural stem cell expansion and differentiation, but further studies are needed in order to fully characterize the influence of electrical cues on nerve injury and repair and to benefit from their use in the development of said therapeutic strategies.

The main objective of this work is the development of transparent, electroconductive scaffolds for NSC culture, able to fulfil two purposes:

- Being established as viable platforms to study the influence of an electric field on cell expansion, morphology and differentiation;
- Validate the use of the materials and techniques explored in this work, namely the use of conjugated polymers and additive manufacturing technologies in future developments of cell-based therapeutic strategies for neurodegenerative diseases or neural injury.

To work towards this goal, two different pathways were explored: i) 3D Printing of commercial filaments to make highly customizable, low-cost, easy and quick to produce platforms; ii) combination of a transparent hydrogel, poly(ethylene glycol) Diacrylate – PEGDA – and an electroconductive conjugated polymer – poly(3,4-ethylenedioxythiophene):poly(styrene sulfonate) (PEDOT:PSS). Proof-of-concept biological studies of NSC expansion and differentiation were then performed on these scaffolds to assess their viability in future investigation on the effect of electrical fields on cell culture.

In parallel, characterization and optimization studies were made on the latter materials, namely the enhancement of PEDOT:PSS electrical conductivity, the modification of PEGDA mechanical properties and the enhancement of PEGDA hydrogel transparency.

Introduction

I. Tissue Engineering Strategies for the Central Nervous System

A. The promise of Tissue Engineering on Neurodegeneration and Neural Injury

Neurodegeneration is the progressive loss of structure and function of neurons, characteristic in many neurodegenerative diseases, such as Alzheimer's, Parkinson's, Huntington's or Amyotrophic Lateral Sclerosis[1]. Despite differences in the pathophysiology and the pathological markers of these diseases, there are important common characteristics, such as atypical protein folding that results in the formation of intracellular aggregates such as, for example, the creation of Lewy bodies in Parkinson's[2] or the formation of β-amyloid plaques in Alzheimer's[3], and the trigger of neural inflammation and apoptotic pathways[1,4].

Alzheimer's is the most prevalent neurodegenerative disease, with reported 5.2% prevalence of associated dementia[5], followed by Parkinson's disease, which affects 2% of the world population over 65 years[6]; both diseases having increased prevalence each year. To address neurodegeneration on these diseases, there is a strong research effort to develop Tissue Engineering strategies that combine Stem Cell and Biomaterial Research to address neurodegeneration and neural injury.

The Tissue Engineering market is growing at an increasing rate every year – the compound annual growth rate between 2014 and 2020 is 23.2%, with the Central Nervous System (CNS) the fastest growing application segment, with a reported compound annual growth rate of 30.8% for the same period worldwide[7]. For all Stem Cells-based applications, those involving Biomaterial Scaffolds are the fastest expanding ones, with a worldwide annual growth rate of 13.4% until 2021, when compared to other Stem Cell-based therapies or medicine sales growth rates[8]. The growing market allied to the strong research effort and increasing number of clinical trials on stem cell-based therapies[9] place Tissue Engineering as a very promising pathway for future medical therapies for the CNS.

B. Neural Stem Cells

Neural Stem Cells (NSCs), as the most primordial cells in the CNS, are responsible for the generation of the entire framework of the Central Nervous System during pre-natal development, giving rise to both several subtypes of neurons and glial cells[10]. As Stem Cells, NSCs have two special properties: (i) NSCs are self-renewing, that is, they are able to proliferate, going through numerous cycles of cell division, maintaining an undifferentiated state; (ii) they are multipotent cells, having the ability to differentiate into specialized cell types of the CNS, mainly neurons, oligodendrocytes and astrocytes.

Besides these properties, NSCs also have unique characteristics that make them a strong pillar for Tissue Engineering and Cell therapies: NSCs can be isolated, proliferated, genetically manipulated and differentiated *in vitro* and reintroduced in the patient; they are highly migratory[11,12], having the ability to populate a region during development, or to repopulate a region that suffered ablation or neurodegeneration; and they can act to reduce

the inflammation and cell death by releasing neurotrophic factors, such as Nerve Growth Factor (NGF), Brain-derived Neurotrophic Factor (BDNF) and Neurotrophin-3 (NT-3)[13–15].

The process by which NSCs generate different subtypes of neurons is called Neurogenesis. Besides having a central role during pre-natal neural development, Neurogenesis also occurs in the Adult Brain in specific niches: the Subventricular Zone (SVZ)[16], lining the lateral ventricles, where NSCs and progenitor generate new neurons that migrate along the rostral migratory tract to the olfactory bulb; and the Subgranular Zone (SGZ)[17] of the dentate gyrus, in the hippocampus. Tissue homeostasis is maintained in these two regions, as new neurons are continually born throughout adulthood. Although the functional relevance of these niches is still uncertain, it is thought that it correlates with the cognitive functions of the regions – for example, as the hippocampus is important in learning and memory, it is hypothesized that neurogenesis in the SGZ allows the improvement of learning and hippocampal plasticity[18].

It has been shown that these cells can migrate from these niches along blood vessels in the brain to regions of neurodegeneration[12]. However, the limited stem cell number on the adult CNS in specific locations, the formation of glial scar tissue upon injury and the progressive neuronal death associated with neurodegenerative diseases[19] has the obvious implication that the ability of NSCs to migrate and promote neurogenesis to counteract the onset of these diseases is limited.

C. Scaffolds for NSC-based Tissue Engineering Strategies

The golden standard of Tissue Regeneration is the use of autologous grafts, where stem cells are isolated from the patient and put under *ex vivo* culture to generate a graft tissue to be implanted in the patient (Figure 1). However, neural autografts made solely of NSCs have several drawbacks, namely the failure to repair and regenerate the lost neural tissue and the lack of functional integration and recovery of the *ex vivo* neurons when introduced in the tissue[20–22]. In fact, in some studies on animal models, such as the one for spinal cord injury in mice, the introduction of NSCs lead to cell homing to the injury site with release of neurotrophic factors and chemokines that diminish neural inflammation, but cells were phagocytised after some time without integrating with the surrounding tissue[23].

Given this limitation, Tissue Engineering strategies are being developed linking Stem Cell culture with Biomaterials has led to the creation of Scaffolds, which are structures that attempt to function as an artificial Extracellular Matrix (ECM), mimicking the physiological microenvironment that control cell growth and differentiation. As an artificial microenvironment, scaffolds can be used to enhance NSC *ex vivo* culture and as delivery vehicle for the graft tissue, promoting the integration of functionalization between host and graft[19,24,25].

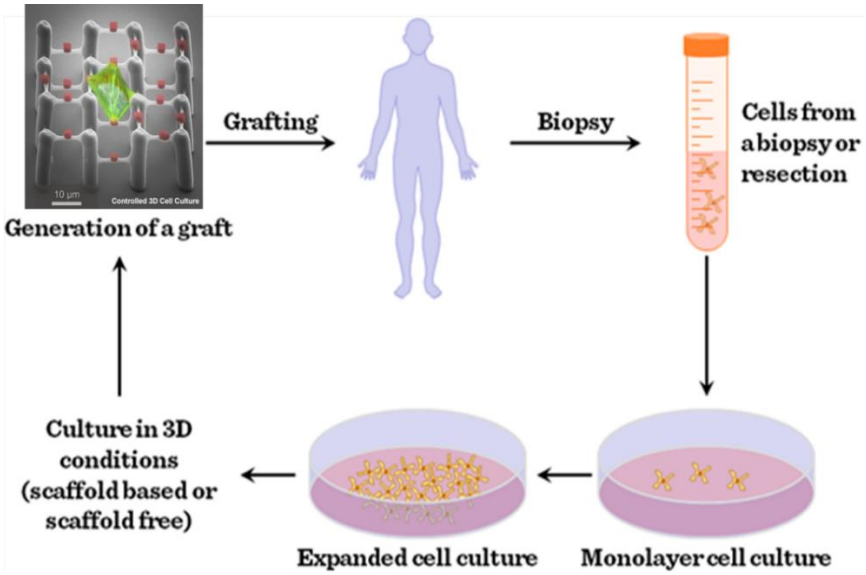

Figure 1. Golden Standard of Tissue Regeneration Strategies. Adapted from Bartis et al[26].

II. Mimicking Cell Microenvironment with Scaffolds

To be used for graft development with Neural Stem Cells, a desirable scaffold has to be biocompatible, causing no cytotoxicity and minimal inflammatory response; the degradability should be controlled to account for tissue integration from the graft into the host; it has to provide the appropriate biochemical and physical cues to mimic a neuroregenerative microenvironment, promoting NSC adhesion, viability and proliferation, as well as allowing functional integration with the surrounding tissue.

A. Scaffold Architecture and Biomaterials

There are several scaffold structures reported in the literature, making use of different materials. As it is intended to mimic ECM, attempts have been made in creating scaffolds made from decellularized ECM, as for example for peripheral nerve regeneration[27] or rat sciatic nerve regeneration[28]. These decellularized matrices can serve as *in vitro* ECM models to understand the roles of ECM in NSC growth and differentiation[29].

More common strategies involve the use of polymeric biomaterials due to the wide choice of biocompatible materials with different characteristics, such as mechanical properties, porosity and potential for biochemical modification[30]. Some examples of these scaffolds are hydrogels, nanofibers, nanofoams, nanotubes and sintered matrix. From these, hydrogel and electrospun nanofiber-based scaffolds have been the most explored[22], as will be detailed below.

Hydrogel-based Scaffolds

Hydrogels are 3D networks of water-insoluble, hydrophilic polymers, characterized by swelling, that is, the capacity to hold water within the interstices of such networks. Their hydrophilicity results from the presence of hydrophilic functional groups in the polymeric backbone, while their stability in water is due to the crosslinks established between the network chains[31].

Hydrogels have been extensively explored as scaffolds due to their characteristics: biocompatibility; ability to tune mechanical properties in a wide range of elastic moduli, allowing to replicate those of several soft tissues[32]; and low interfacial tension and are good for strategies involving simple injection[22]. The mesh size of the polymeric backbone and swelling properties of hydrogels are of extreme importance to cell culture, especially in strategies of cell encapsulation in hydrogels[21,33]. Hydrogels with different mesh size will have different pore diameters which, being dependent on the swelling, affect nutrient supply to cells cultured in the material pores. Some examples of hydrogels used on NSC culture include poly (ethylene glycol) (PEG)[34], poly(ethylene glycol) diacrylate (PEGDA)[35] and alginate[36].

Nanofibrous Scaffolds

Nanofibers constitute another widely explored approach at constructing scaffolds for Tissue Engineering due to their structural resemblance to natural ECM[37,38]. A scaffold architecture that mimics the physiological environment provides a more appropriate environment for cell adhesion, migration, proliferation and differentiation[39].

Electrospinning is the most used method to create nanofibrous structures due to its relative ease of use and ability to form fibers from a wide range of materials. The dimensions of the fibers can be controlled through the polymer solution concentration, viscosity and dispense rate, and it is possible to tweak the alignment of the fibers by controlling the electric field strength and pattern applied to the system[37]. Some examples of electrospun nanofibrous scaffolds for NSC culture include poly(L-lactic acid) (PLLA)[40], poly(lactic-co-glycolic acid) (PLGA)[41] and poly(ε-caprolactone) (PCL)[42].

B. Scaffolds as Artificial Cell Microenvironment

Mimicking the cell microenvironment with scaffolds is a rather complex task – the natural cues in ECM that direct cell fate involve different biochemical cues – such as ECM adhesion proteins, soluble factors, growth factors and hormones – and physical cues – such as three-dimensionality of cell culture, mechanical stiffness, surface topography and, importantly for neural tissue development and function, electrical signalling.

Here, there is a brief description of the types of scaffolds explored in the literature, as well as the biomaterials used. Then, several of these cues are briefly presented, with an emphasis on the mechanical properties and electrical cues. As will be noted throughout this section, the most efficient scaffold systems use a combination of the several cues and not isolated ones as the first case tends to be more approximate to the physiological environment where cells develop.

3D Cell Culture

Two-dimensional, monolayer Tissue culture has been widely used in Stem Cell Biology and Tissue Engineering due to the easy culture protocols and cell visualization. However, the formed cell monolayer does not account for the complex cell-ECM or cell-cell interactions found within the physiological environment; as so, the transition from 2D to 3D culture conditions is an important step towards a more physiological-like microenvironment,

resulting in biological studies whose results are closer to the physiological conditions, and in improved regeneration of injured tissue on therapeutic strategies[43].

There is, however, a limitation regarding optical imaging of 3D scaffold culture systems, implying the need of complex and less accessible techniques, such as Confocal Microscopy, Optical Coherence Tomography or Multiphoton Microscopy for transparent scaffolds[44]. Also, Label-free magnetic resonance imaging has been an emerging technology that allows live cells detection that are developing deep in a porous scaffold, even in non-transparent ones, circumventing the need to perform immunohistological sections of the scaffolds for cell distribution studies[45].

The encapsulation of cells in biodegradable hydrogels, such as poly(ethylene glycol) (PEG) is one common strategy to create 3D porous scaffolds, were pore sizes depend on the mesh size of the polymer used[21]. Electrospun nanofibrous scaffolds have also been used to establish 3D scaffolds with a vast network of interconnected pores[38,40].

Recent advances in Additive Manufacturing (AM) technologies have allowed the creation of 3D-bioprinted scaffolds[46–48], such as biodegradable polyurethane hydrogels for NSC culture[49], or the bioprinting of neural stem cells, collagen hydrogel and vascular endothelial growth factor (VEGF) to create artificial neural tissue constructs[50]

Biochemical Cues

As already mentioned, NSCs have a trophic effect on the surrounding tissue by secreting neurotrophic factors. These same factors are also commonly used in NSC culture. In addition, other soluble differentiation inducers, such as Retinoic Acid[51], and growth factors, such as Epidermal Growth Factor (EGF) and Fibroblast Growth Factor-2 (FGF-2)[52], can be used with scaffolds for cell culture to provide biochemical cues to control proliferation and differentiation.

These biochemical cues can also be immobilized on the materials surfaces. In fact, it has been proven that immobilization of BDNF on 3D electrospun PCL nanofibers has improved NSC proliferation and neural commitment upon differentiation when comparing with cultures on simple PCL nanofibers, with soluble BDNF in the culture medium[42].

Drug delivery strategies with hydrogels and electrospun nanofibers can be used to construct scaffolds where there is a sustained release over a long period of time of biochemical cues. For example, Nt-3 has been loaded onto electrospun PLGA nanofibers, where sustained release of the neurotrophin lasted for 4 weeks in NSC culture, increasing differentiation into neurons, when co-cultured with Schwann cells[41].

Surface Functionalization

The surface chemistry of scaffold materials is an important parameter[53], as the ECM is mainly responsible for cell adherence and migration, as well as to provide the means for the cells to interact with each other. Without functionalization, most materials would be bioinert and fail to provide an ECM-like environment favourable to

neural development. The most common strategy used is the surface functionalization of materials with ECM proteins, such as Fibronectin, Laminin and collagen. Laminin is a key adhesion molecule widely used for NSC culture: besides promoting adhesion, the binding of laminin to the correspondent receptors in cell's integrins triggers conformational changes on integrin, activating intracellular pathways such as mitogen-activated protein kinases (MAPK) that regulate self-renewal and maintenance of NSCs[54,55].

The ECM proteins routinely used in research are isolated from animals, which can have high batch-to-batch variability and limits their use for clinical applications due to the potential immune response[56]. Xeno-free surface functionalization could be performed by using functional peptides derived from these ECM proteins that promote cell attachment.

Laminin is constituted by peptide sequences such as arginine-glycine-aspartic acid (RGD) or isoleucine-lysine-valine-alanine-valine (IKVAV) that are known to guide cell adhesion and neurite outgrowth[55,56]. As an example, incorporation of IKVAV on self-assembled nanofibers made from amphiphilic peptides have shown to favour neural differentiation in detriment of glial differentiation pathways[57], and their use on spinal cord injury model in mice led to the reduction of neural cell death[58]. Still, these peptides fail to allow cell attachment and growth for periods of time similar to the ones obtained when the full ECM proteins are used[56].

Material surface functionalization can also be performed by incorporating some chemical moieties – it has been shown that different surface groups promote different NSC differentiation pathways. Ren *et al.* showed that NSCs grown on surfaces functionalized with sulfonic ($-SO_3H$) underwent preferential oligodendrocyte differentiation, while carboxyl groups (-COOH) were more prone to induce astrocyte differentiation and neural differentiation would occur only on amino-functionalized surfaces[59].

Biochemical cues and ECM molecules or their peptide derivatives can also be used together to direct differentiation in a synergic manner, improving the output of differentiated population when compared to the sole use of each strategy[60].

Mechanical Cues

To guaranty functional integration of grafts in the surrounding CNS tissue, there is the need to provide scaffolds with similar elastic moduli as the ones found on, for example, the brain. There are various values reported for the elastic moduli of brain tissue, depending on the sample in question and method of estimation; nonetheless, the values obtained over the literature point to values on the order of 1 kPa or less[61,62]. Brain tissue also typically shows a viscoelastic behaviour, and differences in dynamic modulus are found between grey and white matter[63].

Mechanical cues, namely material substrate stiffness, are known to act on the NSC growth and differentiation. On a study by Leipzig et al.[64] of NSCs cultured on substrates of methacrylamide chitosan with different elastic moduli, it was found out that proliferation occurred preferentially on scaffolds with moduli below 10 kPa, with a maximum proliferation on 3.5 kPa. Besides that, differentiation into oligodendrocytes was favoured on stiffer scaffolds (bigger than 7 kPa), while neural was favoured on softer ones (smaller than 1 kPa). Astrocytic

differentiation only occurred at substrates moduli smaller than 1 kPa, as shown by the Glial fibrillary acidic protein (GFAP) immunofluorescence marker.

Following the work by Saha *et al.*[65] on interpenetrating polymer network gels made from poly(acrylamide-co-ethylene glycol/acrylic acid), it was found that gels with moduli higher than 100 Pa promoted proliferation of NSC; gels ranging from 100 to 500 Pa of elastic moduli favoured neural differentiation, while harder gels, with plastic moduli ranging from 1-5 kPa, promoted glial cultures. Tuning the elastic moduli of several Alginate hydrogels with encapsulated Neural Stem Cells also showed an increased rate of proliferation with decreasing modulus. The neuronal marker β-Tubulin III (TuJ1) was mostly expressed on the softer hydrogels[36].

Hydrogels present a good scaffold system to tweak mechanical properties by, for example, polymerizing the same monomer with different resulting polymer chain lengths, and thus molecular weights, such as in the creation of PEGDA with different molecular weights[66]. Also, molecules commonly used as plasticizers can be used with hydrogels, as explored in this work and further detailed.

Surface Topography

Micro and nanostructured topographical cues, like grooves, ridges, nodes and pores, influence the interactions between cells and materials, as well as providing cues for cell proliferation, differentiation and orientation[22,67]. Research has shown that topographical features are important in axon growth guidance, thus providing a mean to control neural architecture – research by Mahoney *et al.*[68] with photolithographic-patterned polyimide substrates showed that neurites tend to grow parallel in narrow microchannels (20-30 μm in width), but perpendicular on wider ones (40-60 μm) until reaching the channel walls.

The oriented growth induced by the geometry of the biomaterial has led to development of neve guidance channels[53]. A study by Nomura *et al.*[69] showed that NSCs grown on chitosan tubes could, just due to the topography of the microtubes, promote regeneration of a tissue bride in a rat model of spinal cord injury. The creation of oriented nanofibers also allows the orientation of neurite growth and can be used for the development of nerve guidance channels. For example, PLLA aligned electrospun fibers have shown increased neurite growth when compared to randomly arranged electrospun fibers[40].

Electrical Cues

A key characteristic of the functioning CNS is the propagation of electrochemical signals upon action potentials through the neuron, and from neuron to neuron through synaptic transmission. Designing electroconductive scaffolds to electrically stimulate cells should allow a better nerve regeneration on culture and functional integration of the graft by providing the means to elicit action potentials and improve synaptic interconnections[19,22].

Studies have been made to elicit the effects of electric fields on the neural cells – for example, Sisken *et al.*[70] showed that stimulation of rat sciatic nerved with pulsed electromagnetic fields increased nerve regeneration. Importantly, fibroblast adhesion and viability was also assessed by Shi *et al.*[71], which found that a DC electric field

of 1 V/cm enhanced cell adhesion, without measurable variations in pH or temperature during the period of cell culture.

Regarding the effects of electric field on NSCs, there has been some recent research in literature by Chang *et al.*[72], where a biphasic electrical current chip made from indium-tin oxide (ITO) was made to assess the effect of electrical stimulation on the expansion and differentiation of NSCs over a range of current densities. It was suggested that current densities ranging from 1-30 μA/cm^2 at 100 Hz pulse positively affect NSC proliferation and neural differentiation, with a maximal rate of proliferation obtained at a current density of 8 μA/cm^2, and a maximum increase in differentiation at 4 μA/cm^2. In a work by Kam *et al.*[73], Single-Walled Carbon Nanotubes (SWCNT) were used to create films with Laminin for the culture of NSCs. Upon current stimulation, it was shown that extensive formation of functional neural network occurred, as indicated by the increase in neurite outgrowth and by the presence of synaptic connections. Recent work by Pires *et al*[74] showed a promising strategy in the use of the conductive polymer poly(3,4-ethylenedioxythiophene):poly(styrene sulfonate) (PEDOT:PSS). Increase in neurite growth, cell elongation and in neural differentiation was obtained with quadratic voltage pulses of 1 V/cm at 100 Hz. Similar results are obtained on conductive nanofibrous scaffolds made from electrospun PCL nanofibers doped with the conductive polymer polyaniline[75].

However, the mechanisms behind the effect of electric fields on cell culture are still not clear. It is hypothesized that changes in membrane potential and intracellular signal transduction pathways due to the electric field are responsible for the alterations in cell behaviour[74,76]. Further studies are needed to elicit the mechanisms behind the effect of electric field on expansion and differentiation of NSCs.

III. Approaching Transparent and Electroconductive Scaffolds

On this section, the two materials used for the development of transparent, electroconductive scaffolds are presented. The synthesis of these materials, as well as several aspects important for characterization and optimization studies realized in this work are discussed.

A. Transparent Substrate – Poly(ethylene glycol) Diacrylate Hydrogels

Emergence of PEGDA Hydrogels for Tissue Engineering Applications

Poly(ethylene glycol) Diacrylate (PEGDA) is a hydrogel with increasing use in biotechnological applications involving cell culture. It is formed by a polymeric chain of poly(ethylene Glycol) (PEG) with variable size and acrylate groups attached to both ends, which are responsible for the establishment of crosslinks (Figure 2).

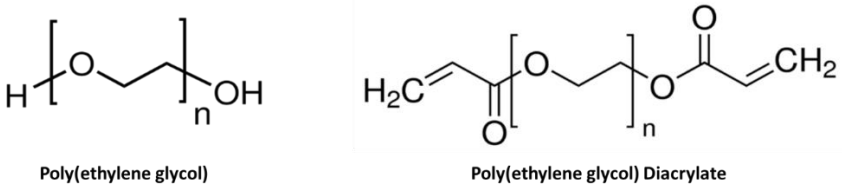

Figure 2. Chemical structures of Poly(ethylene glycol) (PEG, left) and Poly(ethylene glycol) Diacrylate (PEGDA, right) molecules. It is possible to observe the terminal acrylate (CH_2CHCOO) groups in the PEGDA molecule.

Just like its counterpart, PEG, its increasing use in literature is greatly due to its characteristics: PEGDA is biologically inert, as it is non-toxic and does not generate an immunogenic response[77]; it is transparent, allowing the development of scaffold systems for easy microscopy imaging[78]; chemical and structural properties can be extensively modified, as well as its mechanical properties, which can be varied over a range of moduli and swelling ratios comparable to many soft tissues[35,79]. It has been envisaged as a scaffold material for tissues with different stiffness, such as bone[80] and cornea[81], and has been extensively used in cartilage[82–84]. The usage of PEGDA in neural-related systems is recent: it has been used in the fabrication of neurocompatible hydrogels[85] or in the development of injectable drug-delivery systems for the treatment of spinal cord injuries[86], such as delivery of nerve growth factor[87].

Besides its use as a biomaterial for cell and tissue culture, PEGDA is being explored as an alternative for poly(dimethylsiloxane) (PDMS) for microfluidic device fabrication – PEGDA has bigger stiffness and lower nonspecific adsorption of molecules than PDMS[88], while achieving high aspect ratio of structures fabricated by lithographic patterning, similar to those obtained with PDMS[89–91].

PEGDA, however, does not support cell attachment by itself[92]. There is the need to perform surface functionalization by promoting the adsorption and/or covalent attachment of biomolecules that serve as ligands between substrate and cells. In this work, there is the need to coat the PEGDA substrates (as well as the ones made from commercial filaments in 3D-printing) with Laminin.

Another important aspect of PEGDA usage as a hydrogel for cell culture is its relative stability during cell culture due to the insolubility of the hydrophilic PEG backbone[93]. Several tissue engineering strategies rely on grafts with a degradable material, where implanted cells will proliferate and eventually produce their own natural ECM, which will substitute the degrading scaffold material. For such end, hydrogels with induced biodegradability can be obtained by tweaking the molecular backbone; for example, the incorporation of a matrix metalloproteinase (MMP)-sensitive peptide into the polymer backbone has been used by Ali *et al.*[94] to create degradable PEGDA hydrogels for endothelial cell culture, as MMP-2 and MMP-9 released by these cells promote polymer degradation at the peptide location. A similar strategy could be envisaged for NSC grafts, as astrocytes and some neuronal lineages secrete these MMPs[95].

UV-Crosslinking of PEGDA

As mentioned above, the terminal acrylate groups allow the creation of crosslinks between PEGDA oligomers. Crosslinking can traditionally be done either by gelling[96] or UV activation of a photoinitiator[97,98] - in this work, the latter method will be used via the photoinitiator 2,2-dimethoxy-2-phenylacetophenone (DMPA). DMPA generates radical species upon absorption of UV radiation, and is specifically used in the preparation of polymers whose monomers contain acrylate groups, such as poly(methyl methacrylate) (PMMA), polyacrylamide (PA) or, in the case of PEGDA, these terminal acrylate groups. The main reactions involved in UV-crosslinking of PEGDA are shown in Figure 3.

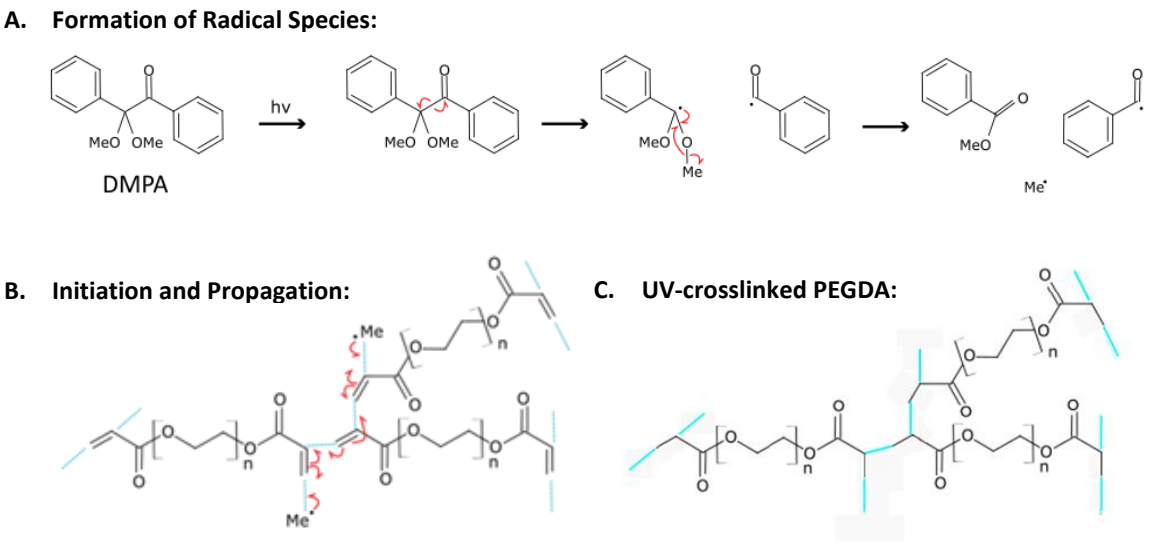

Figure 3. Main Steps in the UV-crosslinking reaction of PEGDA: (A) The absorption of UV radiation by DMPA, resulting in the formation of radical species, namely a benzyl radical (PhC•O) and a methyl radical (Me•); (B) Initiation and Propagation of PEGDA radical polymerization – although only the Me• radical is represented, the same mechanism applies for the initiation with the benzyl radical; (C) Final UV-crosslinked PEGDA – blue lines represent the covalent crosslinks that can be formed between PEGDA molecules.

Upon exposure to UV, DMPA cleavage results in a benzyl radical and a dimethoxy substituted carbon centred radical; the dimethoxy radical will rearrange to form a methyl radical and methylbenzoate (Figure 3.A)[99]. These radicals will be transferred to the monomer, cleaving the double bond present in the vinyl group of the acrylate ends and leading to the formation of bonds between different PEGDA monomers. The unreacted radicals and photoinitiator can be washed away after crosslinking. Once crosslinked, hydrogels are thermoset plastics, as the polymer matrix can't be changed with temperature variations without decomposing the polymer[100].

Tailoring Mechanical Properties of Hydrogels – The use of Plasticizers in Hydrogel Development

In this work, an attempt to tailor the mechanical properties of UV-crosslinked PEGDA was made, aiming to both show the mechanical tunability of this hydrogel and optimize mechanical properties for neural tissue culture, while maintaining substrate transparency for microscopic visualization. Modification of PEGDA mechanical properties can be achieved by two main paths: creating PEGDA hydrogels with different PEG chain lengths, as increasing PEG chain length leads to decreased mechanical modulus[90]; or by molecular additives, such as plasticizers. In this work, we studied the addition of N-(2-Hydroxyethyl)piperazine-N'-(2-ethanesulfonic acid) (HEPES, Figure 5) Buffered Saline (HBS) and several plasticizers, such as glycerol, sorbitol and its counterpart, PEG, in different concentrations to a single PEGDA oligomer solution with a molecular weight of 575 Da[101].

Plasticizers typically are low-molecular weight polyalcohols, such as glycerol, sorbitol, ethylene glycol and its resulting polymer, PEG. The presence of more than one hydroxyl (-OH) groups (Figure 4) on polyalcohols allows the establishment of hydrogen bonds between these molecules and the main polymer – in this case, PEGDA.

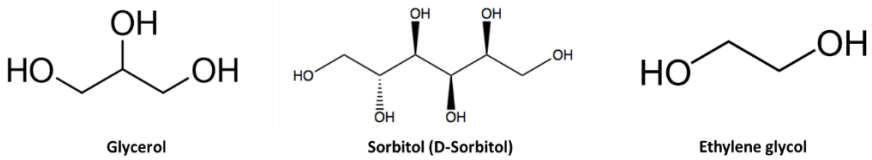

Figure 4. Chemical structures of some polyalcohols commonly used as plasticizers: glycerol, sorbitol and ethylene glycol. The low molecular size and presence of more than one hydroxyl (-OH) groups are responsible for their plasticizing effect.

The low molecular size of plasticizers allows the molecules to occupy intermolecular spaces between polymer chains and interacting with them by establishing these hydrogen bonds, altogether with other weak interaction forces such as van der Waals. It is thought that these interactions are responsible for the effect of plasticizers on polymer mechanical properties: as plasticizer molecules attach along polymer chains, they lead to the decrease of interactions between polymer chains and increasing the space between them, thus reducing polymer rigidity[102]. Some studies also hypothesize the behaviour of plasticizers as lubricants which reduce friction between molecules in the polymer and thus polymer rigidity[103,104]

.

In this work, PEGDA hydrogels with different mechanical properties are prepared using different dilutions of PEGDA on two different systems: a solution of HEPES-Buffered Saline (HBS), and PEG with two different molecular weights: 400 and 600 Da. The mechanical properties assessed are stiffness, represented by the compressive modulus and compressive strength.

HEPES is a zwitterionic organic chemical buffering agent, widely used in cell culture[105] to maintain pH at physiological temperature. Several works in the literature used PEGDA solutions diluted in HEPES at different concentrations to obtain hydrogels with different stiffness[97,98,106]. The molecular structure of HEPES can be seen in Figure 5.

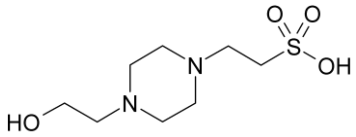

Figure 5. Chemical Structure of HEPES.

Enhancing the Transparency of PEGDA Hydrogels

Pure PEGDA is transparent, with high optical transmittance throughout the visible spectra, as shown in this work. However, soft hydrogel substrates are normally prepared from diluted monomer in aqueous solutions, such as culture medium for direct cell encapsulation[107], or saline solutions, such as phosphate-buffered saline (PBS) or HBS, which turns them opaque, imposing a barrier for cell visualization on this hydrogels and in the development of 3D culture systems in general. Thus, it is of great importance to develop strategies to improve hydrogel transparency, enabling the study of cell behaviour through microscopy in 3D hydrogel-based scaffold systems.

Glycerol has been investigated as a tissue optical clearance agent[78,96,108]. It was shown that the injection of glycerol into dermal tissue increased transparency both *in vitro* and *in vivo*, as the light scattering was decreased by the close proximity of refractive index of glycerol to the surrounding tissue[108].

A breakthrough tissue preparation method developed by Chung and Deisseroth *et al.*[78] allows high resolution imaging of tissue samples by creating a tissue-hydrogel hybrid, allowing intact tissue imaging of long neural circuit projections, wiring and cellular relationships, while also preserving fine structure, proteins and nucleic acids. In such work, tissue is fixed with common fixative agent, and is covalently linked to acrylamide and bis-acrylamide monomers which are then polymerized into a transparent, PA hydrogel mesh. During preparation for optical imaging, this tissue-hydrogel hybrid is treated with glycerol, creating a match between the glycerol solution surrounding the sample and the clear tissue.

In the work by Zhao *et al.*[96], it was assessed for the first time if this clearance mechanism could be used for improving hydrogel transparency, namely in PEGDA, PA, PLGA and gelatin. Due to the encouraging results of this report, it will further be explored in this work the possibility of using plasticizers, such as glycerol, sorbitol and PEG, to further enhance the transparency of the PEGDA hydrogels.

B. "Adding" Conductivity – Poly(3,4-ethylenedioxythiophene):Poly(styrene sulfonate)

Emergence of PEDOT:PSS in Organic Electronics and Tissue Engineering Applications

Conductive or conjugated polymers are organic polymers which intrinsically conduct electricity. The backbone of these polymers has contiguous sp^2-hybridized carbon centres, each having a valence electron residing in a p_z orbital, orthogonal to the other σ-bonds. The π bonds resulting from the combination of these orbitals allow the delocalization of these electrons throughout the polymer backbone[109,110]. There are several extensively explored conductive polymers, such as polypyrrole, polyaniline and several polythiophene derivatives[109,111].

One of these polythiophenes – poly(3,4-ethylenedioxythiophene):poly(styrene sulfonate) (PEDOT:PSS) – has gained especial relevance over the years, especially in applications as a biomaterial. PEDOT:PSS has several advantages over other conductive polymers, such as high transparency in the visible spectral range, high flexibility, thermal stability and processability in aqueous dispersions[112,113], finding several applications in organic electronics, such as organic light-emitting diodes[114,115], organic photovoltaic cells[116,117] and other energy conversion and storage devices, such as supercapacitors[118,119], fuel cells[120] and stretchable devices[121,122].

Recent medical applications of PEDOT:PSS in the fields of tissue engineering and bioelectronics have emerged due to its biocompatibility[123] and ability to be effortlessly modified in order to promote the immobilization of proteins, creating ideal interfaces with biological systems for organic bioelectronics applications[124]. In the context of tissue engineering applications, as discussed before, PEDOT:PSS has the ability to provide electrical cues on scaffolds for NSC growth, differentiation and cell orientation[74,111].

In the area of bioelectronics, important developments on neural electrodes have recently been made with conductive polymer coatings, as they provide improved charge transfer capacity and lower impedance values between neural tissue and the electrode when compared to metallic ones[125–127]. Notoriously, progress has been made towards bioelectrodes that combine tissue engineering with neuroprosthetic electrode coatings to incorporate neural stem cells, providing a neural interface that both minimizes foreign body response and

promotes neural survival of the target neuron in close proximity with the electrodes. A layered construct is proposed by Green *et al.*[128] were NSCs are developed *in vitro* on a conductive scaffold above the metallic electrode, forming a network of neural cells and glia. This neural graft will then be integrated within the target tissue and serve to conduct electrochemical signals to the electrode for recordings.

One limitation of PEDOT:PSS for applications in organic electronics is its low conductivity[113,129]. Several methods have been extensively researched to improve the conductivity, involving addition of organic solvents acids and ionic liquids to solution or film treatment methods with these solvents[129]. Some of the methods will be explored in this work, as detailed below.

Synthesis of PEDOT:PSS

PEDOT is obtained by the oxidative polymerization of the monomer ethylenedioxythiophene (EDOT), which is initiated when an oxidizing agent, such as Iron salts, forms a radical cation by removing an electron from the thiophene moiety (Figure 6) The oxidized EDOT monomer tends to form a dimer with other monomer in the same oxidation state, and the resulting dimer has a higher propensity to be oxidized - it is thought that this reaction is propagated by successive oxidation and dimerization of sequentially longer oligomers[130,131].

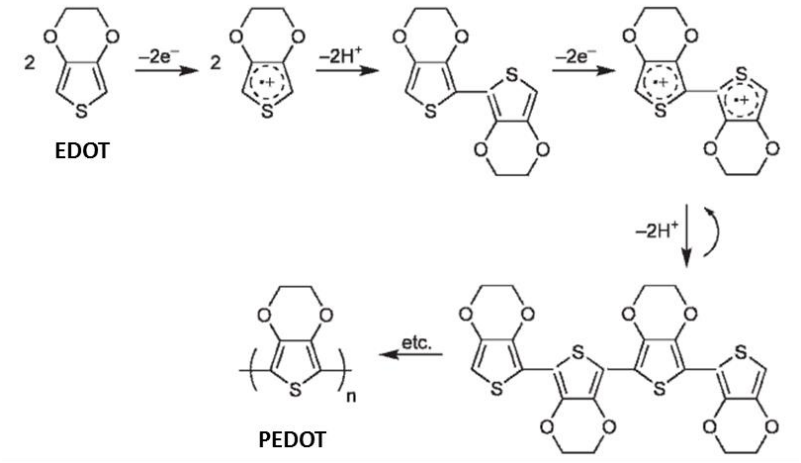

Figure 6. Oxidative polymerization of PEDOT through successive oxidation/dimerization of growing oligomers. Adapted from Kirchmeyer et al.[130].

PEDOT precipitate formed from this polymerization cannot be used by itself for transparent conductive coating, as it cannot be re-dissolved and re-dispersed. To coat a substrate with PEDOT, polymerization *in situ* can be performed, but at the expense of obtaining films with high surface roughness and needing extra rinsing steps to remove the oxidation agent[132]. One of the alternative methods is to have a form of PEDOT ready for processing by polymerizing the cationic PEDOT within an aqueous counter ion polyelectrolyte – the most effective and widely used is polystyrenesulfonic acid (PSS). The resulting polyelectrolyte complex – PEDOT:PSS – is soluble in water, has good film forming properties and has high optical transmittance in the visible spectra (Figure 7)[131].

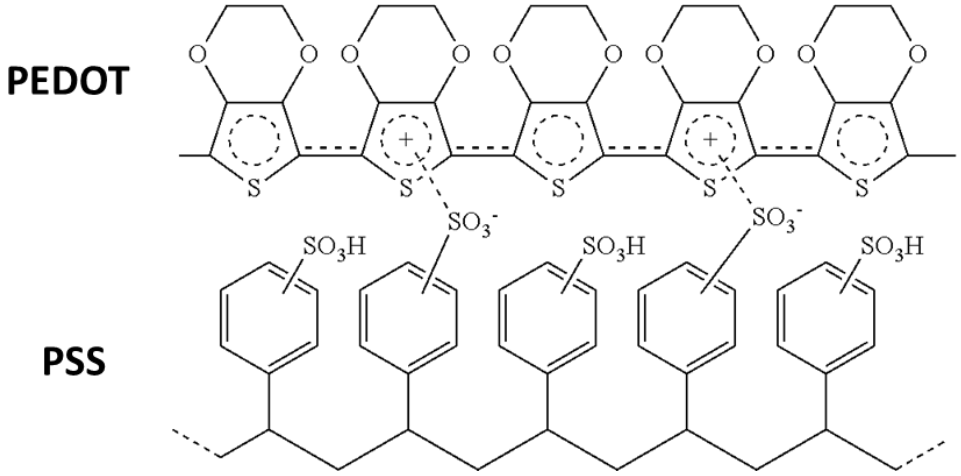

Figure 7 Molecular structure of PEDOT:PSS polyelectrolyte complex. The oxidized PEDOT chain is linked to the PSS anions through electrostatic interactions. Taken from Law et al.[133].

The characteristics of PEDOT:PSS films, namely its surface topography and electrical conductivity, are dependent on several factors, such as particle size, viscosity, fraction and phase segregation of PSS polyanion. The latter two are especially important in the conductivity of the final films because PSS is an electric insulator, increasing the energy barrier for charge transport, as it lacks the delocalization mechanism of conjugated polymers. As so, lower proportion of PSS[74,134] to PEDOT and higher degree of phase segregation of excess PSS[135] are associated to higher film conductivity values, and are the processes behind several strategies reported in literature for increasing PEDOT:PSS conductivity[136–139].

Stability of PEDOT:PSS films in aqueous environment

To test the effect of an electric field during the culture of NSCs, the scaffolds made with inkjet-printed PEDOT:PSS will be exposed to an AC voltage source while submerged in the culture medium. As PEDOT:PSS is hydrosoluble, it is important to guaranty the stability of these films throughout the duration of the experiment. This could be done by exploiting the crosslinking properties of (3-glycidyloxypropyl)trimethoxysilane (GOPS, Figure 8). GOPS molecule allows the creation of PEDOT:PSS films that are stable under water.

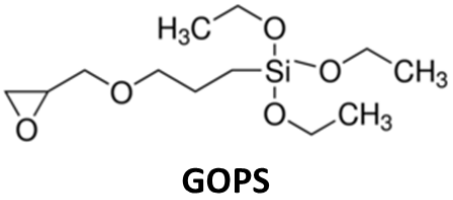

Figure 8. Molecular structure of crosslinker GOPS. The establishment of crosslinks can be made through the epoxide ring, on the left, and the three methoxy groups, on the right, depending on the molecules that interact with GOPS.

It is not clear what are the mechanisms behind increased stability, as several reactions can take place between GOPS, the substrate supporting the PEDOT:PSS films and common additives added to the solution for conductivity enhancement[124,140]. It is thought that ether bonds may be created between the epoxide ring of GOPS and the hydroxyl (-OH) groups of common additives of PEDOT:PSS, such as ethylene glycol or glycerol ,and glass.

Also, condensation reactions can occur between the three methoxy groups (-O-CH_3) in GOPS and –OH groups on these additives[124,141]. This may result in an entanglement between the GOPS-crosslinked network of substrate and additives with the PEDOT:PSS that difficult its delamination when immersed in water. When additives are not added to solution, GOPS may interact with itself or with PEDOT:PSS to create stable films, but such interactions have yet to be explored[141,142].

PEDOT:PSS Conductivity Enhancement

For the intended application, given the amplitudes of current reported in the literature for the application of electric fields on NSC culture[72,74], it is reasonable for the scaffold material supporting the cells to be able to sustain currents with magnitudes of 0.1-100 µA, allowing a broad range of currents to be used in future studies for the systematic characterization of the electric field effects on NSCs.

There is, however, a key limitation which has to be taken into account in the development of the material and its resulting electrical conductivity – the applied tension should be lower than 1.23 V, which is the electrical potential at which water electrolysis occurs[143]. Electrolysis of culture medium should be avoided, as it negatively affects cell growth and survival: ionic compounds released to the media through electrolysis can directly inhibit cell growth[144], or result in prejudicial change in the pH of the media. Taking into account the voltage limitation and the desired range of current values, the material should have a minimum conductivity on the order of $1 \times 10^{-4}\ S/cm$ to provide current up to 100 µA with a maximum voltage of 1V, assuming that the conductive material has 1 cm length.

As will be shown later in this work, conductivity of PEDOT:PSS as obtained from the supplier is around $9 \times 10^{-4}\ S/cm$, and is further decreased when the crosslinking agent GOPS is added. As so, some approaches to improve PEDOT:PSS electrical conductivity discussed by Shi *et al.*[129] were explored, as conductivity could be improved up to 10^3-fold. Four of these approaches were explored, due to their simple and off-the-shelf implementation:

1. Addition of organic solvents to PEDOT:PSS – The idea is for organic solvents to induce phase separation between the conductive PEDOT and the insulating PSS, decreasing the energy barrier for carrier mobility. The addition of ethylene glycol (EG)[145] at different concentrations was explored.
2. Post-Treatment of PEDOT:PSS films with organic solvents. Here, the same principle applies as the addition of organic solvents, but the treatment occurs on the surface of the already-formed PEDOT:PSS film. Post-treatment with EG[136] and methanol (MeOH)[146] were explored.
3. Surfactant treatment – The addition of surfactants can improve film formation and adhesion to the substrate, thus contributing to an increased film conductivity[129]. In this case, the addition of poly(ethylene glycol) (PEG) to PEDOT:PSS was explored[138].
4. Acid treatment – The addition of acid to the PEDOT:PSS solution has also been shown as an alternative method for increasing conductivity[137,139]. Recent work by Kim *et al.*[147] showed that the conductivity of PEDOT:PSS films could be improved with sulfuric acid treatment up to about 4000 S/cm due to phase segregation between PEDOT and PSS and secondary doping mechanism for PEDOT; however, sulphuric

acid is a strong and corrosive acid, which limits its use in biological applications. In this work, the use of trichloroacetic acid as an alternative is explored.

IV. Research Strategy

As already mentioned, this work aims to create transparent, electroconductive scaffolds for NSC culture, serving as platforms to study the influence of electric fields on cell behaviour and to validate the use of the materials and techniques explored in future developments of scaffolds for cell-based therapeutic strategies.

In Figure 9 it is possible to see a workflow evidencing the materials and techniques explored in scaffold development, the physical chemical characterization performed on scaffold materials, the biological studies performed on the scaffolds, and the parallel optimization studies performed on PEGDA and PEDOT:PSS.

In an early stage of the project, not depicted in Figure 9, it was intended to create 3D transparent, electroconductive scaffolds that could overcome the cell visualization problems of common 3D scaffolding systems, while being able to provide electrical cues for NSC growth and differentiation. Three different strategies were used, and are detailed in Annex A.

To fabricate scaffolds, two different pathways were explored:

- On the first, 3D Printing by Fused Deposition Modelling (FDM) of commercial filaments was used to make highly customizable, low-cost, easy and quick to produce platforms – a transparent filament of poly(ethylene terephthalate) (PET)[148] and a recently developed electroconductive filament made from poly(L-lactic acid) (PLLA or, more commonly, PLA) mixed with Carbon-Black (cPLA)[149] were used;
- On the second, a transparent hydrogel – PEGDA – and an electroconductive conjugated polymer – PEDOT:PSS – are used.

The materials in scaffolds were characterized by electrical conductivity, optical transmittance and wettability studies. Proof-of-concept biological studies of NSC expansion and differentiation were then performed on these scaffolds to assess their viability in future investigation on the effect of electrical fields on cell culture.

Optimization studies were also performed in parallel, namely the electrical conductivity enhancement of PEDOT:PSS to create an optimal formulation to be used in inkjet-printing of PEDOT:PSS films; the exploration of PEGDA hydrogel mechanical properties with high concentrations of plasticizers; and the enhancement of PEGDA hydrogel transparency by using molecules commonly used as plasticizers as clearance agents.

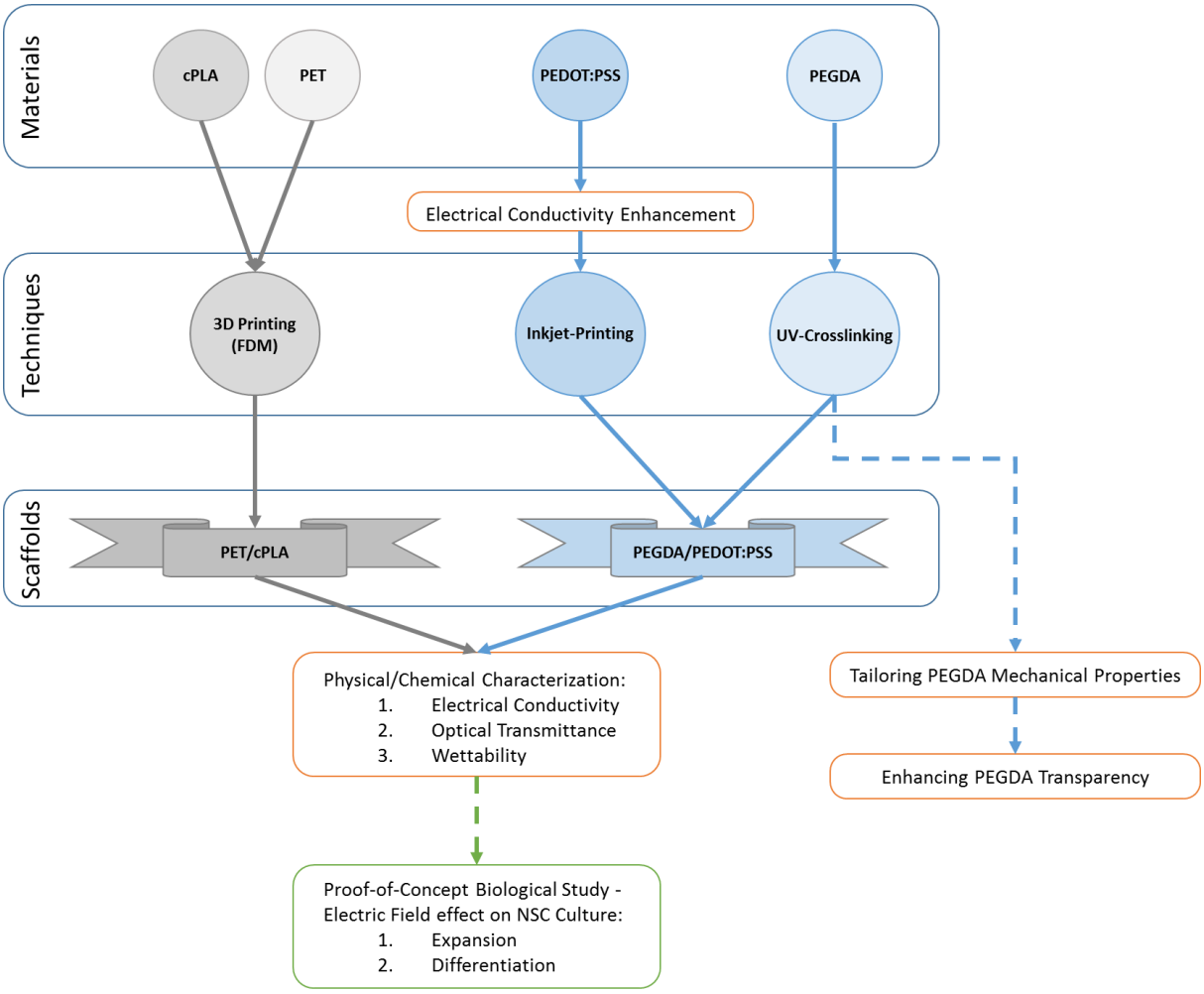

Figure 9. Research Strategy followed in this work.

Methods

I. Scaffold Design and Development

A. 3D-Printed Scaffold using Commercial Filaments

In this prototype, the scaffold was designed using CAD software and directly 3D-printed by FDM of two commercial filaments: transparent PET (t-glase, Taulman 3D[148]) and conductive PLA (cPLA – ProtoPasta conductive PLA, ProtoPlant[149]).

1. **3D Modelling using CAD.** The scaffold was designed using SolidWorks 2015. The overall design of the scaffold consists on a 2D cell culture platform containing three different parts: a medium container (Figure 10.A); the cPLA filaments in the middle, which provides the electrical cues to the cells; (Figure 10.B) and the transparent PET base, where cells will be cultured and can be observed (Figure 10.C). In a first iteration of the scaffolds, gaps between cPLA filaments (which are the observable cell regions through the transparent PET base below, Figure 10.D) were designed with different sizes (200, 300, 400, 500 and 1000 µm) in order to assess possible differences in the electric field effect on cells. The squared cPLA regions are outside of the cell culture area and are used as electrodes to make the connection with the voltage source, as shown in the Electric Field Experiment Setup. The height of the objects are 400 µm for both PET base and cPLA filaments and 1 cm for the medium container. The inner diameter of the medium container is 1 cm, which translates in a cell culture area of about 0.875 cm^2, approximate to that of 48-well plate[150]. The several CAD designs are saved as *Standard Triangular Language* (.STL) file extension.

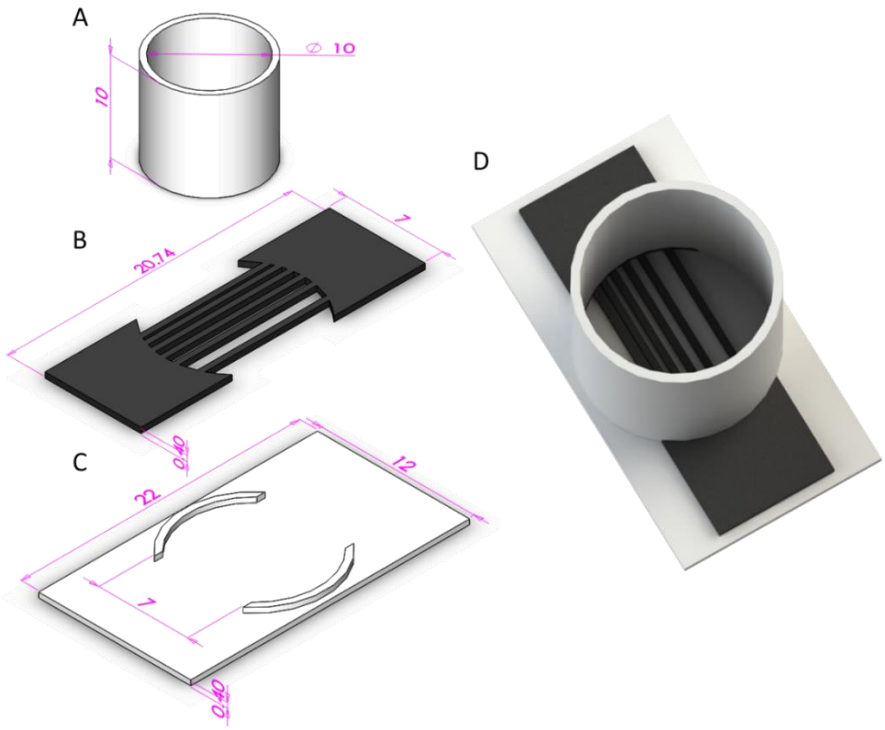

Figure 10. cPLA Scaffold Design: (A) Medium Container; (B) cPLA filaments; (C) PET base; (D) Assembled scaffold. Dimensions shown are in mm.

Later, a second iteration was designed, where two cPLA filaments (distanced at 400 µm) ran parallel to each other, forming a conduit with two regions: one where the cPLA is parallel to the orientation of the subjacent PET filaments, the other where it is perpendicular (Figure 11).

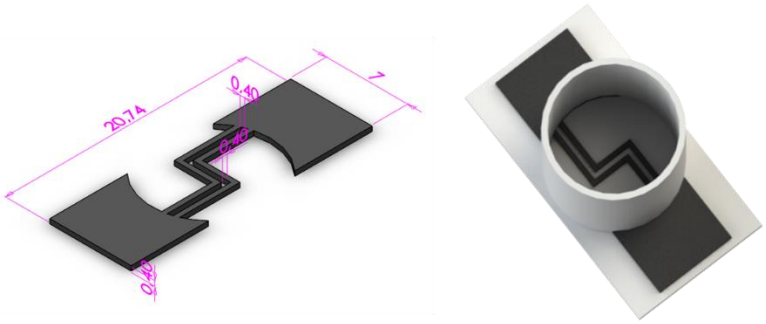

Figure 11. Design of the Second iteration of 3DP PET/cPLA scaffold: cPLA filaments (left); assembled scaffold (right). Dimensions shown are in mm.

2. **3D Printing using FDM.** The several .STL. files created were assembled on MakerBot MakerWare 3.7 software according to Figure 12 and printed on a MakerBot Replicator 2X (MakerBot).

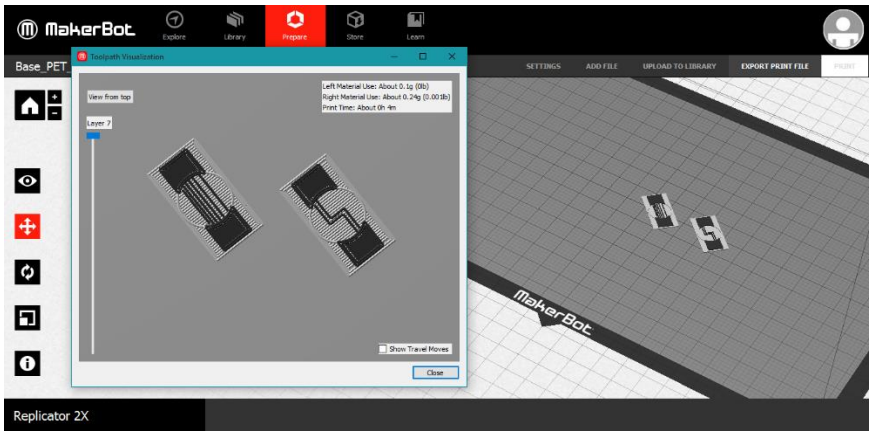

Figure 12. Assembly of 3DP PET/cPLA scaffold. The parts are assembled in a 45º angle as to orient the PET filaments perpendicularly to the cPLA filaments (as can be observed in the 'Toolpath Visualization' window on the left). It is possible to observe, in the 2nd iteration of the scaffold, the areas where the cPLA filaments run either parallel or perpendicular to the underlying PET.

The printing settings used are presented in Table 1. The Layer Height corresponds to the height of the PET base and cPLA filament designs, as it is intended to create these objects with one layer only – this height was optimized for better visualization through the PET filaments extruded on the base of the scaffold. The extrusion and build plate temperatures are optimized for both filaments, according to the manufacturer's instructions[148,149]. It is important to note that low extrusion speeds, in this case 10 mm/s, are needed to print parts with small dimensions in order to maintain high level of detail, as it increases the time needed for the previous filament layer to cool down.

Table 1. Settings introduced in MakerBot MakerWare to print the Scaffold.

Layer Height:	0.40 mm
Extruder Nozzle Diameter	0.40 mm
Right Extruder (PET):	232°C
Left Extruder (cPLA):	210°C
Build Plate:	70 °C
Speed while Extruding:	10 mm/s

To obtain detailed images of the results, photos were taken on a trinocular stereomicroscope with a digital camera, on magnifications ranging between 0.67-4.5x. Measurements on gap size and cPLA filament width were performed on FIJI software.

B. Hydrogel- and Conductive Polymer-based Scaffold

In this second prototype, a scaffold was created by UV-crosslinking of the transparent hydrogel PEGDA and inkjet printing of the conductive polymer PEDOT:PSS.

1. **UV-Crosslinking of PEGDA.** To fabricate the transparent substrates, a PEGDA oligomer solution with a molecular weight of 575 Da (Sigma-Aldrich) was used. First, the UV photoinitiator 2,2-dimethoxy-2-phenyl-acetophenone (DMPA, maximum absorption at 365 nm, Sigma-Aldrich) was dissolved (300 mg/ml) in N-vinylpyrrolidone. 10 µl/ml of the DMPA solution are then added to the PEGDA. To create substrates for ink-jet printing, the solution is filtered with a 0.2 µm syringe filter and is placed on a mold made of two glass slides separated by a 0.8 mm PET spacer created on the 3D printer, and exposed to UV light (Newport 94023A Sol3A solar simulator, with an intensity of 100 mW/cm^2) for 2 min. The glass slides were previously plasma-treated at 60 W for 6 minutes. The resulting PEGDA substrates are taken from the mold, rinsed with distilled water and dried under a Nitrogen stream.

2. **Inkjet Printing of PEDOT:PSS on PEGDA.** Dimatix Materials Printer 2831 (DMP, Fujifilm) was used to print PEDOT:PSS onto the PEGDA substrates. A solution of PEDOT:PSS (Clevios P VP AI 4083) with 10 v/v% EG, 0.5 µl/ml TCAA and 10 mg/ml crosslinker GOPS was filtered with 0.45 µm cellulose acetate filter tips and injected into a DMP cartridge. The DMP cartridge print head in use dispensed drops of 1 pl. Similarly to the layout created for the conductive filaments in the previous scaffold, a design was created in Inkscape software where PEDOT:PSS stripes of varying widths were designed – in this case, the design had strips with 500, 100, 50 and 20 µm, with gaps of 500 µm (Figure 13).

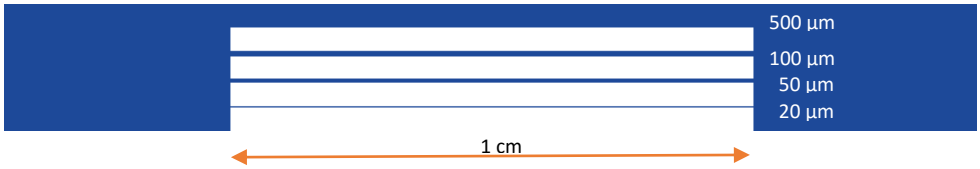

Figure 13. PEDOT:PSS feature used for Inkjet-printing on PEGDA.

The design is saved as a monochromatic .BMP file, and opened in the Dimatix Drop Manager software for printing. The printer settings used in the ink-jet printer are depicted in Table 2: the substrate height was set to

0.85 mm, (0.05 mm higher than the actual substrate height) as to prevent collision between the printer head and the substrate; out of the 16 nozzles present in the DMP cartridge print head, 4-5 consecutive nozzles were used; a total of 40 layers were printed, with 30 s of rest time between them. The cartridge temperature and print height were left at the default values of 30°C and 1 mm, respectively. A Cleaning program was set to run after every 5 printed bands, or until reaching 240 seconds after the last cleaning cycle.

Table 2. Settings introduced in the Dimatix Drop Manager to print the PEDOT:PSS design.

Substrate Height:	0.85 mm
Platform Temperature:	OFF (Room Temp.)
Number of Nozzles:	4-5
Number of Layers:	40
Cartridge Temperature:	30°C
Cartridge Print Height:	1.00 mm
Pause time between layers:	30 s
Cleaning Cycle during printing:	Spit-Purge-Spit-Blot
Cleaning Program during printing:	Every 5 bands OR 240 s

After printing, the substrates were put on a hot plate at 150°C for at least 5 minutes to activate the crosslinking mechanism of GOPS. To obtain detailed images of the resulting IJP PEDOT:PSS, photos were taken on a trinocular stereomicroscope with a digital camera, with magnifications ranging between 0.67-4.5x. Also, photos were obtained with the inbuilt DMP camera. Feature measurement was performed on FIJI.

3. **Medium Container.** The Medium container used in the previous scaffold was 3D-printed and glued to the PEGDA/PEDOT:PSS scaffolds with Medical Adhesive Glue (Dow Corning), which was left to solidify for 2 days.

II. Material Characterization

A. Electrical Conductivity

Electrical conductivity was assessed by four-point probe method, using an in-house built setup as depicted in Figure 14. First, four gold contacts with 40 nm of thickness were deposited on the spin-coated samples by thermal evaporation using the Edwards Coating System E306A; secondly, each probe (copper wire) was attached to the gold contacts using adhesive silver paint (Figure 14.B). A DC current source was applied between the outermost electrodes (1 and 4, Figure 14) and values of 0.1, 0.2, 0.5, 1.0, 2.0 and 5.0 µA were applied in both directions by inverting its signal, while the corresponding voltage values were measured between the two innermost electrodes (2 and 3, Figure 14).

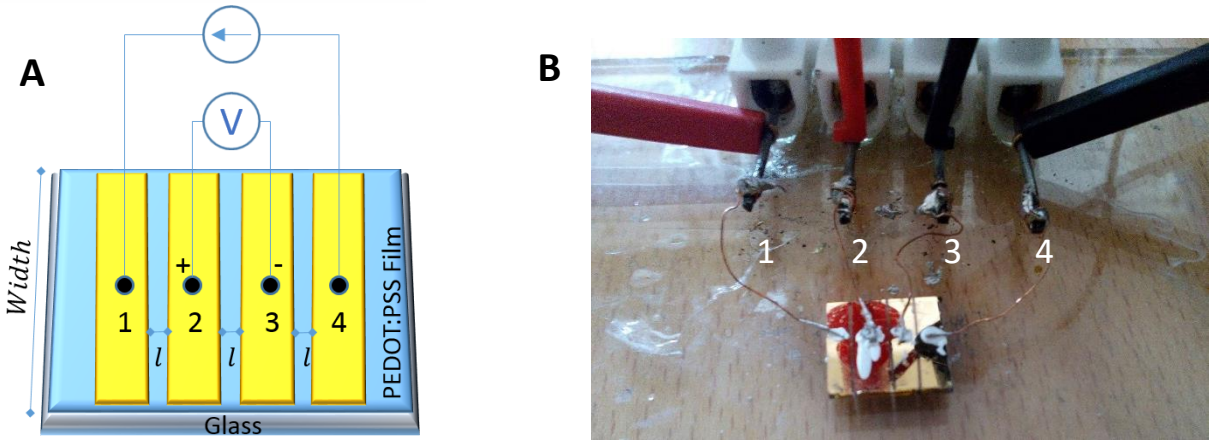

Figure 14. Resistivity measurement by four-point probe method; (A) Schematic representation of the four-point probe method - a current source is connected to the outer contacts (1 and 2), and the resulting voltage across length l of the material is measured between contacts 3 and 4 with a digital voltmeter; (B) Assembly of four-point probe method – the 4 gold contacts, as well as the connections of each probe with silver paint can be observed. Although the figure represents a PEDOT:PSS-coated glass, the same procedure was used for other substrates, namely PEGDA.

Least squares regression analysis in Excel was used to find the Resistance R of the film, given by the linear relation:

$$R = v/i\ [\Omega] \tag{1}$$

The electrical resistivity ρ is related to the resistance by the following equation:

$$R = \rho\frac{l}{S} \Leftrightarrow \rho = R\frac{S}{l}\ [\Omega.\mathrm{cm}] \tag{2}$$

where l is the length of the piece of the material, in this case, the distance between gold contacts, and S is the cross-sectional area of the film, that is, the product of the film thickness by the width (Figure 14.A).

Finally, electrical conductivity σ is defined as the reciprocal of resistivity:

$$\sigma = \frac{1}{\rho}\ [\Omega^{-1}.\mathrm{cm}^{-1}\ or\ S/\mathrm{cm}] \tag{3}$$

For film thickness measurement, each film was scratched with a razor blade, and the scratch was scanned with Veeco Dektak 6M Stylus Profiler with a 1kN stylus force. The resulting valley height, and thus film thickness, was measured with Dektak 3.31 Software.

B. Optical Transmittance

To assess the transparency of both PEGDA substrates and PEDOT:PSS films, Transmittance Spectra was calculated from Absorption spectra obtained with a Cecil CE7200 Double Beam UV-Vis Spectrophotometer. Spectra analysis ranged from 300 to 900 nm to include the visible range (approximately 390-700 nm). The resulting spectra was then analysed in Excel to calculate % of Transmittance according to:

$$T = 10^{-A} \tag{4}$$

$$\Rightarrow \%T = 100 \times 10^{-A} = 10^{(2-A)} \tag{5}$$

C. Wettability

Contact angle was measured for the materials used in cell culture, namely PEGDA, PEDOT:PSS, cPLA and PET, both with and without Laminin coating, and also for the PEGDA substrates with different mechanical properties. It should be noted that contact angle of PEDOT was measured on an ink-jet printed feature on top of PEGDA substrate, while cPLA and PET was measured on the 3d-printed scaffolds. The sessile drop profile method was used, and the contact angle was assessed with the Kruss DSA25B goniometer and Drop Shape Analysis 4 Software by measuring the tangent angle at the three-phase contact point (Figure 15).

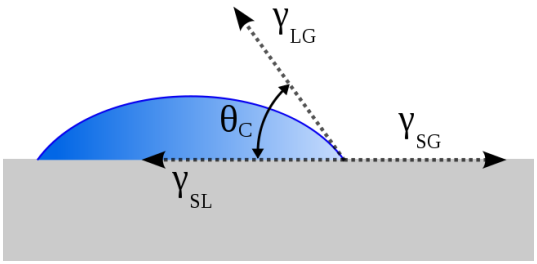

Figure 15. Contact angle (θ_C) of a liquid droplet measured at the three-phase (Solid, liquid and gaseous) contact point, between the solid-liquid interfacial tension (γ_{SL}) and liquid surface tension (γ_{LG}); γ_{SG} is the solid-vapour interfacial tension.

D. Mechanical Properties

Compressive Modulus and Strength of different PEGDA hydrogels were assessed using a Zwick Z100 machine, with an extension rate of 1 mm/min and a load cell of 5kN. At least five samples of each hydrogel were tested, each with a minimum of 4x4 mm surface area and 3 mm height. The obtained force-extension curves were then transformed into stress-strain plots given the sample dimensions, where strain, ε, is the percentage of height variation of the sample and stress, σ, is given by:

$$\sigma = \frac{F}{A} \; [Pa \; or \; N/m^2] \tag{6}$$

where F is the force load applied and A is the area of the sample being tested. The linear region of each plot was used to determine, by least squares regression, the Compressive Modulus E, according to:

$$E = \frac{\sigma}{\varepsilon} \; [Pa \; or \; N/m^2] \tag{7}$$

where while σ is the stress and ε the strain. Compressive strength corresponds to the maximum stress value in stress-strain curves from which material rupture occurs. The obtained values for each hydrogel condition were averaged between the 5 samples to obtain compressive modulus and strength, and results are reported as the mean ± standard deviation (SD).

E. Swelling Behaviour

The hydrogels were first left to soak on PBS right after UV-crosslinking. The wet hydrogels were then weighted after 10, 20, 90 and 180 minutes of soaking – care was taken to remove the excess PBS from the surface of the hydrogels, so that only the weight of incorporated PBS was taken into account. As the weight stabilized around 90 minutes under PBS, it was concluded the hydrogels have reached the swelling equilibrium after that time. The

hydrogels were then dried overnight at 50°C, and the dry weight was obtained. The swelling equilibrium weight (w_s) and the the dry weight (w_d) were then used to calculate the % of swelling ratio, SW:

$$SW(\%) = \frac{w_s - w_d}{w_d} \times 100 \quad (8)$$

III. Enhancement of PEDOT:PSS Electrical Conductivity

To assess ways to improve the electrical conductivity of PEDOT:PSS with organic solvents, samples were prepared according to previous work in literature[74,136–138,145,146]. First, glass substrates with approximately 1x1 cm^2 of area were cut, and washed with acetone and 2-propanol – for both solvents, samples were placed in an ultrasonic bath for 5 minutes, and rinsed using a nitrogen stream. The glass substrates were then O_2-plasma treated at 30 W for 6 minutes before use in order to increase their hydrophilicity by creating hydroxyl (-OH) groups on the surface. The conductivities of glass and PEGDA substrates are negligible, as both showed high resistance when measured with the four-point probe method. The samples were then prepared according to the protocols described below; in all solutions, the same PEDOT:PSS starting dispersion (Clevios P VP AI 4083) was used, and films were spin-coated at 1800 rpm for 60 seconds, unless stated otherwise.

1. **PEDOT:PSS (Control).** Simple aqueous PEDOT:PSS dispersion was used to spin coat glass substrates, which were thermally annealed at 120 °C for about 10 minutes.
2. **Crosslinked PEDOT:PSS[74].** Crosslinker GOPS was added to PEDOT:PSS at a 10 mg/ml (1 wt%) concentration. After spin-coating, the substrates were thermally annealed at 150°C for at least 2 minutes in air in order to activate the crosslinker.
3. **PEDOT:PSS with EG[145].** 10 and 20 v/v/% of EG (Sigma-Aldrich) were added to PEDOT:PSS and stirred for 24 hours. The solutions were then used to spin coat glass substrates, which were dried under vacuum at 60°C in a vacuum oven for 24 hours.
4. **Post-treatment with EG[136].** PEDOT:PSS spin-coated films were obtained in a similar procedure as the control sample. The substrate was then dipped in EG for 3 minutes, followed by drying under vacuum at 80°C for 24 hours.
5. **Post-treatment with MeOH[146].** PEDOT:PSS spin-coated films were obtained in a similar procedure as the control sample; however, before annealing, a drop of MeOH was placed on top of the film; the sample was then annealed in air at 130°C for 20 minutes. As reported by Alemu *et al.*[146], the conductivity can be further enhanced by dipping the substrates in MeOH for 10 minutes, followed by annealing in air at 140°C for 5 minutes.
6. **Surfactant Treatment with PEG[138].** 2 v/v% of PEG (M_n=400, Sigma-Aldrich) and 6 v/v% of EG were added to PEDOT:PSS. Glass substrates were then spin-coated with this solution at 3000 rpm for 60 seconds, and thermally annealed at 130°C for 30 minutes.

7. **Acid Treatment with TCAA**[137]**.** TCAA was added to PEDOT:PSS in a concentration of 0.5 µl/ml (0.05 v/v%). After spin-coating glass substrates, they were annealed at 150°C for 2 minutes.
8. **Crosslinked PEDOT:PSS + EG.** 10 mg/ml crosslinker GOPS and 10 v/v/% of EG were added to PEDOT:PSS and stirred for 24 hours. Glass Substrates were then spin coated, thermally annealed at 150°C for at least 2 minutes to activate the crosslinker and dried under vacuum at 60°C for 24 hours.
9. **Crosslinked PEDOT:PSS + EG + MeOH post-treatment.** A drop of MeOH was placed on top of substrates prepared in 8 and thermally annealed at 130°C for 20 minutes. The substrates were then dipped in MeOH for 10 minutes, and annealed at 140°C for 5 minutes.
10. **Crosslinked PEDOT:PSS + EG + TCAA.** Substrates were prepared in a similar procedure as condition 8, with the difference that 0.5 µl/ml TCAA were also added to the PEDOT:PSS solution.
11. **Crosslinked PEDOT:PSS + EG + TCAA + MeOH post-treatment.** Substrates prepared in 10, were post-treated with MeOH in a similar procedure as the one described for condition 9.

Electroconductivity was measured and the transmittance spectra was obtained for the several conditions. In the transmittance spectra, since the solutions were spin-coated onto glass, the substrates were measured against a clear glass slide as control.

IV. Tailoring PEGDA Mechanical Properties

A base solution of PEGDA oligomer (M_n = 575 Da, Sigma-Aldrich) with DMPA photoinitiator was prepared in a similar method described above for the creation of scaffolds and was used to create solutions with different concentrations of HBS and PEG (M_n = 400 and 600 Da, Sigma-Aldrich). The hydrogels tested are described in Table 3.

Table 3. PEGDA-HBS/Plasticizer Hydrogels used in Compression tests.

		Plasticizer Concentration (as wt% on PEGDA)	Sample Name
PEGDA		0%	PEGDA (dry)
		0%	PEGDA (wet)
PEGDA + Plasticizer	HEPES-Buffered Saline (HBS)	50%	HBS-50%
		75%	HBS-75%
		90%	HBS-90%
	PEG(400)	50%	PEG(400)-50%
		75%	PEG(400)-75%
		90%	PEG(400)-90%
	PEG(600)	50%	PEG(600)-50%
		75%	PEG(600)-75%
		90%	PEG(600)-90%

10 mM of HEPES (Sigma-Aldrich) and 10 mM NaCl were added to deionized water to prepare a HBS solution, similarly to some works in the literature[98,151]. The pH was adjusted with a Metrohm 827 pH meter to the physiological value of 7.4. To create the hydrogels for mechanical testing, the solutions were poured on Petri Dishes, while for wettability and transmittance analysis, the same mold system with two glasses used to fabricate

the PEGDA/PEDOT:PSS scaffolds was used. The solutions were then UV-exposed for 2 min to activate PEGDA crosslinking.

For the mechanical properties of different PEGDA hydrogels, compressive modulus and strength were assessed on the hydrogels specified in Table 3. Wettability was assessed by measuring the contact angle on the hydrogels of Table 3 using the sessile drop profile method. To obtain the transmittance spectra, the PEGDA substrates were measured against air as control.

V. Enhancement of PEGDA Transparency

A base solution of PEGDA oligomer (M_n = 575 Da, Sigma-Aldrich) with DMPA photoinitiator was prepared in a similar method described above for the creation of scaffolds and was used to create solutions with different concentrations of plasticizers glycerol (Sigma-Aldrich), sorbitol (Sigma-Aldrich), and PEG (M_n = 400 and 600 Da, Sigma-Aldrich). The solutions tested can be observed in Table 4.

Table 4. PEGDA-Plasticizer Solutions tested to enhance transparency.

Plasticizer	Concentration (as (wt)% on PEGDA)	Sample Name
-	-	PEGDA
Glycerol	1%	Gly-1%
	10%	Gly-10%
	25%	Gly-25%
	50%	Gly-50%
Sorbitol	1%	Sorbitol-1%
	10%	Sorbitol-10%
PEG(400)	10%	PEG(400)-10%
	50%	PEG(400)-50%
PEG(600)	10%	PEG(600)-10%
	50%	PEG(600)-50%

To prepare the samples for transmittance, the solutions were poured on the same mold system described before to fabricate the PEGDA/PEDOT:PSS scaffold, and UV-exposed for 2 min to activate PEGDA crosslinking. To obtain the transmittance spectra, the PEGDA samples were measured against air as reference.

VI. Cell Culture

A. Cell Line

The Cell line used was ReNcell VM human neural progenitor cell line from Millipore, which is derived from the ventral mesencephalon region of human fetal brain and immortalized by retroviral transduction with *v-myc* oncogene. Cell doubling time is 20-30 hours, and can be differentiated *in vitro* to a high level of human neurons which have been shown to be electrophysiologically active[152], and thus suitable to use for these experiments.

B. Culture Media

The Basic Culture Medium used in the experiments was prepared using a 1:1 mixture of Dulbecco's Modified Eagle Medium with Nutrient Mixture F12 (DMEM/F12, Life Technologies) supplemented with 1% N-2 (Life Technologies), 20 µg/ml insulin (Life Technologies), 1.6 g/l additional glucose (Sigma) and 1% Penicillin/Streptomycin (Pen/Strep, Gibco®). For expansion, the basic culture medium was further supplemented with 20 ng/ml EGF, 20 ng/ml FGF-2 (both from Peprotech) and 20 µl/ml B27 (Life Technologies). For differentiation, Neurobasal Medium (Life Technologies) was supplemented with B27 (20 µ/ml) and mixed in a ratio of 1:1 with basic culture medium.

C. NSC Thawing and Expansion

Prior to their use in the experiments, cells were thawed and cultured for at least one passage. This is done in order to recover from the environmental stress caused by the thawing process, allowing them to go back to the normal cell cycle and preventing delayed-onset apoptosis during the experiments, as it has been shown that a great proportion of cells suffer apoptosis up to 48 hours post-thawing, which is likely due to activation of the caspase cascade up to 24 hours[153] or changes in mitochondrial permeability caused by free radicals in the cytoplasm, causing a leakage of cytochrome c, triggering the apoptotic pathway through procaspase 9[153,154]. A T12.5 flask is previously coated with Laminin: the coating protocol consists of incubating with 2 ml Poly-L-Ornithine (Sigma) at the cell incubator (37°C; 5% CO_2) for at least 30 minutes, wash once with PBS and incubate overnight at the cell incubator with 1ml diluted solution of Laminin (20 µg/ml in PBS). ReNcell VM (*Millipore*) Neural Stem Cells were thawed at passage 40 from the -80°C freezer by submerging the cryovial in the water bath (37°C) for 30 seconds and quickly resuspending in basic culture medium. The cell mixture was then centrifuged at 1000 rpm for 3 minutes, the supernatant was discarded and cells were resuspended in expansion medium (growth factor-supplemented basic culture medium). Cells were then seeded onto the previously-coated T12.5 flask with a density of 1.5×10^5 cells/cm^2, and placed in the cell incubator. NSCs were expanded on the T12.5 until reaching 80-90% confluence.

D. NSC Cryopreservation

The remainder of expanded NSCs that were not used for seeding on scaffolds were cryopreserved, with densities of $1.5 - 3 \times 10^5$ cells/vial. The cell suspension was again centrifuged at 1000 rpm for 3 minutes and cells were resuspended with 1 ml expansion culture medium with 10 (v/v)% dimethyl sulfoxide (DMSO), which was placed in a cryovial. The cryovial is quickly placed at -80°C inside a Mr. Frosty™ Freezing Container (Thermo Scientific), which is used to achieve a cooling rate of 1°C/min, optimal for cell preservation[155].

VII. Electric Field Experiment Setup

A. Preparation for Biological Studies

To prevent medium leakage, a watertight enclosure made of polydimethylsiloxane (PDMS) was created around both scaffolds. First, PDMS was prepared using Sylgard® 184 Silicone Elastomer Kit (Dow Corning).The desired amount of elastomer was weighted, and the Curing agent was added in a 1:10 weight proportion. The two were

mixed together for 1 minute using a stirrer, and set down in a desiccator under vacuum for 30 minutes to degass. A small amount of PDMS was then poured onto a 3D-printed cylindrical mold placed on a clean glassware, and the PDMS was thermally crosslinked at 95°C for 15 minutes, forming the bottom of the PDMS case. The scaffold was then placed inside the mold with a weight on top, PDMS was poured around the scaffold and left overnight for crosslinking at room temperature.

Copper wires of 0.35 mm diameter were used to make the connection between the scaffold electrodes inside the well-plate and the electrodes placed on the cell incubator (Figure 16). The tips of the copper wires were first dipped in acetic acid for in order to remove the insulating enamel. Two copper wires were then connected to the scaffold by gluing one of the tips to the scaffold electrodes using conductive silver paint (Electrodag 1415, Agar Scientific).

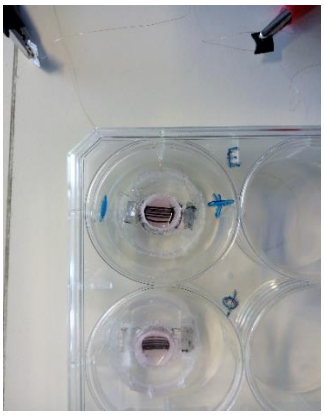

Figure 16. The PET/cPLA scaffolds are glued to a well plate and the thin copper wires establish the circuit between the cPLA electrodes outside the well-plate.

B. Scaffold Sterilization

Before cell seeding, the PET/cPLA scaffolds can be sterilized by immersing in ethanol until they are brought to a sterile environment in the laminar flow chamber; the PEGDA/PEDOT:PSS scaffolds, however, are brought dry in order to not compromise the PEDOT layer, as well as to prevent absorption of ethanol by the PEGDA hydrogel and subsequent release during cell culture. Under the laminar-flow chamber, the scaffolds are glued to 6-well plates using Medical Adhesive Glue (Dow Corning) – the glue was placed around the cell culture area in order to allow cell visualization using the microscope. Scaffolds were then further sterilized using Gibco® Antibiotic-Antimycotic solution for at least 2 hours.

C. NSC Seeding on Scaffolds

The scaffolds are washed 3 times with PBS to remove any trace of the antibiotic-antimycotic solution and coated with Laminin - in the same fashion as the T12.5 flask coating, except 300 µl/scaffold of both Poly-L-Ornithine and diluted Laminin were used this time, and Laminin was left at the cell incubator for at least 2 hours. Expanded NSCs were dissociated from the T12.5 flask by removing the culture medium, adding 1 ml Accutase and placing the flask in the incubator for a maximum of 5 minutes. Then, the enzymatic effect of accutase was stopped by diluting it with 1 ml of basic culture medium, the resulting cell suspension was centrifuged at 1000 rpm for 3

minutes, the supernatant was taken out and the cell pellet was resuspended. Gibco® Trypan Blue was then used in a 1:1 mixture with cell suspension to count cells on a haemocytometer. Cells were then seeded onto scaffolds with a density of 30 000 cells/cm^2 using the expansion culture medium.

D. Experiment Setup

The setup for the application of an electrical field to the scaffolds is shown in Figure 17. Overall, the equivalent circuit is a simple voltage divider where the scaffolds, represented as a resistors, are connected in series with a rheostat. The connection from the voltage source positive terminal to the scaffolds (node 1, Figure 17.C) and from these to the rheostat (node 2, Figure 17.C) is made through the rightmost red and black cables in Figure 17.A, respectively, which enter the cell incubator and are connected to the copper wires (Figure 17.B) – red cable for the positive scaffold terminal, black for the negative. The rheostat is then connected to the negative terminal of the voltage source, which is grounded (node 3, Figure 17.C).

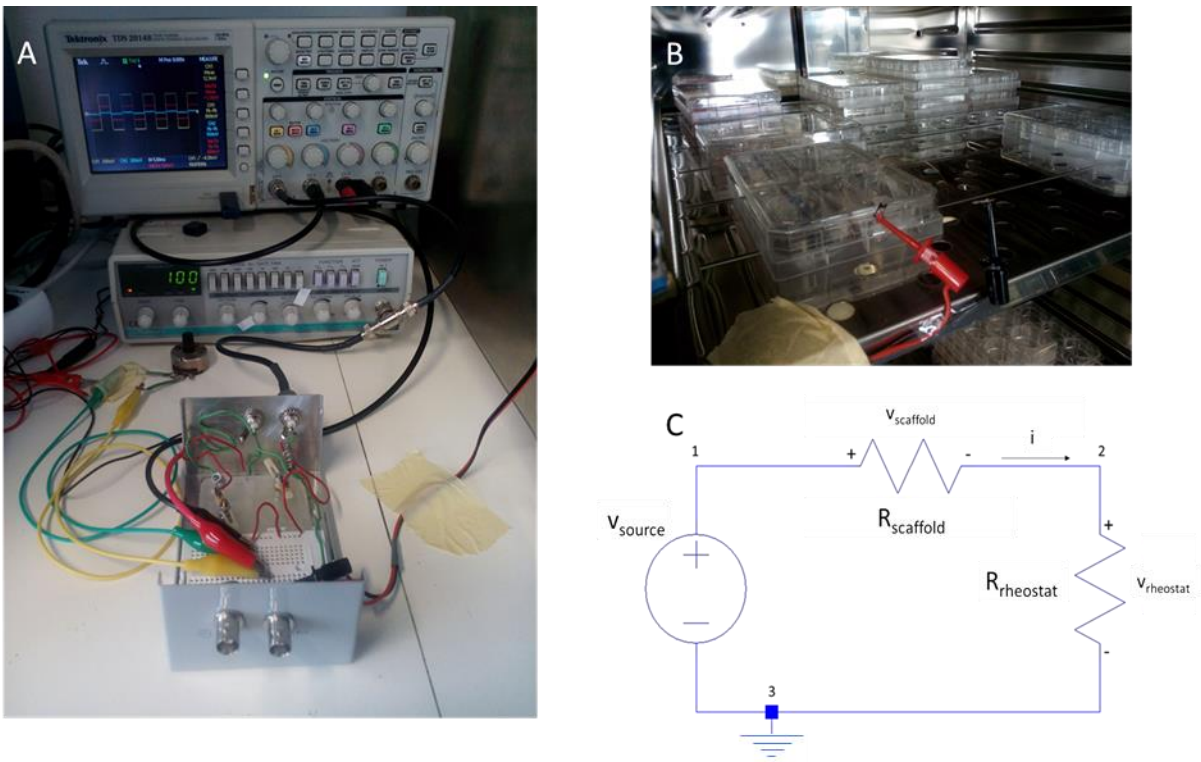

Figure 17. Experimental setup for the electrical field effect on NSCs: (A) "Electrical" Setup mounted next to the cell incubator, where it is possible to see the voltage source, the oscilloscope, the rheostat and the white circuit board that establishes the circuit; (B) Interior of the cell incubator, where the connection of the scaffolds to the circuit is made; (C) Scheme of the equivalent circuit mounted for the experience.

The rheostat main purpose is to indirectly measure scaffold voltage $v_{scaffold}$, as this is the difference between the source (v_{source}) and the voltage at the rheostat ($v_{rheostat}$), both measured at the oscilloscope. This method is preferable to direct measurement at the scaffolds inside the incubator because it is easier to setup and avoids possible contamination from probes directly located at the scaffolds. Also, the rheostat serves as an alternative method to adjust $v_{scaffold}$, by changing its resistance value.

The scaffold resistance $R_{scaffold}$ is measured with a multimeter before connecting them to the rest of the circuit. As so, knowing the resistance, the voltage $v_{scaffold}$ necessary to obtain a desired current value can be determined by equation 1. This voltage is then adjusted to this value by adjusting v_{source} or by changing the rheostat resistance.

E. NSC Expansion Protocol

The expansion protocol used in this work is similar to the one reported in previous studies[74,156]: an AC Electric Field was applied as a voltage quadratic pulse of 100 Hz during 4 consecutive days after seeding; the expansion culture medium was changed every 2 days. After 4 days, cells are fixed, fluorescence staining and imaging is performed and then cells are dehydrated for Scanning Electron Microscope (SEM) imaging.

F. NSC Differentiation Protocol

The differentiation protocol used in this work is similar to the one conducted in the work by *Pires et al.*[74]: first, cells are expanded by applying an AC Electric Field as a voltage quadratic pulse of 100 Hz during 4 consecutive days after seeding, with the expansion medium being changed every 2 days; after 4 days, differentiation is induced by changing the medium into the differentiation one (with Neurobasal Medium and lack of EGF and FGF-2 growth factors) and replaced every 3 days, while the AC electric field is applied during 7 days intermittently with a daily 4-6h rest period. In some trials, live cell Calcein AM staining was performed at day 4. After 7 days, cells are fixed and immunocytochemistry is preformed, fluorescence images are taken and cells are dehydrated for SEM imaging.

VIII. Imaging and Analysis

A. NSC Expansion - Fluorescence Staining

After the 4-days (expansion) experiments, cells were double-stained with Phalloidin–Tetramethylrhodamine B isothiocyanate (Phalloidin-TRITC) and 4',6-diamidino-2-phenylindole (DAPI) in order to access cell visibility on the scaffolds and thus the viability of using immunocytochemistry on the 12-days (differentiation) experiments. Cells were first washed twice with PBS and fixed with 4% paraformaldehyde (PFA) at room temperature (RT) for 30 minutes. They were then washed twice with PBS and permeabilized with blocking solution (89.9% PBS; 10% Normal Goat Serum (NGS) and 0.1% Triton-X) for 30 minutes. The samples were then washed twice with PBS, incubated with 0.1 v/v% Phalloidin-TRITC (1 µl/ml in PBS) for 45 minutes in the dark, washed again twice and incubated with 0.15 v/v% DAPI (1.5 µl/ml in PBS) for 5 min in the dark. The samples were finally washed twice and stored with PBS for microscopic imaging. In some samples, Calcein AM live staining (Life Technologies) was performed: after 4-days of expansion, cells were washed with PBS, and 2 µM of Calcein in expansion medium (diluted from a stock solution of 4 mM) was used to incubate cells at 37ºC for 30 min.

B. NSC Differentiation - Immunocytochemistry

Immunocytochemistry was performed on the 12-days (differentiation) experiments in order to compare differentiation levels on scaffolds of early neurons and astrocytes under electric field stimulus and control. Cells were first washed twice with PBS and fixed with 4% PFA at RT for 30 minutes. The samples were then washed

twice with PBS and permeabilized with blocking solution for 30 minutes. The primary antibodies were then diluted according to data shown in Table 5 in a staining solution (94.9% PBS; 5% NGS and 0.1% Triton-X) and used to incubate the samples at 4°C overnight in the dark. The samples were then washed once with PBS and incubated with the secondary antibodies at RT for 1 hour in a dark cabinet, with the dilutions indicated in Table 5. Finally, samples were rinsed once with PBS, incubated with DAPI at RT for 2 minutes in the dark, and washed twice and stored with PBS for visualization.

Table 5. Antibodies used in the immunocytochemistry protocol and their respective dilutions.

	1st ANTIBODY	*DILUTION*	*2nd ANTIBODY*	*DILUTION*
TuJ-1	Mouse IgG Anti-TuJ-1	1:4000	Alexa Fluor-546 Goat Anti-mouse IgG	1:500
GFAP	Rabbit IgG Anti-GFAP	1:150	Alexa Fluor-488 Goat Anti-rabbit IgG	1:500

All the bright-field and fluorescence images were taken using the Leica® DMI 3000B microscope, Nikon® DXM 1200F digital camera

C. Fluorescence Microscopy Imaging

All the bright-field and fluorescence images were taken using the Leica® DMI 3000B microscope, Nikon® DXM 1200F digital camera and Nikon® AcT1 software, with the 100 and 200x magnifications. At least 3 images were taken for each of the spaces between cPLA filaments, in the case of the PET/cPLA scaffolds, or for each of the PEDOT stripes, for the PEGDA/PEDOT scaffolds. In all experiments, DAPI (Sigma, excitation maximum at 340 nm, fluorescence emission maximum at 488 nm[157]) was used to stain the nuclei, and images were taken with DAPI-FITC excitation filter. For the 4-days expansion studies, images for Phalloidin-TRITC (Sigma, excitation maximum at 540-545 nm, fluorescence emission maximum at 570-573 nm[158]) were taken with TRITC excitation filter. For the 12-days differentiation study, images of TuJ-1 marked with Alexa Fluor-546 (Life Technologies, excitation maximum at 556 nm, fluorescence emission maximum at 573 nm[159]) were taken with TRITC filter, while images of GFAP marked with Alexa Fluor-488 (Life Technologies, excitation maximum at 490 nm, fluorescence emission maximum at 525 nm[160]) were taken with a FITC excitation filter.

D. SEM Sample Preparation and Imaging

After fluorescence staining and microscopy, the samples were dehydrated by sequentially immersing in 25%; 50%; 75% and 99% of ethanol in milliQ water, at 37°C for 30 minutes each. The dehydrated samples were then coated with Au/Pd layer of about 30 nm using a Polaron E5100 coater (Quorum Technologies). All images were obtained using an electron beam with energies in the range of 10-15 keV, with a Field Emission Gun Scanning Electron Microscope (FEG-SEM, JEOL JSM-7001F) at magnitudes of 100x and 400x. At least 3 images were taken for each magnitude and for each of the spaces between cPLA filaments or PEDOT stripes, depending on the type of scaffold in use.

E. NSC Morphology and Alignment Analysis

For the 4-days expansion experiments, cell morphology was analysed according to aspect ratio (ratio between longest and shortest axis of cell body, reported as mean ± standard deviation), while cell alignment was analysed by creating histograms of the angle between the longest cell axis and the direction of the electric field; angle histograms are represented as the frequency percentage, and range from -90^{o} to 90^{o}. The analysis was performed in FIJI software in both cases; at least 15 cells were analysed in a minimum of 3 images for each of the spaces between cPLA filaments, in the case of the PET/cPLA scaffolds, or on top of the PEDOT stripes, for the PEGDA/PEDOT scaffolds.

Results and Discussion

I. Enhancement of PEDOT:PSS Electrical Conductivity

All treatment tested lead to conductivity enhancement of PEDOT:PSS.

As shown in The three most effective treatments were, in decreasing order, post-treatment with MeOH, addition of TCAA and addition of 10 v/v% EG to PEDOT:PSS solution, all with a 103-fold increase of PEDOT:PSS conductivity.

Table 6 and Figure 18, all sample treatments led to an improvement in electrical conductivity. It is important to note that the four-point probe method used was built in-house, and thus lacks some accuracy and reproducibility in the measurements – in fact, some factors, as the effect of temperature, quality of the four-point head and resistance between the head and the silver-glued electrodes, are not considered. For accurate and reproducible measurements, purposely commercial four-point probe heads exist.

Moreover, PEDOT:PSS contains ionic impurities. Therefore, as measures were done with an applied DC bias, this will originate an ion movement that will create an internal electric field that opposes the applied electric field, thereby reducing the effective field that causes electron migration; therefore, the measurement results are only effective conductivity values, as there is a contribution of this ionic space charge effect.

Given the limitations in measurement accuracy and the effect of ionic movement these effective conductivity measurements should be used with caution when drawing conclusions on the absolute conductivity value for a given sample. However, rather than absolute values, we aimed to assess relative conductivity between different substrates – for that purpose, it is assumed that ionic effects are constant for all samples tested.

The three most effective treatments were, in decreasing order, post-treatment with MeOH, addition of TCAA and addition of 10 v/v% EG to PEDOT:PSS solution, all with a 10^3-fold increase of PEDOT:PSS conductivity.

Table 6. Calculated resistance, resistivity and conductivity values for the different films deposited on glass substrates.

	Control	Crosslinker	PEDOT:PSS + Organic Solvent		Film Post-Treatment		Surfactant Treatment	Acidic Treatment
	PEDOT:PSS	GOPS	EG 10 v/v%	EG 20 v/v%	EG	MeOH	PEG	TCAA
R (Ω)	7.98E+06	9.32E+06	3.55E+03	8.51E+05	1.92E+03	1.63E+03	1.37E+05	6.81E+03
Width (cm)	1.005	1.025	1.465	1.025	1.485	1.005	1.000	1.025
Thickness (nm)	48	64	29	54	82	34	63	11
Section Area (cm²)	4.8E-06	6.5E-06	4.2E-06	5.5E-06	1.2E-05	3.4E-06	6.3E-06	1.2E-06
Distance (cm)	0.035	0.035	0.035	0.035	0.035	0.035	0.035	0.035
Resistivity (Ω.cm)	1.1E+03	1.7E+03	4.3E-01	1.3E+02	6.7E-01	1.6E-01	2.5E+01	2.3E-01
Conductivity (S/cm)	9.1E-04	5.8E-04	2.3E+00	7.5E-03	1.5	6.3	4.1E-02	4.4E+00
Relative Conductivity	1.0	0.6	2.6E+03	8.2	1.7E+03	6.9E+03	45	4.9E+03

As expected, the addition of the GOPS crosslinker led to about 40% decrease in conductivity when compared to pristine PEDOT:PSS[74,140].

As stated already, several strategies can be employed in order to increase PEDOT:PSS electrical conductivity. One of the strategies explored in this work, the addition of EG, has already been employed by *Pires et al.*[74], where 20 v/v% EG was added to PEDOT:PSS. Here we compare this concentration against 10 v/v% of EG, which was the most effective concentration obtained by Liu *et al.*[145]. In view of our results, it is possible to conclude that using a 10% concentration is preferable, with a 10^3-fold increase against 10-fold when a 20% concentration is used (The three most effective treatments were, in decreasing order, post-treatment with MeOH, addition of TCAA and addition of 10 v/v% EG to PEDOT:PSS solution, all with a 103-fold increase of PEDOT:PSS conductivity.

Table 6 and Figure 18). As so, an immediate modification of the approach used by *Pires et al.* is to decrease the EG concentration to half.

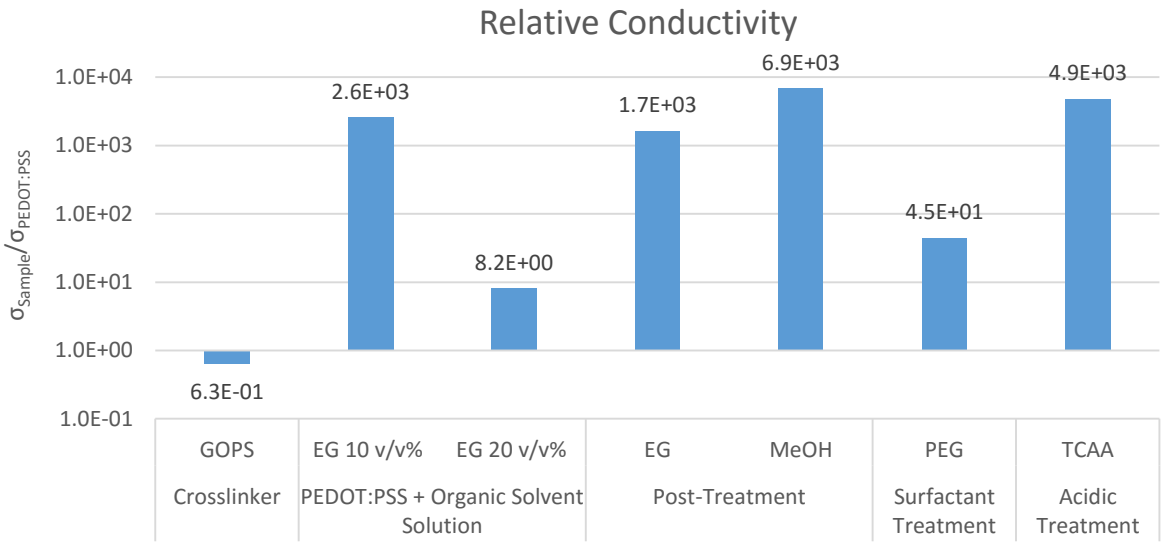

Figure 18. Relative electrical conductivity for the different PEDOT:PSS films, measured as the ratio of conductivity between each sample and control (pure PEDOT:PSS). Relative conductivity is presented as logarithmic scale in order to highlight the differences in magnitude between the different treatments.

The mechanism for the conductivity enhancement when adding an organic solvent is not fully understood. It is believed that the addition to the solution or treating film treatment with hydrophilic, organic solvents with high dielectric constant, such as ethylene glycol or methanol, induces a screening effect on the Coulombic interaction between positively-charged PEDOT and negatively-charged PSS, enhancing phase separation between PEDOT and PSS chains and leading to the dissolution of some hydrophilic, electrical insulator PSS chains[138,146], which results in the conductivity increase.

Atomic Force Microscopy (AFM) topographic images also suggest an increase in PEDOT aggregate particle size as a result of the phase separation induced by the additives, which decreases the number of particle boundaries in a given volume, decreasing the energy barrier associated with charge hopping between different polymer chains[129,146].

Conformational changes in the PEDOT structure can altogether result in increased charge-carrier mobility, and thus enhancement of conductivity[113,129] – it has been shown that there is a shift in the dominant resonant structure of PEDOT from benzoid to quinoid (Figure 19)[113,136] upon the addition to solution or post treatment of films with organic solvents.

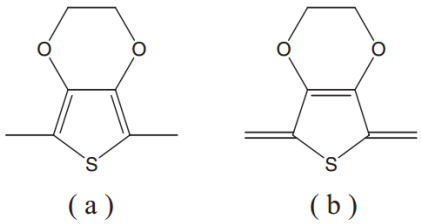

Figure 19. Resonant structures of PEDOT - (a) Benzoid and (b) Quinoid. Taken from [113].

Regarding the treatment with acids, such as trichloroacetic acid, it is believed that a similar mechanism of phase separation between PEDOT and PSS is behind conductivity enhancement[137]. In addition, there may be a secondary doping process, where an ion exchange may happen between PSS^- and the conjugate base of the acids, resulting in improved charge transport; this process has been described for strong acids such as sulphuric acid, and characterized by Raman and Fourier Transform Infrared (FTIR) Spectroscopies, but does not affect the conductivity in the same level as increased phase segregation between PEDOT and PSS[117,139].

Complementary studies are needed to understand the mechanism of conductivity enhancement. The morphology of the films should be studied with AFM to analyse PEDOT:PSS aggregate size variation with these additives or annealing strategies. Chemical analysis such as X-ray photoelectron spectroscopy or absorption in the infrared (IR) spectra by FTIR or Raman spectroscopy can be used to detect conformational changes of PEDOT chains and secondary doping mechanisms.

> The conductivity of crosslinked PEDOT:PSS can be further enhanced addition of ethylene glycol and trichloroacetic acid and post-treatment with methanol.

To use the PEDOT:PSS films for cell culture, these will have to be exposed to the culture medium, a water-based solution. As PEDOT:PSS is hydrossoluble, further modification has to be made in order to guarantee stability of the films in this aqueous environment. The modification used in this work is the addition of a crosslinking agent – glycidoxypropyltrimethoxysilane (GOPS)[74,124]. As so, further modifications were made on PEDOT:PSS with GOPS – designated as crosslinked PEDOT:PSS - by sequentialy testing the addition of 10 v/v% EG, TCAA and post-treatment with MeOH. The following combinations were tested: addition of EG (10 v/v%), with and without post-treatment with MeOH; addition of EG(10 v/v%) and TCAA, with and without post-treatment with MeOH.

Table 7. Calculated resistance, resistivity and conductivity values for the different combinations. Relative conductivity is measured as the ratio between conductivity of each film and conductivity of crosslinked PEDOT:PSS (PEDOT:PSS with the crosslinker GOPS).

	PEDOT:PSS	Crosslinked PEDOT:PSS	Crosslinked PEDOT:PSS + EG (10 v/v%)		Crosslinked PEDOT:PSS + EG (10 v/v%) + TCAA	
			Pristine	Post-treat. MeOH	Pristine	Post-treat. MeOH
R (Ω)	7.981E+06	9.32E+06	1.47E+04	1.115E+04	7.008E+03	1.407E+04
Width (cm)	1.005	1.025	1.025	1.035	0.965	1.030
Thickness (nm)	48	64	31	34	62	25
Section Area (cm^2)	4.8E-06	6.5E-06	3.2E-06	3.5E-06	6.0E-06	2.6E-06
Distance (cm)	0.035	0.035	0.035	0.035	0.035	0.035
Resistivity (Ω.cm)	1.1E+03	1.7E+03	1.3	1.1	1.2	1.0
Conductivity (S/cm)	9.1E-04	5.8E-04	0.8	0.9	0.8	1.0
Relative Conductivity		1.0	1.3E+03	1.5E+03	1.4E+03	1.7E+03

Observing both Table 7 and Figure 20, we conclude that the conductivity of crosslinked PEDOT:PSS has a 10^3-fold increase with the addition of EG, in agreement with previous results. Further addition of TCAA and post-treatment with MeOH increases conductivity, although the increase is small.

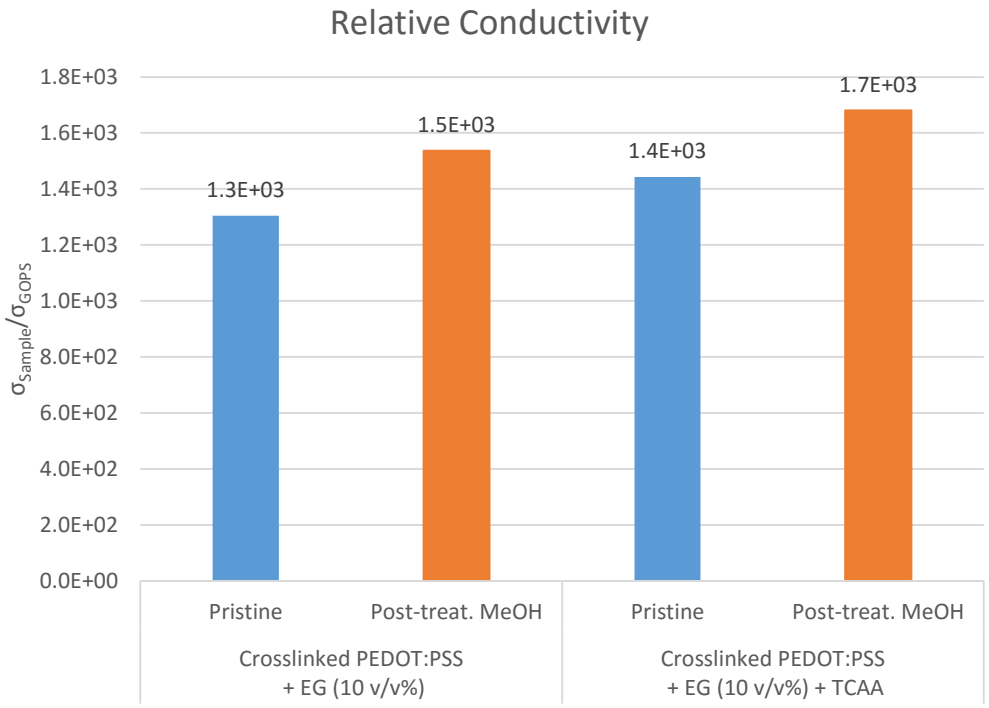

Figure 20. Relative electrical conductivity for the different PEDOT:PSS substrates, measured as the ratio between conductivity of each substrate and conductivity of crosslinked PEDOT:PSS (PEDOT:PSS with the crosslinker GOPS).

However, for scaffold development, as the PEDOT:PSS solution is deposited on PEGDA, it was chosen not to include a post-treatment step, as it would involve dipping PEGDA substrates in MeOH, which would lead to absorption of MeOH by PEGDA that could be released later during cell culture – even with a drying step, there could be some residual MeOH within the PEGDA matrix. Therefore, a solution of crosslinked PEDOT:PSS with 10 v/v% EG and TCAA was chosen for inkjet-printing.

> Besides conductivity enhancement, improvement in optical transmittance can also be achieved when organic solvents are used as additives or upon substrate post-treatment.

Transparency of the several PEDOT:PSS substrates was assessed by taking the UV-Vis absorption spectra and calculating optical transmittance spectra (Figure 21). There iss an increase in transmittance across the whole visible range on most modified PEDOT:PSS films when compared to control, as shown in Figure 21. This biggest improvement came from organic solvents EG and MeOH, either by addition to PEDOT:PSS solution or by film post-treatment. However, surfactant treatment with PEG showed to slightly decrease transmittance – this may be due to poorer film homogeneity when analysed on the profiler, relatively to the other samples, causing light scattering.

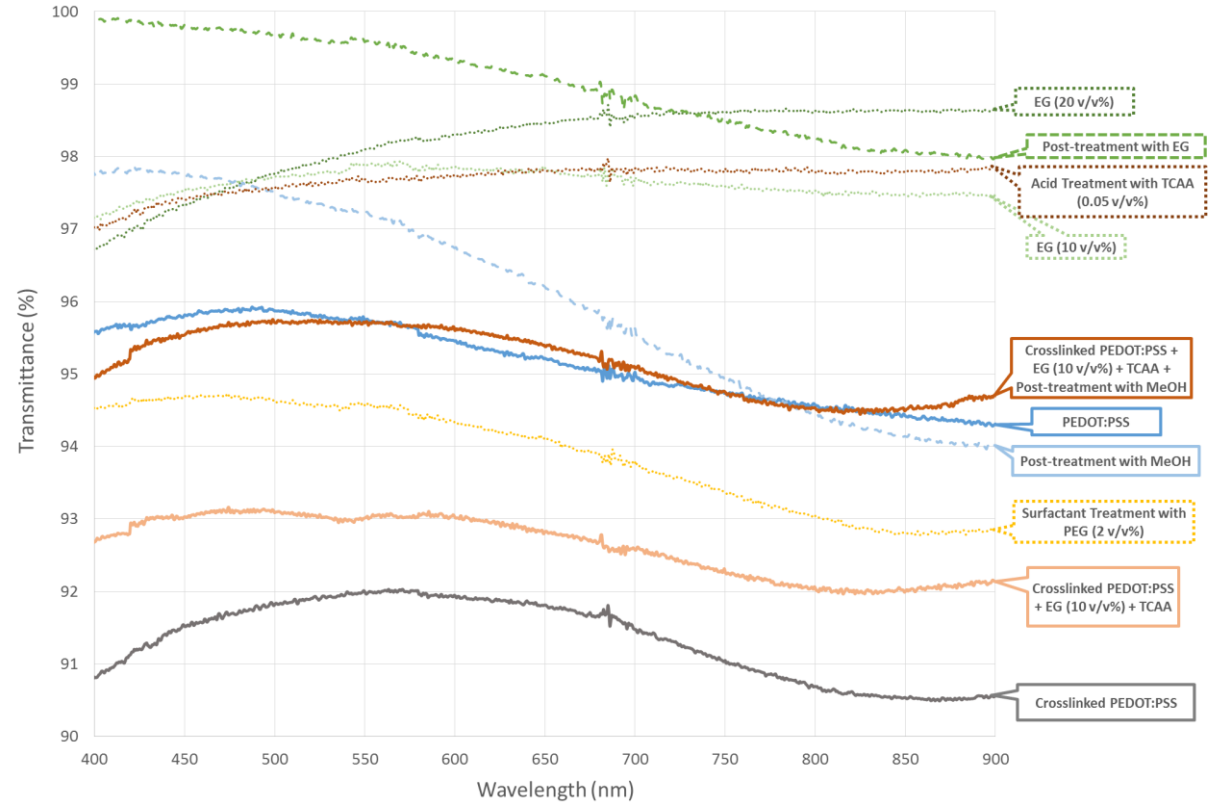

Figure 21. Optical transmittance of the various PEDOT:PSS films.

The transmittance of crosslinked PEDOT:PSS is significantly lower for the whole range when compared to pristine PEDOT:PSS. This could be increased when 10 v/v% EG and TCAA were added, and further improved by post-treatment with MeOH – interestingly, the spectra for the crosslinked PEDOT:PSS to which EG and TCAA have been added and post-treated with MeOH are virtually the same as the one obtained for pristine PEDOT:PSS films.

II. Scaffold Design and Development

The prototypes developed aimed to establish transparent, electroconductive platforms for cell culture where the effect of electric fields on cell growth and development could be studied. It is intended to study the effect of electric fields on NSC expansion, morphological changes and differentiation. In this section, we assess the viability of using the explored materials and techniques for the intended biotechnological application by comparing the constructed scaffolds with the intended design characteristics, while identifying benefits and limitations of using said materials or techniques. A focus will be made on three aspects: transparency and overall visualization of cells; scaffold electrical conductivity and wettability.

A. 3D-Printed Scaffold using Commercial Filaments

The first prototype – PET/cPLA scaffold – refers to the fabrication of a scaffold by FDM using two commercial filaments: the transparent PET and conductive PLA (cPLA). There were two main goals in this methodology: to show the versatility of AM techniques in the development of polymeric scaffolds for tissue engineering strategies; and to validate the use, in biotechnological research, of publicly-available additive manufacturing

resources, like the commercial 3D printer and filaments, which are easy to use and less expensive than systems specially developed for working at the microscale.

The FDM machine used in this work is not appropriate to print features with sizes below 1 mm for applications needing accurate feature size.

Scaffold design and printed result are shown in Figure 22.A and B, respectively.

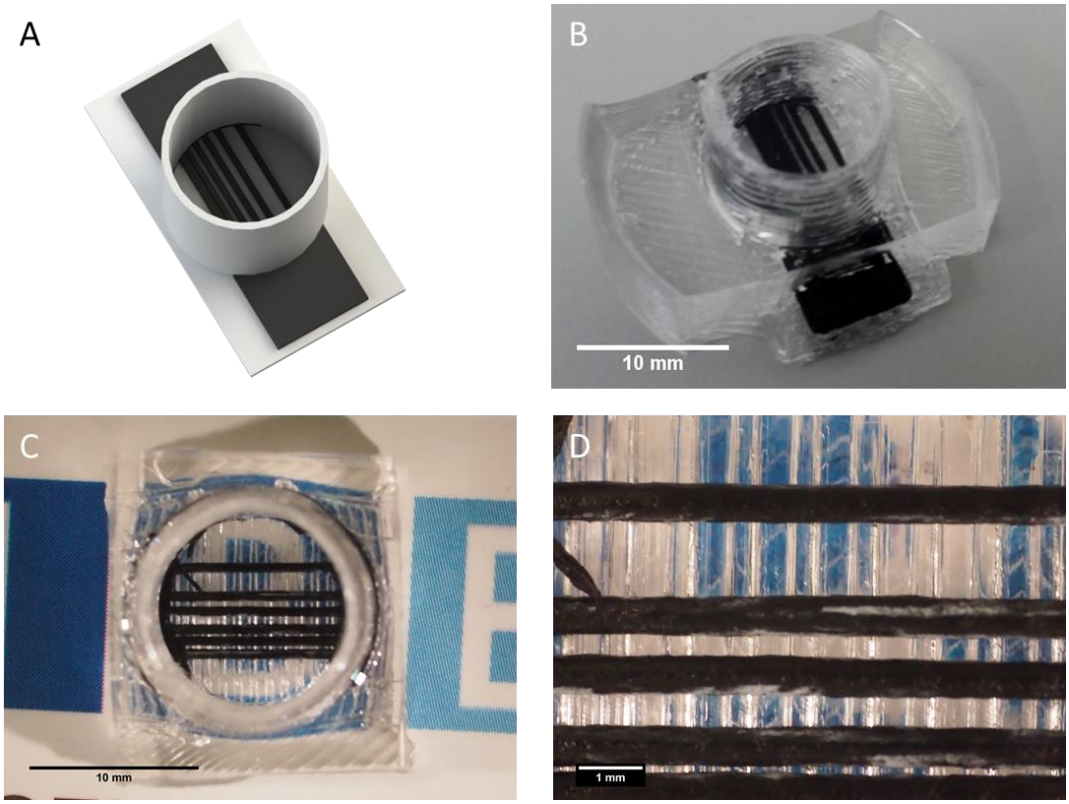

Figure 22. 3D-printed PET/cPLA scaffold: (A) CAD model in SolidWorks; (B) printed result (scale bar at 10 mm); (C) shows the PET transparency (scale bar at 10 mm); (D) gap separation between cPLA filaments (scale bar at 1 mm).

As can be observed macroscopically, the result is very similar to the design. However, when scaffolds were observed in a stereomicroscope, it was possible to observe that gap separation between cPLA filaments on the extruded scaffolds had different sizes than the ones projected on the design. Also, when several scaffolds were extruded, it was observed that gap size between cPLA filaments was not constant through scaffolds – as an example, it is possible to observe in Table 8 the design-scaffold and scaffold-scaffold disparities between two extruded scaffolds.

Table 8. Gap sizes and filament width between 3 different scaffolds, compared to design specifications.

	Design	Scaffold 1	Scaffold 2
Gap Size (µm)	**200**	Closed gap	63.4
	300	243.4	276.4
	400	271.8	231.8
	500	396.6	438.6
	1000	713.4	728.4
Filament width (µm)	**400**	410.7	387.8

It is possible to observe that gap size is roughly 100 µm smaller than the intended value for most cases for both scaffolds, and values are slightly different between the scaffolds for the same gap. In scaffold 1, the smaller gap was actually inexistent, as the two filaments were fused. Filament width is relatively close to the design value.

For the scaffold design with cPLA curves, the same phenomenon can be observed for the gaps on the vertical filaments (Figure 23), where gap sizes were 200 µm when the design had 400 µm. For the horizontal section, the gap size actually increased about 100 µm, as the result had about 500 µm when compared to the projected 400 µm.

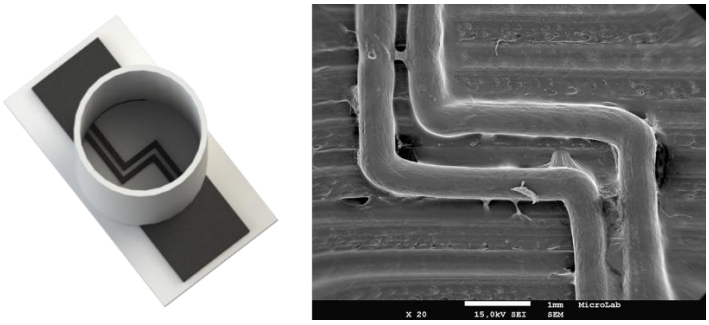

Figure 23. 3D-printed PET/cPLA scaffold with curves: Design in SolidWorks (left); printed result, shown in SEM (scale at 1 mm, right).

Polymers undergo thermal expansion upon heating at the extruder nozzle, and start to contract when they cool as soon as they are deposited on the platform. Intuitively, one is lead to think that the cPLA filaments would shrink and create wider gaps between them – this is the case for the horizontal gap on the scaffold with cPLA curves, but not for the other ones, as the gaps are smaller by 100 µm than the design values, while filament width maintains just a difference of about 20 µm with respect to the design value.

These design-scaffold disparities, namely smaller-than-design gaps and the fact that shrinkage is not observed on the same proportion in filament width is probably because extra polymer is being extruded by the nozzle. This could be due to inadequate printing settings, namely the speed at which the plastic is extruded could be too high, or could be due to the precision of the machine used, as these details are the same size or smaller than the nozzle diameter (Table 1). Also, this could be due to the diameter of the commercial filament. The printer filaments usually have a tolerance associated to its diameter – for cPLA, it is 3%, which means that filament diameter is 1.75 ± 0.0525 mm[149]. When extruding the filament, this error will approximately duplicate that of the extruded filament[161], which may contribute to increase the width and thus counteract thermal contraction.

Overall, these differences in detail size show that the machine used is not appropriate to print features with sizes below 1 mm for applications needing accurate feature size, as this becomes similar to the dimensions of the variations caused by thermal expansion/contraction and extruding errors. Higher-resolution machines that can print smaller features and work with biocompatible materials exist and should be used for applications similar to those addressed in this work.

The transparency of PET is limited by the printing technology.

In terms of transparency, the subjacent PET base is relatively transparent as shown in Figure 22.C and D. However one can observe the “wavy” surface that is a result of the printing process itself, as several cylindrical filaments are extruded during printing and fused together during cooling. This PET surface pattern limits cell visualization, as it is only possible to focus on cells at the same height. As shown in Figure 24.A, this window of visualization is only around 50 µm, while the filament has a diameter of 400 µm. This window of visualization is probably situated on top of the filament as represented in Figure 24.C, where the material surface is practically flat, which leads to minimal deflection of light rays and number of internal reflections, thus higher transmittance. Also, when cells were seeded on scaffolds, it was possible to see that it was not even possible to focus on cells in some areas, most likely due to the scattering of light on the material. This scattering can be caused by internal reflections on the cylindrical threads, which result in these “dark” spots where it is impossible to focus.

Furthermore, irregularities on the extruded filament, both at the surface or inside the filament, can lead to scattering – in fact, as can be observed in images taken on the SEM (Figure 24.B), the PET substrate presented some concave indents on the surface that could interfere with the trajectory of the light rays.

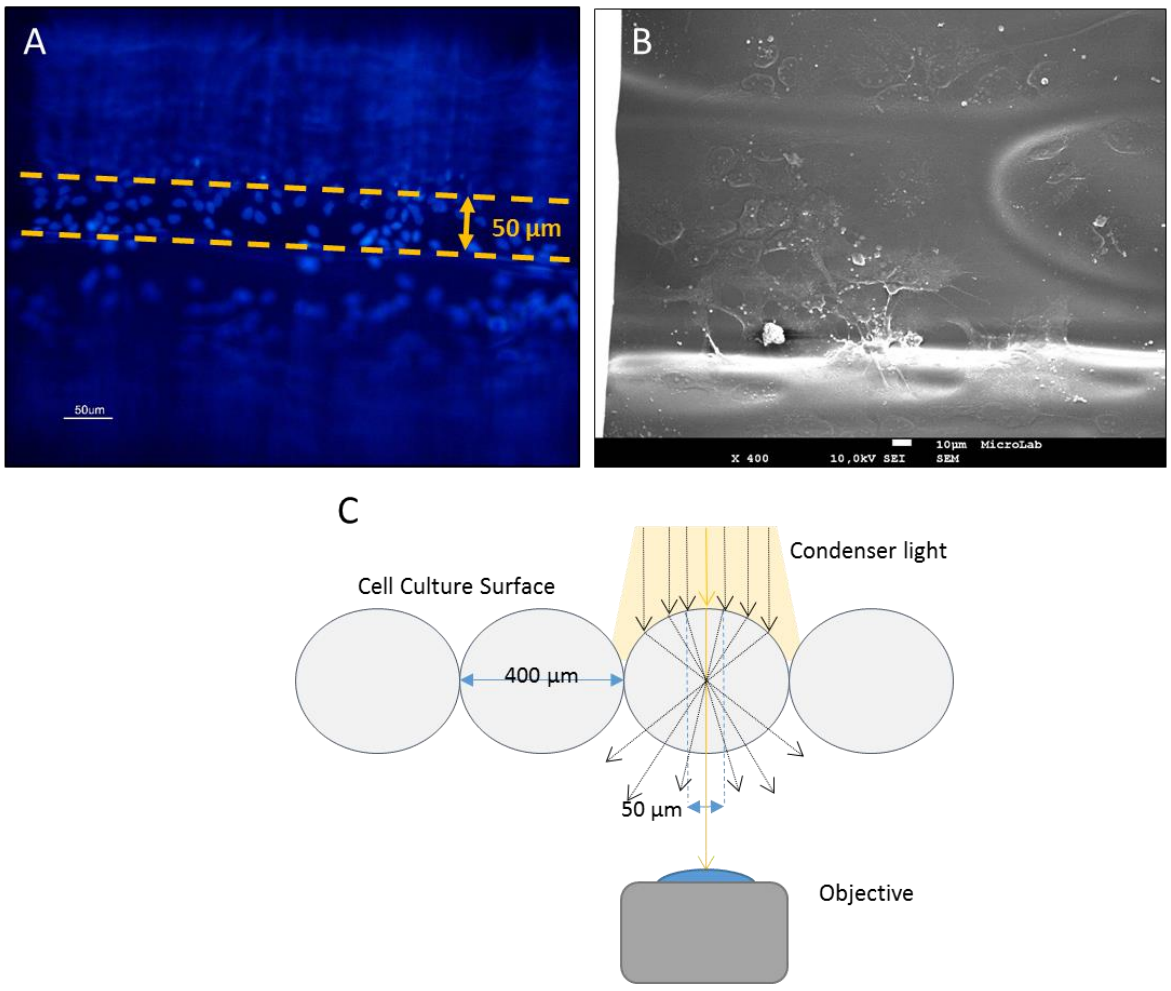

Figure 24. Cell Visualization on PET filaments: (A) FM image of cell nuclei stained with DAPI (scale bar at 50 µm) – it is possible to see a window of about 50 µm width where cells are in focus; (B) SEM image, where cells and the topography of PET filaments

can be seen (right, scale bar at 10 µm); (C) the window of visualization corresponds to the region where there are less internal reflections of light rays, thus it is possible to focus on the transmitted light in the inverted optical microscope and observe cells.

The scattering of light severely impaired the quality of the fluorescence microscopy images taken, as it lead to an increase in intensity on the background light which difficult visualization of the cell structures marked by the probes, especially in red and green-fluorescent images. Also, with these scaffolds, care should be taken on analysing morphological changes or cell alignment, as these could be a result of the topography created on the cell culture surface with this wavy PET pattern. Although this characteristic pattern on surfaces resulting from extrusion of cylindrical threads can be a burden for the intended study, is very useful for studies involving the influence of topography on cell culture and to develop scaffolds with topographical cues for cell orientation and development.

To obtain better images, confocal microscopy should be performed on these substrates in order to eliminate the scattered light, as it eliminates out-of-focus light, and permits to reconstruct a 3D visualization of the several planes created by the PET pattern. Also, a more simple system, where cPLA filaments are extruded onto a clear, smooth substrate (as in a well-plate or a Petri dish) could be used to conduct the NSC experiments described in this work to validate the use of cPLA as a means to convey an electrical field to cells and study its effect, obtaining clear images while reducing any topography effect.

The conductivity of cPLA is fit for the intended application.

The resistivity/conductivity of cPLA was measured before extrusion, in a piece of filament, and after extrusion in a cylindrical feature (Table 9 and Figure 25). The resistivity values obtained are very similar to the ones reported by the manufacturer[149] – 15 and 30 Ω.cm before and after extrusion, respectively – and, as expected[149], the conductivity drops to almost half after printing.

Rearrangement of the conductive carbon-black aggregates present in PLA occurs during extrusion. Upon heating in the nozzle and quick cooling at the platform, it is possible that aggregates of smaller dimensions are formed when compared to the ones obtained during the fabrication of the commercial filaments. In fact, spherulite growth rate in PLA/carbon black blends is very low at the temperature used for solidification of the extruded filaments (70ºC)[162]. These hypothesized smaller aggregates will lead to the increase in particle boundaries in a given volume, increasing the energy barrier for charge transportation between aggregates, thus decreasing conductivity. The reduction of aggregate size after extrusion requires evidence, which can be obtained upon AFM analysis of topographic and phase images of planar cPLA substrates with AFM.

Table 9. Conductivity of cPLA, before and after extrusion.

	Before Extrusion (Filament)	After Extrusion (3DP Feature)
R (Ω)	26.59	127.10
Radius (cm)	0.085	0.165
Section Area (cm^2)	0.023	0.008
Distance (cm)	0.035	0.035
Resistivity (Ω.cm)	17.24	29.95
Conductivity (S/cm)	0.06	0.03
Relative Conductivity	1.00	0.58

The conductivity value of 0.03 S/cm obtained is adequate for the intended purpose, as it is 300 times higher than the established minimum value (10^{-4} S/cm). The scaffolds, however, showed resistance values on the order of 1 kΩ when measured at a distance of 1 cm. This value is still acceptable, as one can deliver a current as high as 1 mA given the electric field limit of 1 V/cm.

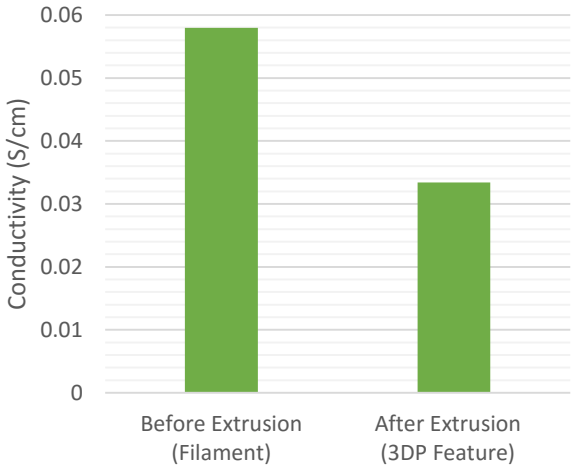

Figure 25. Conductivity of cPLA, before and after extrusion.

B. Hydrogel- and Conductive Polymer-based Scaffold

IJP is a useful technique to print motifs with sizes on the order of 10 µm, but several aspects of the IJP process that affect printing quality and resolution have to be taken into account.

A comparison between the PEDOT:PSS design and the inkjet-printed feature is shown in Figure 26.

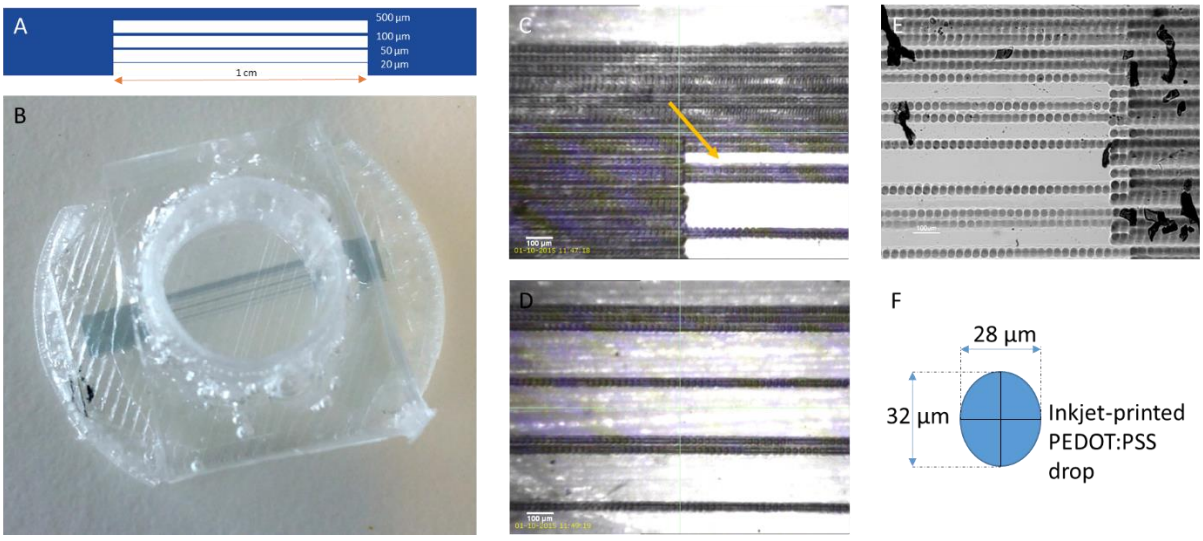

Figure 26. PEGDA/PEDOT:PSS Scaffold: (A) Design of the IJP PEDOT:PSS film; (B) Scaffold with printed PEDOT:PSS (blue) on top of transparent PEGDA – a 3DP medium container was glued on top and covered around with PDMS to enclose the medium and separate the internal cell culture area from the external PEDOT:PSS electrodes (scale bar at 10 mm); (C) and (D) show IJP features taken with the inbuilt DMP camera – the yellow arrow on C shows a region lacking PEDOT:PSS due to nozzle failure during printing (scale bar at 100 µm); (E) IJP feature taken with the Optical Microscope, were it is possible to distinguish printed drops (scale bar at 100 µm); (F) Average size of the inkjet-printed PEDOT:PSS drops.

Figure 26.C, D and E show the printing process of IJP as drops can be discriminated. Printed features measured on scaffold images showed different sizes than the designed specifications – for example, one scaffold resulted in bands with widths of 450, 143, 74 and 36 µm, when compared to the design sizes of, respectively, 500, 100, 50 and 10 µm. These differences are due to the ink drop size, which ultimately affects printing resolution and the size of the printed features. In view of the average size of drops shown in Figure 26.F, which sets the size of the smallest feature (around 30 µm), the band widths are approximately multiples of this value, as the bands are printed as several parallel lines of ink. Nevertheless, opposite to what happened in 3DP, the results are more reproducible in IJP, as several printed PEDOT:PSS designs had essentially the same feature sizes. Therefore, to print features of the same sizes as in the design, the ink drop size should be reduced.

The size of ink drops on the substrate, and thus printing resolution and minimum feature size, is dependent on several factors, such as: fluid viscosity; the speed at which the ink material dries; surface interaction between the ink material and the substrate material; and voltage function used in the piezoelectric nozzle to mold the shape of the ink drop. If one desires to obtain larger dots, one could increase hydrophilicity of the PEGDA substrate by O_2-plasma treatment to increase the spreading of the drop on the substrate surface; if higher resolution is desired, it is a good strategy to decrease this spreading through, for example, increased viscosity, or faster ink drying; the latter could be done by the inbuilt printer function of platform heating.

In IJP applications, it is always much simpler to modify the variables at the substrate lever, such as modifying surface groups at the substrate for higher or lower affinity to ink, influencing ink spreading, or speeding up the drying of the ink with platform heating, than modifying parameters that affect the shape of the drop deposited, such as viscosity and piezoelectric voltage function. One could also create, by lithographic techniques such as soft lithography, a PEGDA substrate with “valley” features with a desired size to confine PEDOT:PSS ink and prevent its spreading.

When looking at the edges of the printed feature, we observe the superposition of different layers of ink (Figure 26.C, D and E). It is important to note that film thickness is not additive, that is, it is not the direct sum of the thickness values of each layers because new layer are not printed directly above the previous ones. This presents a problem if one wants to estimate how many layers should be printed in order to obtain films with a desired thickness.

It is common to see printing “gaps”, that is, absence of ink deposition, like the one indicated by the yellow arrow iFigure 26.C. This is due to malfunctioning of the nozzle attributed to that printing area. The most probable reason is drying of PEDOT:PSS on the nozzle, or accumulation of micro aggregates present in the solution, which clog the nozzle. This phenomenon justifies the need to filter the solution before injecting it in the cartridge. Also, its frequency is diminished thanks to the cleaning cycles, which will pause the printing, move the cartridge to a blotter, and “purge” the cartridge, that is, force the liquid to come out of the nozzles, which clears up the accumulated debris in most cases. Nonetheless, this common occurrence is a severe problem when huge importance is taken into feature size, such as in this case with the width of PEDOT:PSS strips.

Pure PEGDA substrates have an adequate transparency for cell visualization, but its hydrogel behaviour presents as a challenge for its use as platform for microscopy.

As it is observable in **Error! Reference source not found.**, the pure PEGDA substrate is practically transparent, as t is possible to focus on cells and the PEDOT:PSS ink dots.

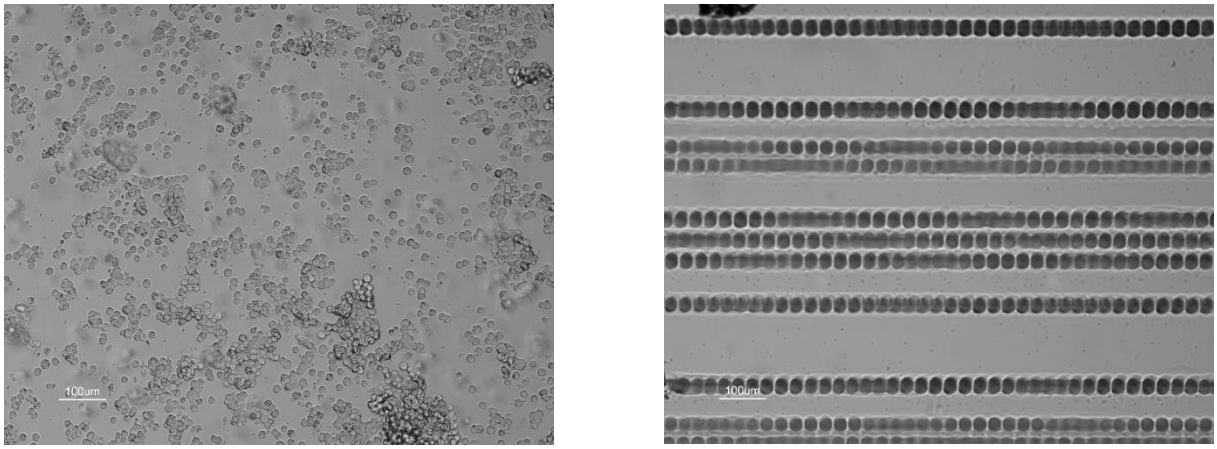

Figure 27. PEGDA substrate showing good cell (left) and Inkjet-printed PEDOT:PSS (right) visualization on the optical microscope (scale bars at 100 µm).

Unfortunately, neither bright field nor fluorescence images were obtained during an expansion protocol on these scaffolds. The problem is related with the bending of the PEGDA substrate in the region designated for cell culture and visualization (**Error! Reference source not found.**). This bending is due to PEGDA swelling after introducing iquid on the cell culture area. Since all available microscopes were inverted, this increased the distance to the objective located below the scaffolds, and prevented any visualization of the cells or the PEDOT:PSS ink.

Figure 28. After wetting the PEGDA/PEDOT:PSS scaffolds, PEGDA swelling caused the region for cell culture (and thus visualization) to bend.

Due to time constrictions, all succeeding experiments with cells were performed on the two variations of the PET/cPLA scaffold. Nonetheless, a simple solution to this problem would be to first soak the substrate with PBS, then creating a medium container from PDMS placed above the substrate, around the area designed for cell culture.

The UV-crosslinked PEGDA presents itself with very good transparency, appropriate to both optical and fluorescence microscopy. However, the material is very stiff and brittle, which makes it difficult to handle, and inappropriate to be used for development of grafts for the CNS, as it will not recreate the physiological mechanical properties of the surrounding tissue. This dictates the need to explore methods to change the mechanical properties of PEGDA, as addressed below in this work. As a consequence, to use a similar system where a softer hydrogel is coated with PEDOT:PSS, there is the need to develop flexible PEDOT:PSS films, as explained below.

The Conductivity of Inkjet-printed PEDOT:PSS is adequate for the intended application.

As shown in Table 9 and Table 10, the conductivity values of cPLA are lower than those obtained with the modified solution of PEDOT:PSS, which is understandable given that cPLA is a blend of pure non-conductive PLA and carbon-based materials, such as graphene. This would lead to the wrong assumption that PET/cPLA scaffolds were less conductive than the PEGDA/PEDOT:PSS ones; however, in practice the first scaffold is created with extruded cPLA filaments, while the latter will have only an inkjet-printed thin PEDOT layer with a thickness in the range of 10-100 µm. Therefore, for the same length of material, the cPLA will have a larger section area, and thus smaller resistance when compared to the PEDOT:PSS film. This is proven by the typical resistance values obtained with scaffolds: the cPLA ones have values on the order of 1 kΩ, while the PEDOT:PSS ones are around 1 MΩ, both measured at a distance of 1 cm.

Table 10. Conductivity of the pristine PEDOT:PSS and the PEDOT:PSS solution used in IJP.

	PEDOT:PSS	Crosslinked PEDOT:PSS + EG (10 v/v%) + TCAA
R (Ω)	7.981E+06	7.008E+03
Width (cm)	1.005	0.965
Thickness (nm)	48	62
Section Area (cm^2)	4.8E-06	6.0E-06
Distance (cm)	0.035	0.035
Resistivity (Ω.cm)	1.1E+03	1.2
Conductivity (S/cm)	9.1E-04	0.8
Relative Conductivity		1.4E+03

The high resistance of PEDOT:PSS scaffolds could be caused by the separation of PEDOT:PSS ink drops as visible in Figure 27, which increases the energy barrier for charge transportation along the film. Also, similarly to the cPLA, the impedance between the silver glue and the PEDOT:PSS film can lead to an increase of the resistivity of the scaffold. In both cases, this could be improved by coating the cPLA or PEDOT:PSS electrodes, that is, outside the area of cell culture, with a thin layer of thermal evaporated gold, as made in the procedure of the conductivity determination.

Although not assessed in this work, there is an obvious need to further study the influence of the modifiers added to PEDOT:PSS on cell viability and attachment to the created films, especially concerning the use of TCAA. The processing steps of PEDOT:PSS can have a huge impact on the toxicity of the resulting films. However, placing the modified PEDOT:PSS films under vacuum with heating can reduce their toxic agents content.

PEDOT:PSS films were stable under an aqueous environment for as long as two weeks when crosslinked.

To determine the stability of the films for the duration of the cell experiments, which have a maximum of 12 days, IJP films of PEDOT:PSS on PEGDA were crosslinked at 150°C for 0, 1, 2, 5 and 10 minutes, and left under PBS for two weeks, with the electrical resistance measured weekly. It was shown that the resistance was practically the same after two weeks, and 1 minute of crosslinking was enough to create stable films. On the other hand, the film that suffered no crosslinking was unstable, as it quickly detached from the PEGDA substrate; it is however interesting to notice that the whole film detached from PEGDA without breaking apart – this could be envisaged as a transfer printing technique for PEDOT:PSS, where thin films are printed on a substrate and then transferred to other substrate that may not be suitable to be used directly in the printer.

Further studies need to be carried out on PEDOT:PSS flexibility and on the influence of mechanical stress on its electrical resistance.

Since substrates made of pure UV-crosslinked PEGDA did not show significant change in volume during swelling, the integrity of PEDOT:PSS was not compromised, maintaining their electrical resistance. In order to establish the viability of using PEDOT-coated PEGDA hydrogels, especially on more flexible, viscoelastic PEGDA hydrogels, methods should be explored to increase the flexibility of PEDOT:PSS films. One of the strategies that could be employed to solve this problem is the addition of plasticizers to PEDOT:PSS, similarly to the modifications made

on the mechanical properties of PEGDA in this work, as described below. These modifications should be assessed by measuring the mechanical properties of PEDOT:PSS, especially ductility and resistance variation of PEDOT:PSS films with bending by performing inner and outer bending reliability tests, as well as fatigue tests[163,164].

C. Scaffold Material Wettability

Wettability was assessed for the materials used for both scaffolds – PET, cPLA, PEGDA and PEDOT:PSS – either with or without laminin coating. The results are shown in Table 11 and Figure 29

Table 11. Contact angle for the materials used for scaffold manufacturing, pristine and laminin-coated. PEDOT:PSS contact angles were measured on IJP printed feature, both on PEGDA and glass substrate.

Material	Pristine Material	Laminin-Coated Material
PET	100.56 ± 4.92	87.08 ± 3.70
cPLA	102.71 ± 7.07	87.69 ± 11.98
PEGDA	56.79 ± 3.11	62.55 ± 2.01
Glass	62.64 ± 2.07	75.09 ± 3.66
PEDOT:PSS on PEGDA	67.20 ± 9.58	80.60 ± 16.71
PEDOT:PSS on Glass	55.41 ± 2.20	71.40 ± 8.83

Looking at pristine materials, as expected, PET and cPLA present higher contact angles, thus being more hydrophobic, while PEGDA, PEDOT:PSS and glass, showed lower contact angles, therefore being more hydrophilic. For the laminin-coated materials, PET and cPLA also present higher contact angles than PEGDA, PEDOT:PSS and glass.

In the work by Hernández *et al.*, AFM phase images were shown to be a viable method to study the conformation of adsorbed proteins on material's surface, as opposed to topographic images, since surface roughness on most substrates are on the same order of magnitude as the adsorbed protein[165]. It was shown through phase AFM that laminin conformation depend greatly on the presence of polar groups on the surface of materials, thus on their hydrophilicity – less density of polar groups generally leads to a more extended conformation of laminin.

In view of this evidence, it is suggested that differences in weak interaction forces (electrostatic, van der Waals and hydrogen bonding) between laminin and materials with different surface wettability play an important role on Laminin coating, affecting its conformation and the wettability of coated materials. Phase AFM should be performed on these materials to assess adhesion and conformation of laminin on the surface, as these have a huge impact on the binding between laminin and cell receptors, namely integrins, thus affecting cell attachment onto the scaffolds. This data can then be correlated with the contact angles obtained in order to understand how the attachment, conformation and spreading of laminin influence its wettability.

Here, Glass and PEDOT:PSS-coated glass were also included in order to compare the effect between PEGDA and another known hydrophilic material on the wettability of PEDOT:PSS films. PEGDA showed a lower contact angle than glass, that is, PEGDA is more hydrophilic than glass, but unexpectedly, the contact angle of PEDOT:PSS on PEGDA was higher than for PEDOT:PSS on glass. The weak interaction forces established between PEDOT:PSS

and the substrate could explain why contact angle on PEDOT:PSS-coated PEGDA is higher than PEDOT:PSS-coated glass: more polar regions of PEDOT:PSS will interact with the more hydrophilic material – PEGDA – to create adhesive forces, thus presenting less polar regions and more non-polar ones to the water drop on the surface, increasing surface tension and contact angle.

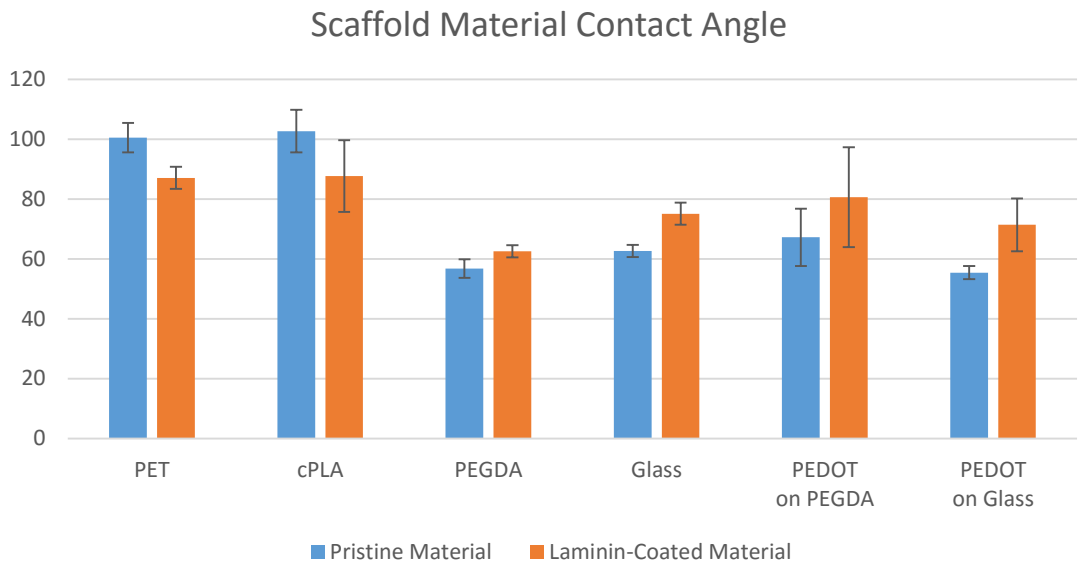

Figure 29. Contact angle for the materials used for scaffold manufacturing, pristine and Laminin-coated.

III. Electric Field Effect on NSC Culture

In this part of the work, the main goal was to establish the scaffolds as viable platforms to study the effect of electric fields on NSCs. For that purpose, proof-of-concept studies were developed to explore the expansion and differentiation of NSCs when an electric field is applied to the culture – in particular, it was intended to explore morphological changes and cell alignment induced by an electric field during expansion, and to assess its influence on the commitment of stem cells to either a neural or astrocyte pathway during differentiation.

An overview of all the experiments realized in this work are shown in Table 12. In this section, the results will be explored in terms of NSC expansion and differentiation: in expansion, results in terms morphological changes and cell alignment on some experiments will be detailed, as well as failures on cell visualization or in quantification in others; in differentiation, a qualitative analysis will be made on the FM images.

Table 12. Experiments performed on the several scaffolds developed, with details of the type, duration and settings of experiments, as well as information about the fluorescence staining used.

Scaffold	Experiment	Duration	Scaff. Resistance	Current Applied	FM Staining
PEGDA/PEDOT:PSS	Expansion	4 days	2.6 MΩ	0.385 µA	Calcein AM/DAPI
PET/cPLA	Expansion	2 days	1 kΩ	300 µA	Phalloidin/DAPI
		4 days	3.5 kΩ	50 µA	Phalloidin/DAPI
	Differentiation	4 days (exp.) + 7 days (diff.)	5 kΩ	50 µA (4-6h rest/day during Diff.)	TuJ1/GFAP/DAPI
PET/cPLA (Curves)	Expansion	4 days	3.34 kΩ	100 µA	Phalloidin/DAPI
	Differentiation	4 days (exp.) + 7 days (diff.)	3.2 kΩ	100 µA (4-6h rest/day during Diff.)	Calcein AM **(day 4)** TuJ1/GFAP/DAPI **(day 12)**

A. Effect of Electric Field on Morphological Changes and Cell Alignment during NSC Expansion.

A total of 5 experiments following an expansion protocol (Figure 30) were realized on the three scaffolds: one on the PEGDA/PEDOT:PSS, two on the PET/cPLA scaffold and two on the PET/cPLA scaffold with curves. NSC morphology and alignment were assessed on the PEGDA/PEDOT:PSS scaffold and on the images of Calcein AM after 4 days expansion of the PET/cPLA with curves. NSC morphology, specifically cell elongation, was assessed according to aspect ratio, while NSC alignment was quantified according to the angle formed between the longest cell axis and the direction of the electric field.

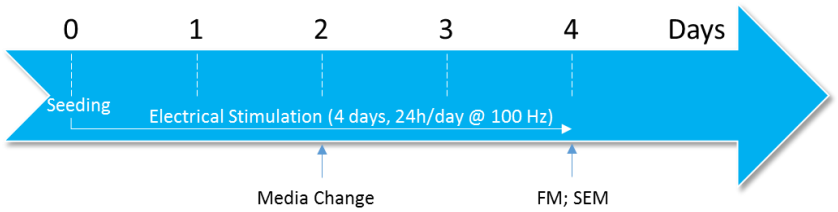

Figure 30. Expansion protocol timeline.

FM images with Phalloidin and DAPI staining showed reasonable visibility of cells, but the poor signal quality of Phalloidin was improper for quantitative analysis of cell morphology and alignment.

In the expansion experiments, Phalloidin was stained together with DAPI mainly to assess the visibility of cells through the PET substrates on PET/cPLA scaffolds. In Figure 31, it is possible to identify some fluorescence images relative to the 4-days expansion experiment on PET/cPLA scaffolds. More pictures of Phalloidin/DAPI staining of the same experiment on PET/cPLA scaffolds with curves are available on Figure S52 of Annex B.

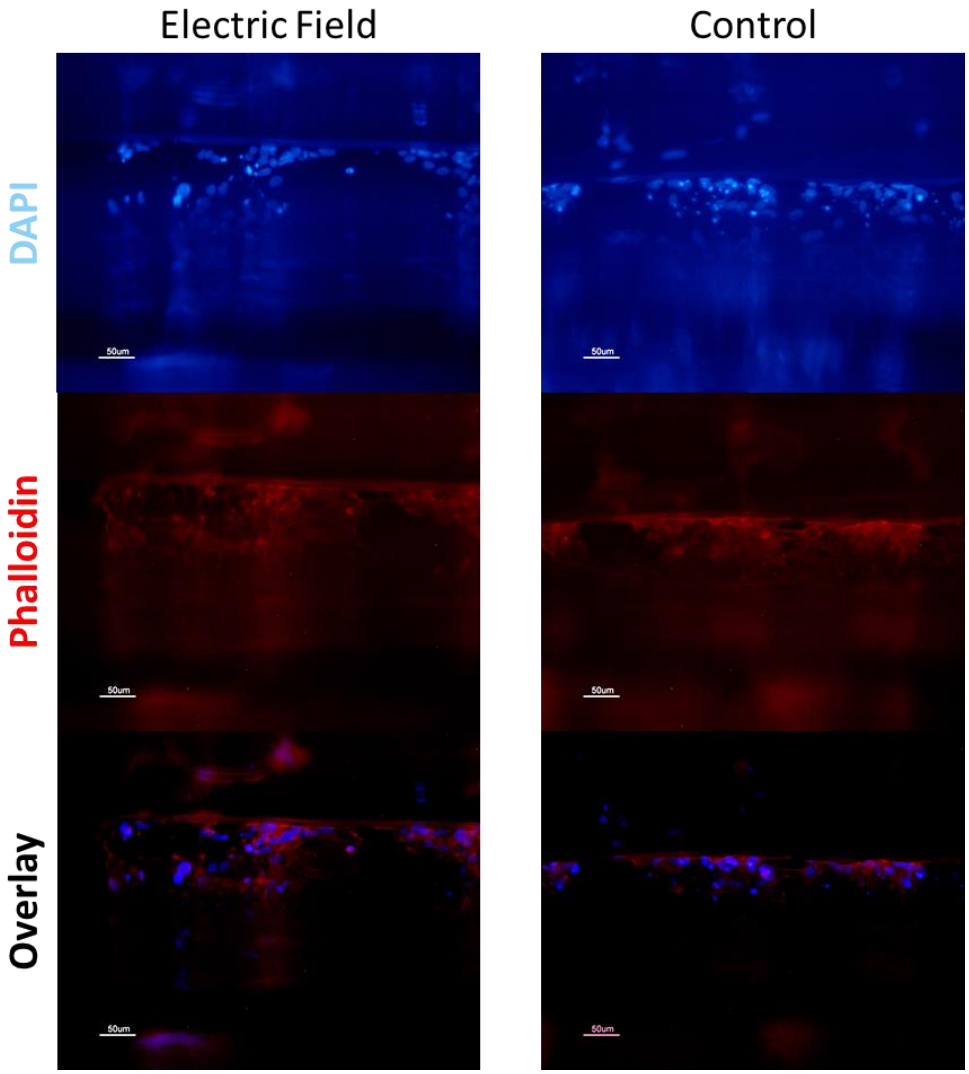

Figure 31. FM Images of DAPI, Phalloidin and their overlay after 4 days of expansion on the PET/cPLA scaffolds, with and without electric field (scale bar at 50 µm).

Although this staining protocol after 4 days expansion shows reasonable visibility of cells through a previously mentioned observation window in PET, the quality of Phalloidin staining is not good enough to perform quantification of cell morphology and alignment, as the resulting fluorescence signal of Phalloidin was weak. The dilution used for Phalloidin was 1:1000 – it is possible that this is too diluted, so in future reiterations of this study the dilution should be optimized by decreasing to, for example, 1:500 or 1:100, which may result in a signal with better quality.

> NSCs on the PEGDA/PEDOT:PSS scaffold showed no preferential cell alignment, but cells were more stretched when an electric field was applied.

As already discussed above in section II of the Results and Discussion chapter, it was not possible to observe cells using optical microscopy nor fluorescence in the PEGDA/PEDOT:PSS scaffolds due to the bending of the substrate. However, SEM images had good quality, so they were used to assess NSC morphology and cell alignment.

The results are discriminated by PEDOT:PSS printed band size, and measurements were made for both conditions (electric field and control) on cells situated on three of the four bands: 500 (wide band), 100 (medium band) and 50 µm (narrow band). The actual sizes of the bands are different as explained in section II, but for simplification purposes they are referenced with the design sizes.

Figure 32 shows SEM images of the three bands for electric field and control samples, as well as the angle histograms for each condition.

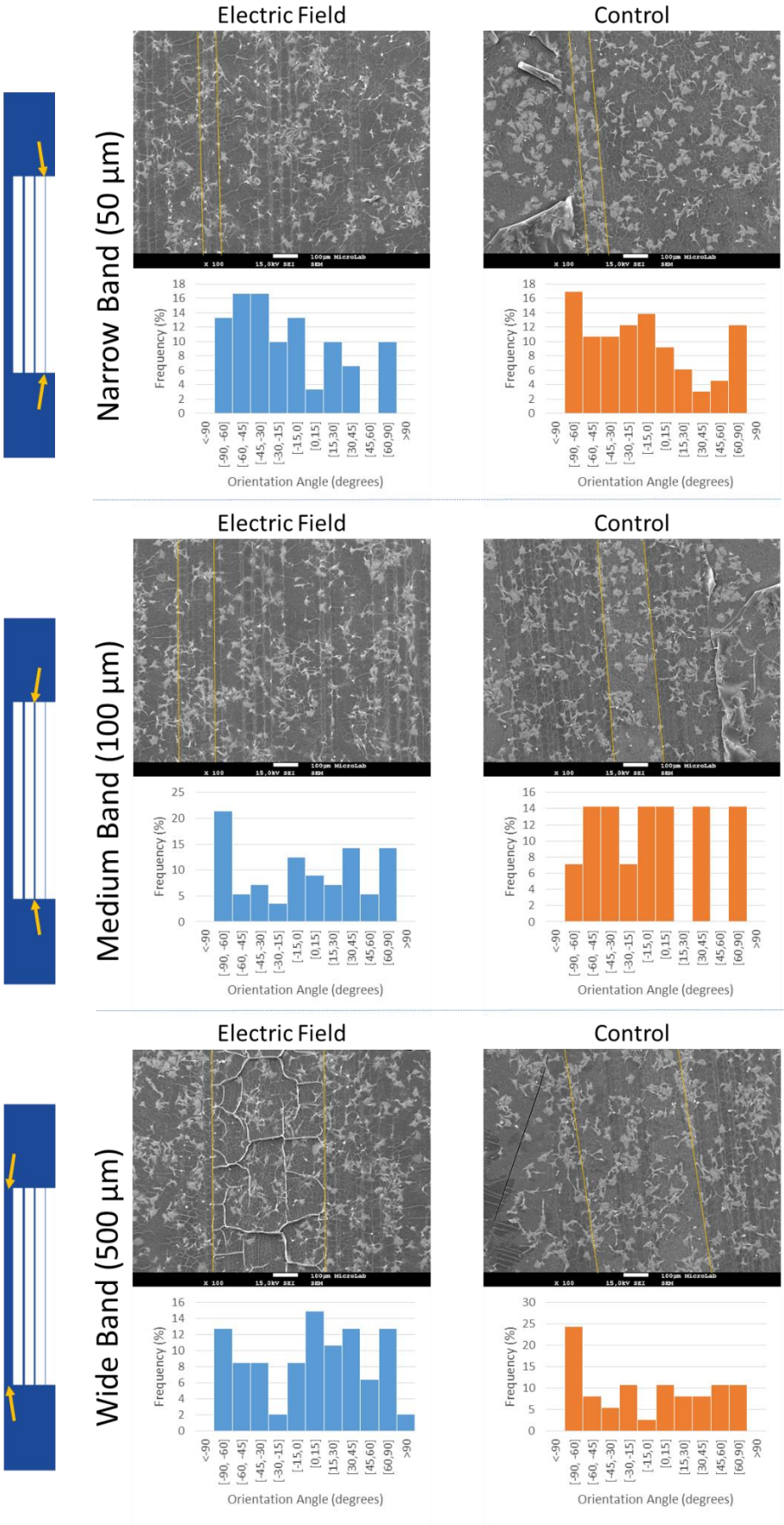

Figure 32. SEM Images (scale bars at 100 µm) and electric field vs. control angle histograms on PEDOT:PSS bands.

It was expected for control that orientation was random, with the histograms representing an uniform distribution across the angle range. This is relatively evident on the histograms for electric field and control conditions on the wide and medium bands. Under electric field, it was expected that cells would be oriented according to the electric field for the three bands, that is, it was expected that angles near 0º were more frequent, with the histogram following a Gaussian curve centred at 0º.

There is, however, a high frequency for orientation angles of 90º for the control condition on the wide band and for the electric field condition on the medium band. A 90º angle indicates a cell alignment perpendicular to the electric field, which may be a result of the surface topography of the PEDOT:PSS band, namely the valleys created between adjacent ink dots. These valleys run both parallel and perpendicular to the orientation of the electric field, so they may also increase the parallel (0º) orientation.

Regarding NSC morphology, the aspect ratios for the cells on different bands and conditions are shown in Figure 33. It is evident that the aspect ratio is higher, that is, cells are more elongated when an electric field is applied, as expected from the literature[72,74]. Also, there seems to be a slight increase in aspect ratio as the band size is increased – this may be due to an increased effect of the electric field on NSCs for wider bands, as the resistance will be lower due to the higher cross section, thus the current that passes them will be higher.

As expected, aspect ratio for control situations is practically the same, except for the wide band. This could be due once again to the topographical cues on the wider PEDOT:PSS band.

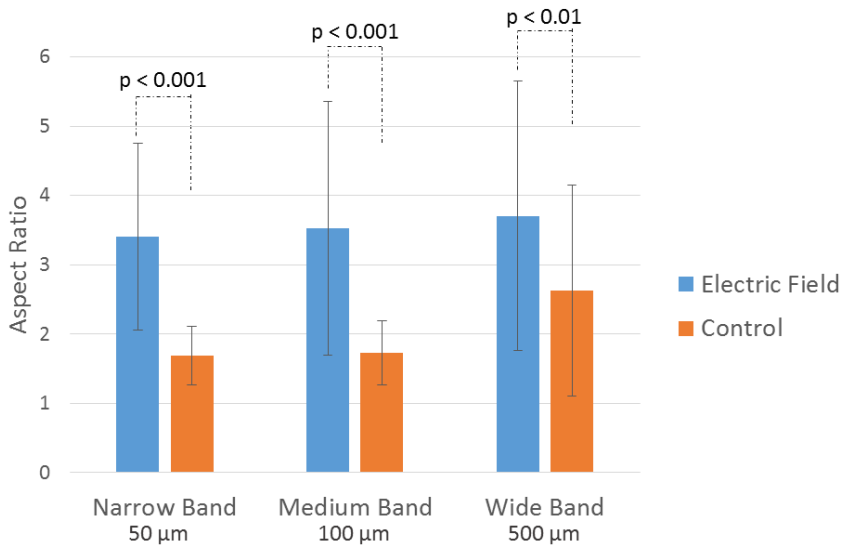

Figure 33. Effect of the electric field on the aspect ratio of NSCs on PEDOT:PSS.

Further studies are needed to assess the electric field-induced cell alignment. Future work on these scaffolds should focus on diminishing the topographic effects on elongation and alignment, in order to have a platform where these variables are only dependent on the electric field applied. There is also the need to study the effective electric field that act on cells; even if the voltage applied was lower than the one that causes electrolysis of water, there is still probably an effect on the culture medium, which is basically an electrolyte. When subjected

to an electric field, this induces ionic currents in the medium that can, for example, alter the pH and influence cell viability.

> NSCs on the PET/cPLA scaffold with curves were more stretched when an electric field was applied and would preferentially align according to the direction of the electric field.

As previously stated, both FM images, obtained with Phalloidin and DAPI, and SEM images for the scaffolds of PET/cPLA with curves were unsuitable for these measurements. However, during the differentiation protocol on these scaffolds, live imaging of cells was performed after 4 days of expansion by staining with Calcein AM, which is a probe commonly used in Live/Dead cell assays[166], and can be used on cells without fixation, allowing them to stay in culture.

In Figure 34, it is possible to observe FM images of the three bands for electric field and control samples, as well as the angle histograms for each condition. These are a superposition of bright field images with fluorescent ones.

For horizontal gaps, there is a Gaussian curve centred at angles near 0^{o} when the electric field was applied, while in the control there was no preferential orientation, as the histogram showed a uniform distribution. This suggests that the orientation is induced by the electric field, but care has to be taken in jumping into such a conclusion, as this is also the orientation of the topography of the PET substrate. There is the need to separate the topographical cues from the electrical ones in cell alignment in future studies.

For vertical gaps, there is a strong evidence for the influence of the electric field on cell orientation, as its application resulted in cell alignment parallel to the electric field, when compared to control, where cells had a tendency to align according to the orientation of the PET substrate topography, that is, perpendicular to the direction of the electric field. However, there is a lack of statistical significance on the histogram for the electric field condition, as a reduced number of cells were observed and their orientation established.

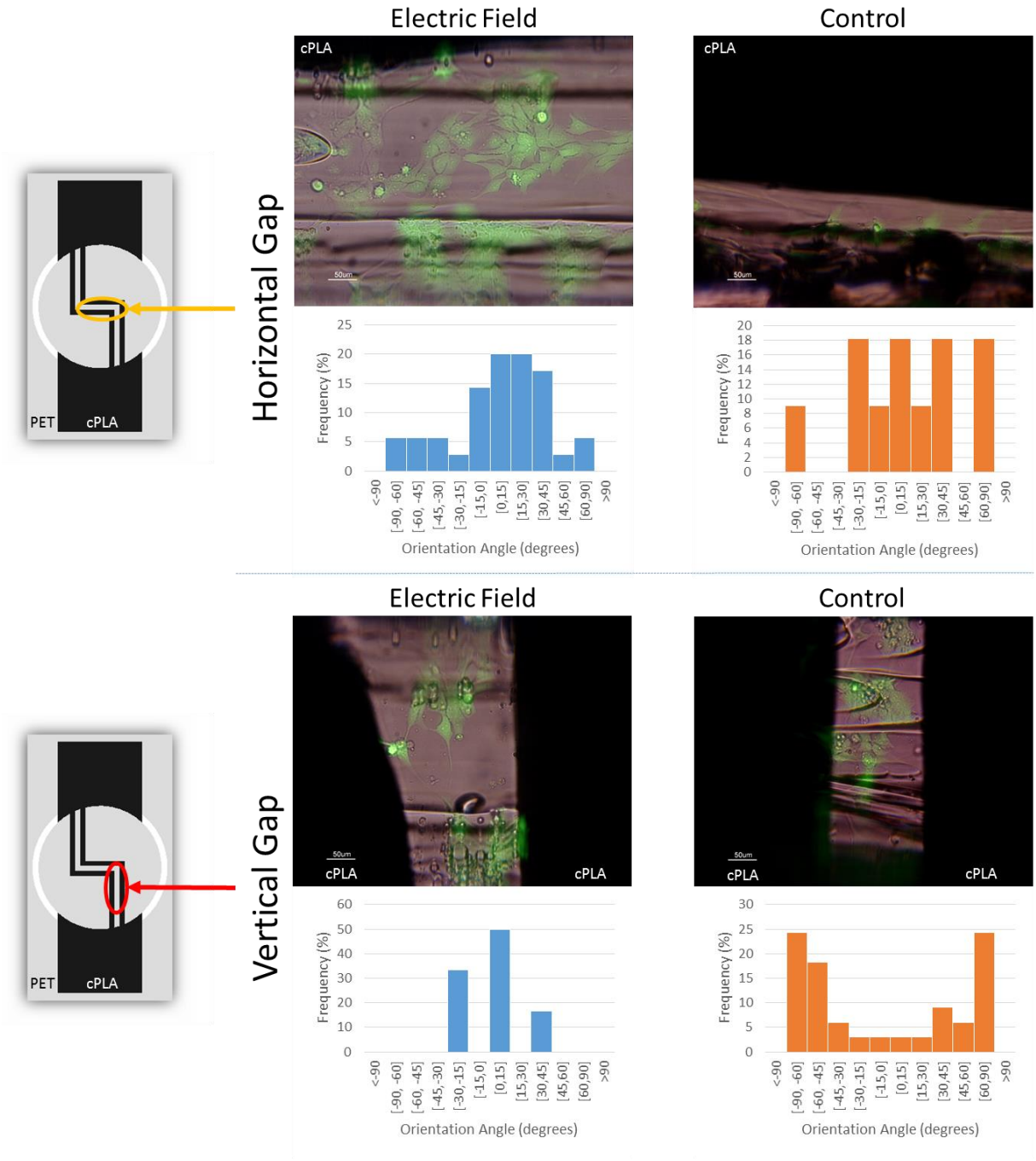

Figure 34. Overlay of bright-field and FM Images of Calcein AM-stained cells (scale bars at 50 µm) and electric field vs. control angle histograms on cPLA filament gaps.

Regarding aspect ratio (Figure 35), it increases for cells on the vertical gaps when electric field is applied, thus we may conclude that elongation is influenced by the electric field. For the horizontal gaps, however, both cells under electric field and on control had statistically the same aspect ratio. This is in agreement with the hypothesis that a small electric field parallel to the horizontal filaments exist, but is very weak when compared to the one formed from the vertical filaments, and is not strong enough to elongate the cells. This may also indicate that the orientation of cells parallel to the direction of the applied electric field on horizontal gaps may be, in fact, the result of the topography of the PET substrate rather than the result of the electric field.

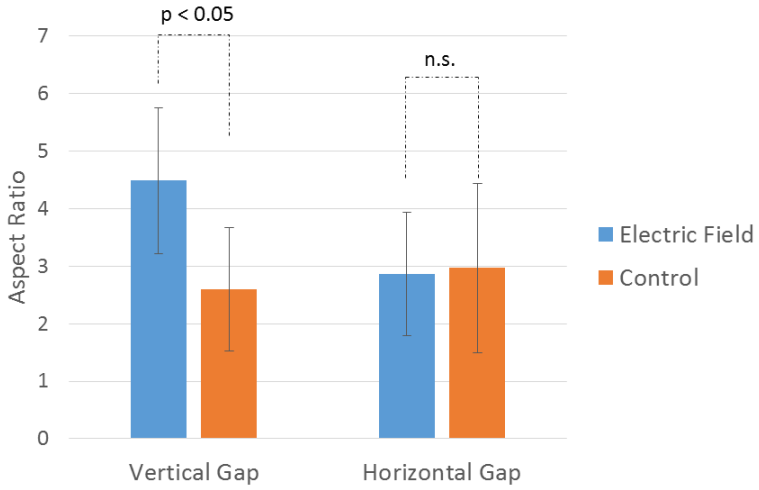

Figure 35. Electric field vs. control aspect ratio for NSCs on vertical and horizontal gaps in scaffolds of PET/cPLA with curves.

Once again, further studies are needed to assess the electrolyte behaviour of the culture medium. Also, there is the need to study the electric field generated in the scaffold through computational simulations. Theoretically, the electric field generated runs parallel to the two cPLA filaments, but minor differences in resistance between the filaments leads to different currents passing through them for the same applied voltage potential, thus creating a small electric field perpendicular to the filaments, which can also have an influence on cell orientation.

B. Effect of Electric Field on the Commitment to Neural or Astrocyte Differentiation Pathways.

Two experiments were performed following a differentiation protocol (Figure 36): one for the PET/cPLA scaffold, another for the PET/cPLA scaffold with curves. FM images were recorder in both experiments, while SEM images were acquired in the PET/cPLA scaffold, as the scaffolds of PET/cPLA with curves were stored with *Vectashield* mounting antifade medium (Vector Labs) to preserve fluorescence staining for future optical and confocal microscopy studies.

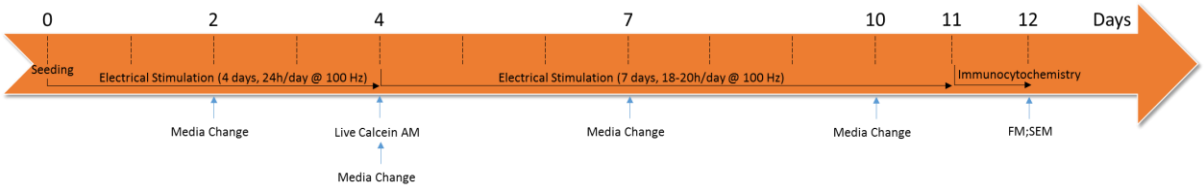

Figure 36. Differentiation protocol timeline.

TuJ1 and GFAP staining are superimposed on the FM images, which prevents the selective identification of neural or astrocytic populations.

It is possible to observe on Figure 37 the results after differentiation on the PET/cPLA scaffold with curves. Images for the differentiation experiment for PET/cPLA scaffold are shown in Figure S53 of Annex B. In a first analysis, it seems that the signal for GFAP is stronger than for TuJ1, which is in agreement with previous studies, given that the NSCS committed to a neuronal lineage are less common than those committed to astrocytes. However, after a more careful analysis it is possible to conclude that there is a majority of cells stained both with GFAP (Glial

Fibrillary Acidic Protein) and TuJ1. This eradicates any possible attempt to further analyse the effect of electric field on the differentiation of NSCs by analysing the relative populations of TuJ1-positive cells (early and mature neurons) or GFAP-positive cells (early and mature astrocytes).

It is difficult to assess with the available information what led to failure of the immunocytochemistry experiments. There is a remote possibility that cells are in fact expressing both markers. A population of GFAP-positive cells also expressing the marker for β-III Tubulin TuJ1 has been found in samples of human fetal (18 to 20 weeks of gestation) brain tissue[167]. It may be that the fetal NSC line used in these experiments are, after differentiation, giving origin to these GFAP-positive cells that also express β-III Tubulin, but these is not in agreement with similar experimental conditions in previous studies with the ReNcell VM NSC line[74,156].

Besides this problem with immunocytochemistry, a large part of cells on the scaffold were death after differentiation – curiously, most of the death cells were outside the cPLA filaments, so in principle less exposed to the electric field. Again it is possible that electrolyte currents in the culture medium are being induced, which may be affecting these cells outside the filaments.

Troubleshooting would involve optimizing culture conditions without electric field to understand when is viable to start inducing differentiation, and assess cell viability with and without electric field conditions. Also, appropriate controls for primary and secondary antibodies used in immunocytochemistry to mark GFAP and TuJ1 should be performed.

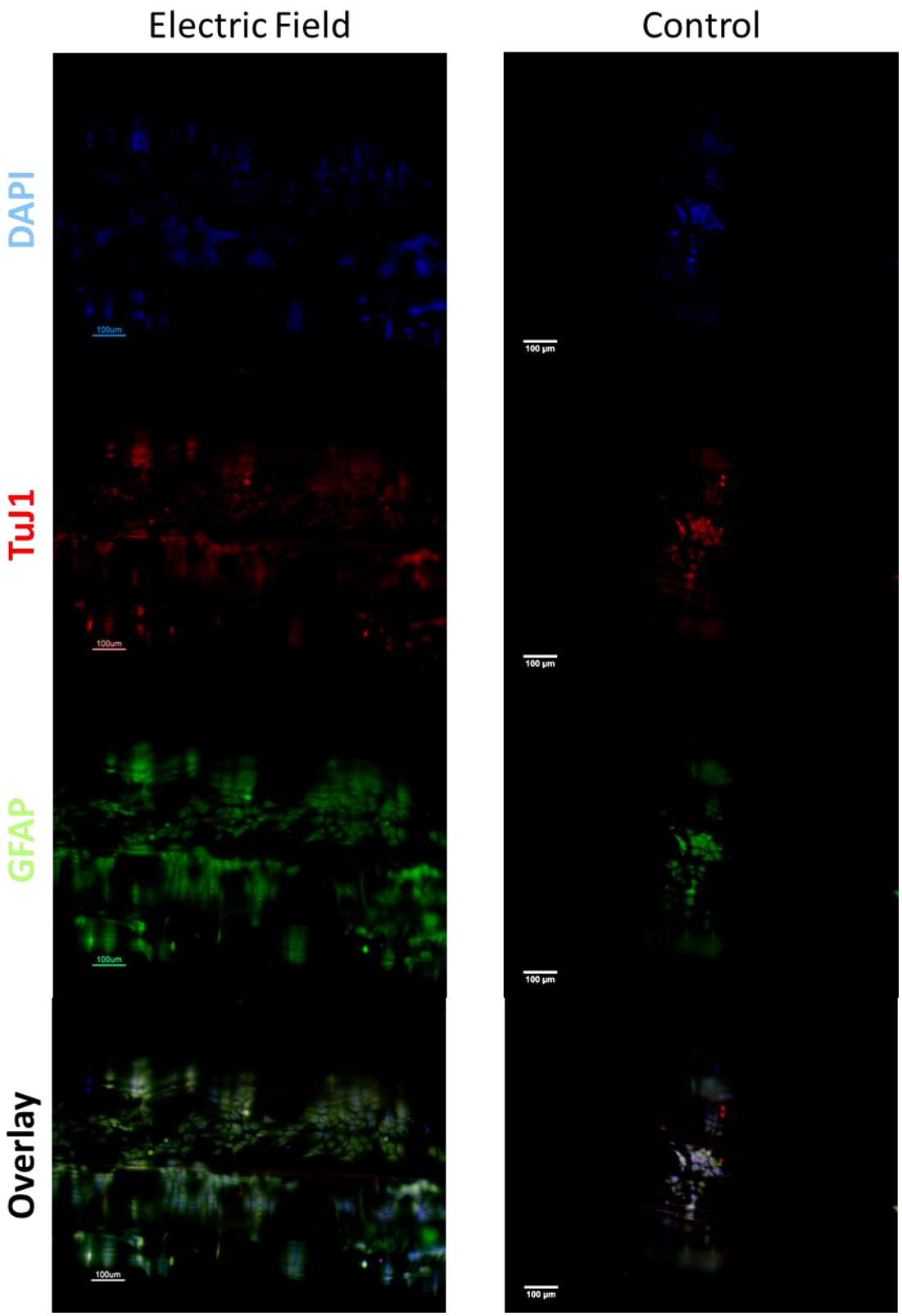

Figure 37. FM Images of DAPI, TuJ1 and GFAP staining, and their overlay after differentiation on the PET/cPLA scaffolds with curves, with and without electric field (scale bar at 100 µm). It is possible to note the overlay between TuJ1 and GFAP signal by the yellowish colour on the bottom images.

III. Tailoring PEGDA Mechanical Properties

In this part of the work, an attempt was made to tweak PEGDA mechanical properties with the addition of plasticizers. It should be noted that as it was intended to maximize the softness of the hydrogels, high concentrations of plasticizer were used, being its maximum concentration limited by the ability to crosslink PEGDA upon UV irradiation to form a hydrogel. This leads to a loose usage of the term "plasticizer", as normally they are added at lower concentrations. Nonetheless, for simplification purposes, they are referred in this section of the results and the next one as plasticizers, including HBS, unless there is the need to establish differences between HBS and PEG.

> Both mechanical properties – compressive modulus and ultimate strength – decrease by increasing concentration of plasticizer. However, the values of compressive modulus are far superior to the ones desired for CNS tissue scaffolding.

Mechanical properties were assessed by determining the Compressive Moduli and Strength of the several hydrogels. The results for Compressive Modulus and Compressive Strength can be found on Table 13 and Figure 38.

Table 13. Mechanical properties (compressive modulus and ultimate strength) of different hydrogels. Results are expressed in MPa.

		Plasticizer Concentration (as wt% on PEGDA)	Sample Name	Compressive Modulus (MPa)		Compressive Strength (MPa)	
				Mean	SD	Mean	SD
PEGDA		0%	PEGDA (dry)	189.30	34.85	40.07	8.82
		0%	PEGDA (wet)	138.30	21.39	19.27	3.04
PEGDA + Plasticizer	HEPES-Buffered Saline (HBS)	50%	HBS-50%	18.58	3.87	4.97	1.50
		75%	HBS-75%	2.93	0.33	1.20	0.28
		90%	HBS-90%	0.18	0.03	0.18	0.07
	PEG(400)	50%	PEG(400)-50%	17.10	3.13	4.46	0.98
		75%	PEG(400)-75%	0.79	0.14	0.97	0.12
		90%	PEG(400)-90%	-	-	-	-
	PEG(600)	50%	PEG(600)-50%	13.44	2.13	5.48	0.98
		75%	PEG(600)-75%	0.50	0.04	1.01	0.19
		90%	PEG(600)-90%	0.12	0.04	0.03	0.00

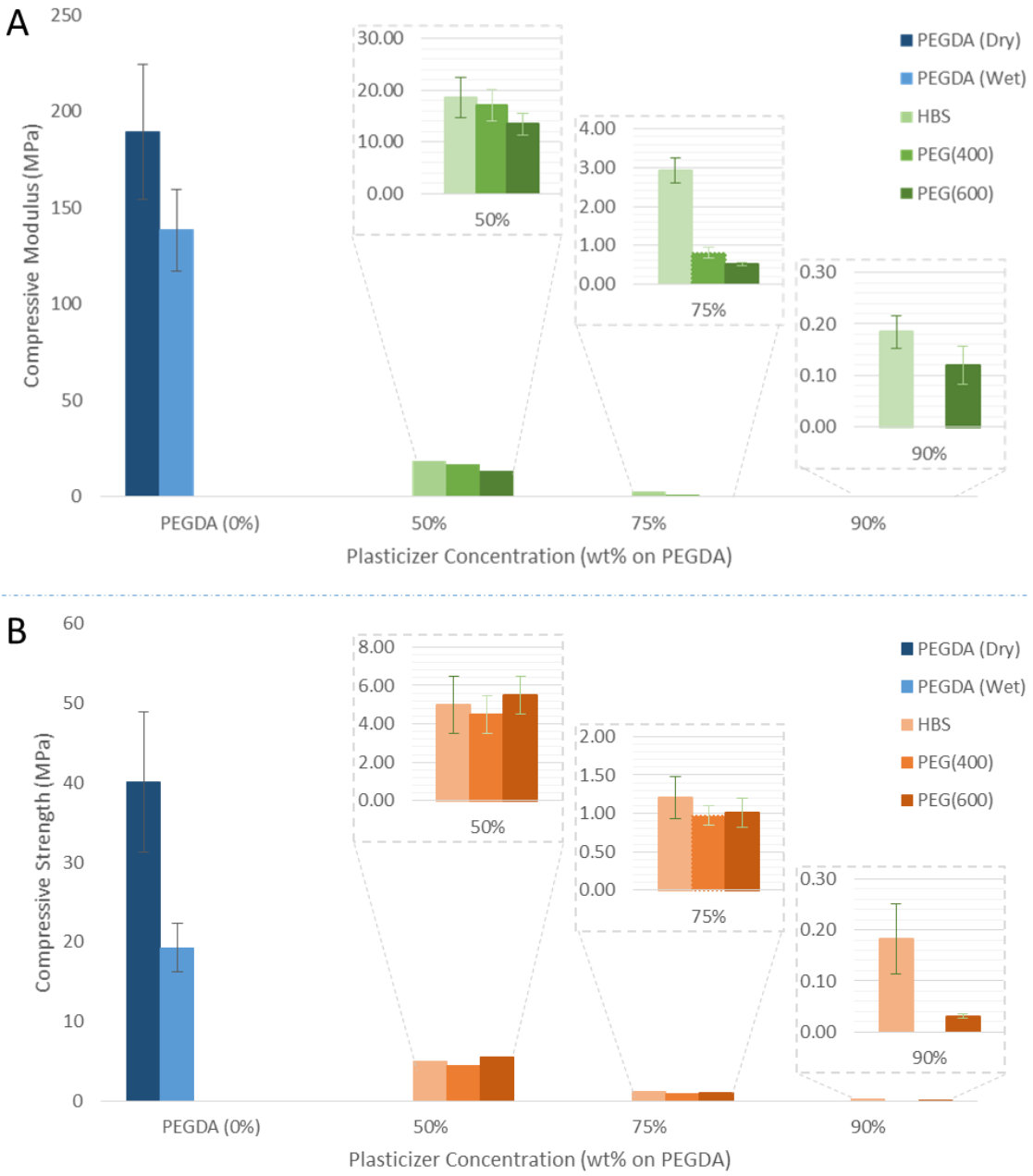

Figure 38. Compressive modulus (A) and ultimate strength (B) for dry and wet pure PEGDA and for different plasticizer types and concentrations in PEGDA-Plasticizer hydrogels.

All PEGDA-plasticizer samples were tested after wetting in PBS, while pure PEGDA hydrogels were tested dry and wet in PBS to see the effect of wetting in mechanical properties. PEGDA soaked in PBS has lower modulus and ultimate strength than dry hydrogels. The presence of the buffered saline solution within the polymer matrix allows a lower local polymer backbone density, as opposed to the compact matrix present in a dry hydrogel. As so, the wet hydrogel will be less stiff (decreased compressive modulus), and more prone to break to higher loads (decreased ultimate strength) than its compact form.

As expected, both compressive modulus and strength decreased when Plasticizer concentration was increased, or in other words, when PEGDA was more diluted. The magnitude of this decrease is 10-fold from pure PEGDA (0%) to 50%, from 50% to 75% and from 75% to 90% of plasticizer concentration. This suggests an exponential

relation between mechanical properties and concentration, and is in agreement to previous reports found in literature[168]. Increasing the concentration of plasticizer, that is, decreasing the concentration of polymer in the solutions, leads to a decreased crosslink density of the polymer matrix, as there is a smaller number of reactive diacrylate groups. Smaller crosslink density leads to a decrease in the compressive modulus and ultimate strength.

Regarding the absolute values obtained for the mechanical properties, the pristine PEGDA and dilutions of PEGDA in HBS have compressive modulus similar to previous reports[36,151,169–171]. No data was found for the PEGDA-PEG hydrogels, as there was only one work found that used different blends of the two polymers with different molecular weights for chondrogenesis from mesenchymal stem cells[35].

In qualitative terms, the stiffness ranged from hard, brittle glass-like hydrogels for pure PEGDA to soft, jelly-like PEGDA-plasticizer hydrogels, where softer hydrogels were obtained with higher concentrations of plasticizers. Stress-strain curves could not be obtained for hydrogels made from PEGDA with 90% PEG(400), as they quickly crumbled when subjected to the load.

The compressive modulus (Figure 38.A) in not strongly dependent on the nature of the plasticizer, yet a clear distinction between HBS and PEG can be made, as HBS-containing hydrogels possess a higher modulus for every concentrations, thus being stiffer. The difference between PEG(400) and PEG(600) is more significant at 50% concentration, where PEG(400) produces hydrogels 5 MPa more stiff than PEG(600); for 75% and 90%, the moduli for the hydrogels based on both molecular weights of PEG are similar at each concentration. Compressive strength (Figure 38.B) follows a similar trend to the compressive moduli when concentration is changed, given a certain plasticizer.

HBS is mainly water, with a small concentration of HEPES (10 mM), whose molecules have much lower molecular weights than the PEG oligomers used (400 and 600 Da). Therefore, molecules present in HBS are much smaller than the long polymeric chains of PEG, so it is expected that the addition of PEG lead to a higher number of possible interactions, through weak interaction forces, between the plasticizer and PEGDA backbone when compared to the number of interactions between the small HBS molecules and PEGDA. This higher number of possible interactions results in increased mobility of the PEGDA backbone, and is associated with decreased stiffness, thus decreased compressive moduli[168].

Regarding overall mechanical behaviour, the compressive stress-strain curves showed a typical curve for viscoelastic materials (Figure 39), as expected for PEGDA hydrogels[34,172]. Also, this behaviour is in agreement with the behaviour described for brain tissue.[63]

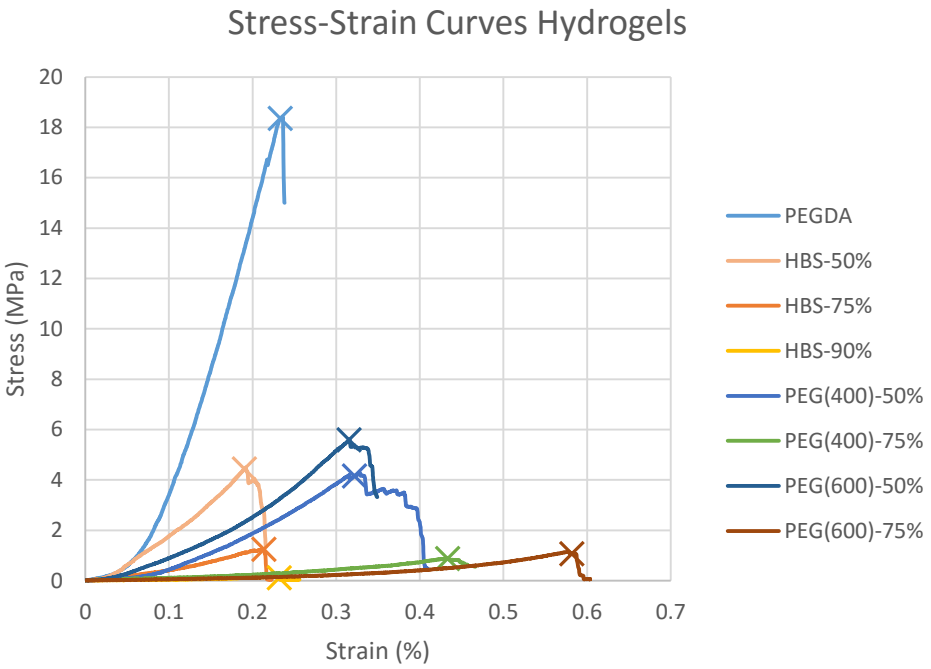

Figure 39. Compressive stress-strain curves for some hydrogels: pristine PEGDA (wet); PEGDA with HBS at 50, 75 and 90 wt% concentration; PEGDA with PEG(400) and PEG(600) at 50 and 75 wt% concentration. The "X" marks the fracture point, at which ultimate strength is measured.

Optical transmittance is reduced when plasticizers are added and there is a shape change of the spectra due to scattering phenomena, which suggests the presence of domains within the hydrogel.

Transmittance was assessed by UV-Vis spectrophotometry. Figure 40.A, B and C show the spectra of hydrogels with different concentrations of HBS, PEG(400) and PEG(600), respectively. The corresponding absorption spectra are shown in Figure S54 on Annex C. Figure 40.D, E and F represent the transmittance of the several plasticizers and concentrations at 400, 600 and 800 nm.

As can be observed in Figure 40.A, B and C, there is a decrease in transmittance from pure PEGDA to hydrogels created from a PEGDA-plasticizer blend and, more importantly, there is a difference between the shape of the spectra of PEGDA-PEG hydrogels when compared to pure PEGDA. For HBS, the spectra are similar except at 75%.

The change in spectra in particular at higher concentration of plasticizer is attributed to light scattering occurring in the polymer matrix. Light scattering in hydrogels is mainly caused by gel inhomogeneity, which causes the hydrogel to be whiter, opaque, than the liquid solution[173,174]. This is characterized by an inhomogeneous crosslinked polymer density distribution and the formation of several domains of polymer-plasticizer that increase the number of internal reflections, thus scattering. The amount of scattered light could be assessed with integrating spheres to obtain the true absorption spectra.

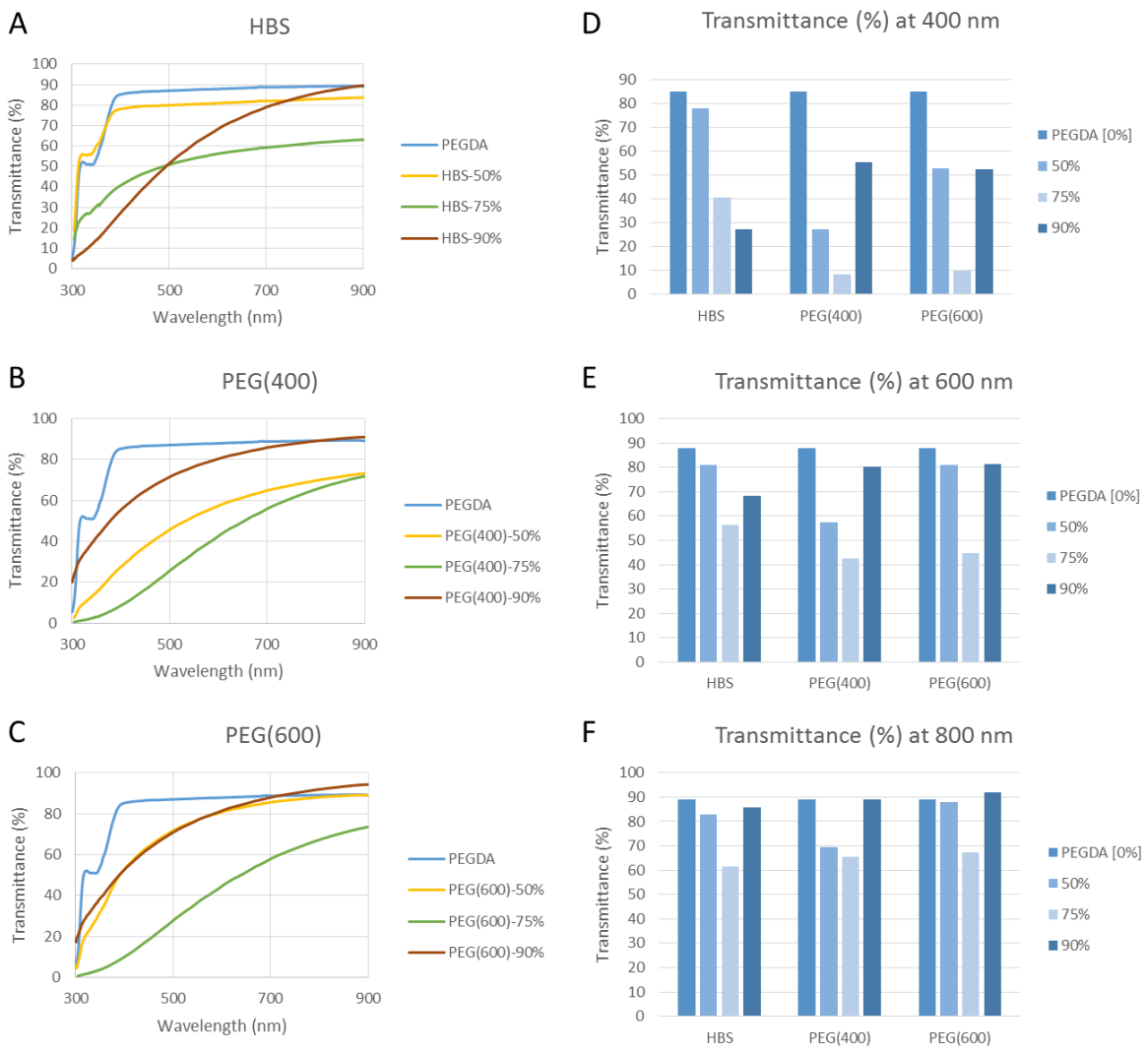

Figure 40. Transmittance spectra for hydrogels with HBS, PEG(400) and PEG(600) at different concentrations (A, B and C); Transmittance at different wavelengths (400, 600 and 800 nm) for the different plasticizers and concentrations (D, E and F).

For hydrogels made of PEGDA-HBS blends another fact can be related to the decrease in transmittance: when compared to the clear PEGDA-PEG solutions prepared, PEGDA-HBS ones were opaque. This is due to the cloud point of HEPES being around 20°C[175], close to room temperature, while PEG polymers have cloud points above room temperature.

Looking at specific wavelengths across the spectra, such as 400, 600 and 800 nm (Figure 40.D, E and F), transmittance seems to decrease as a function of plasticizer concentrations for all plasticizers until 75%. At 90%, the transmittance is higher than the obtained for minor concentrations, and at 800 nm it seems to be higher than the transmittance for pure PEGDA. It is possible to assume that at plasticizer concentration of 90%, the residual PEGDA has a lower probability of forming domains, which means that the scattering in the hydrogel will be reduced, thus having higher transmittance.

In all spectra there is a local minimum of transmittance, that is, a local maximum in absorption which can be discerned at the near-UV around 340 nm in the absorption spectra on Figure S54 of Annex C. This is due to the

presence of residual photoinitiator DMPA, whose absorption peak is at this wavelength, at the concentration used in all solutions[176].

Further studies should be done on swelling, as it was not possible to draw conclusions with the obtained data.

Looking at the swelling degree of the different hydrogels (Figure 41), it is not possible to draw clear conclusions. It is possible that the drying step was not carried out long enough to remove the water present in the hydrogel matrix, thus affecting the measurement of the "dry" weight.

It was expected to find an increase in swelling degree with an increase in concentration for HBS or plasticizers, as more water can occupy the less dense polymer matrix formed. The low swelling degree values obtained for both types of PEG can be explained by the presence of PEG within the PEGDA matrix even after drying the water – this is a severe limitation if one wants to use these hydrogels as materials for cell encapsulation, as culture medium flow to the cells, and thus nutrient transportation will be impaired.

A future study on swelling should first focus on optimizing the drying process in order to confirm these results, and the chemical composition of the dried hydrogels should be assessed to check the fraction of plasticizer PEG still present within the matrix. Also, the swelling kinetics of the hydrogels can be further studied; although hydrogels with plasticizers have a limited capacity of absorbing water due to a decrease in the free space that is occupied by the plasticizer molecules within the PEGDA matrix, it is expected that the presence of hydrophilic plasticizer molecules lead to a faster absorption of water, reducing the time for the hydrogel to reach equilibrium. The hydrophilicity of PEG is supported by the small contact angles obtained for hydrogels with PEG as plasticizers when compared to pure PEGDA and hydrogels with HBS (Figure 42).

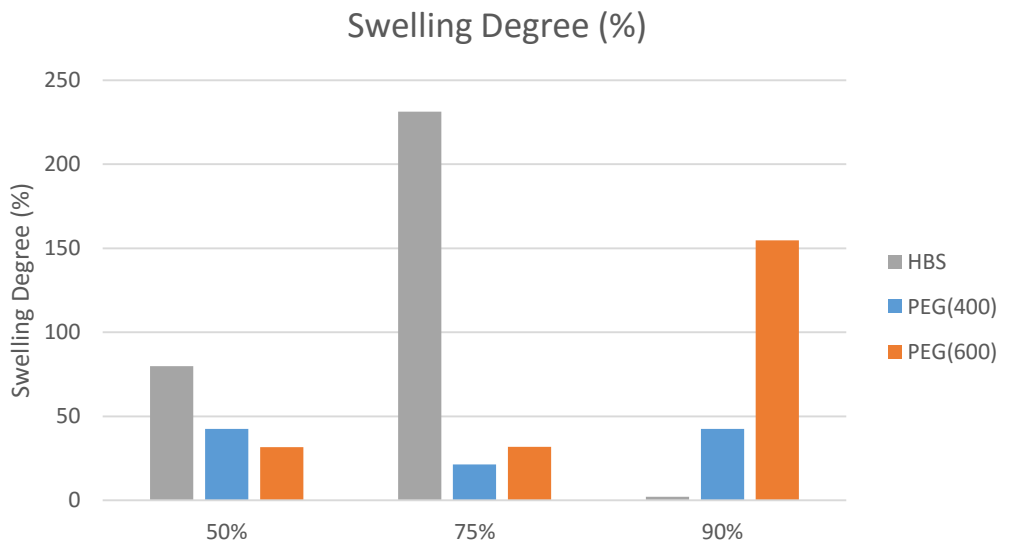

Figure 41. Swelling degree for the several hydrogels: Pristine PEGDA; with HBS, PEG(400) and PEG(600) plasticizers at 50, 75 and 90 wt% concentration.

The wettability of hydrogels is increased when the plasticizer concentration increases.

The contact angle values obtained for the different hydrogels are shown in Figure 42. The addition of PEG leads to a decrease of the contact angle, being this decrease more pronounced as the concentration increases. This is probably due to the higher percentage of hydrophilic plasticizer present in the hydrogel. The values obtained for pure PEGDA and the solutions in HBS also are in agreement with the literature[170]. At 75 wt% of HBS, the contact angle is much higher than for normal PEGDA. Also, when looking at the spectra for PEGDA-HBS blends, the spectrum for 75% sample had a different shape when comparing with the spectra obtained for PEGDA and the other concentrations. Further studies on blends with concentrations around 75% should be performed to explore this peculiar behaviour.

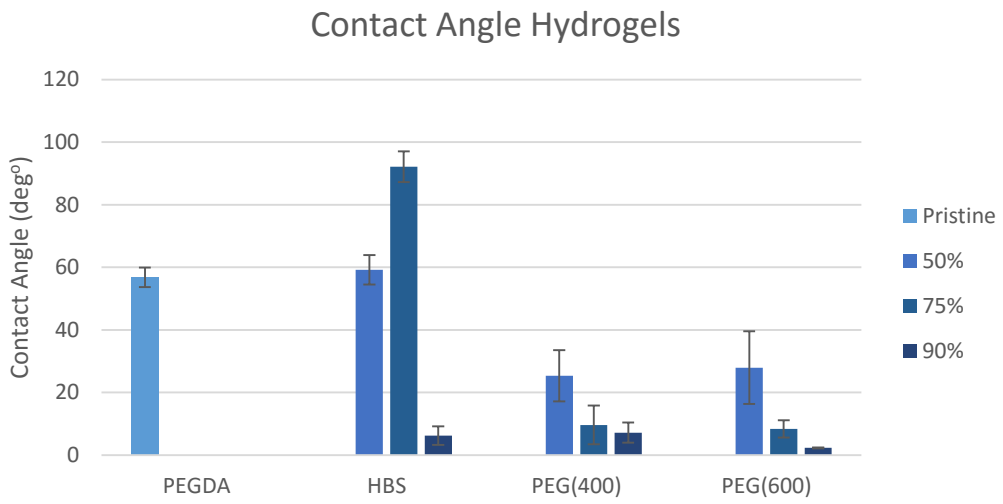

Figure 42. Contact angle obtained for the several hydrogels: Pristine PEGDA; with HBS, PEG(400) and PEG(600) plasticizers at 50, 75 and 90 wt% concentration.

Further studies should be performed to assess the formation of plasticizer domains in the hydrogels, and correlate that morphology with optical and mechanical properties.

In sum, the addition of plasticizers in high concentrations are a good way to modify mechanical properties of PEGDA, resulting in hydrogels with modulus ranging from 100 kPa to 100 MPa; still, for applications involving PEGDA scaffolds for NSCs culture to create grafts for the CNS, the obtained hydrogels have mechanical properties that are still too different from the typical values that affect cell behaviour on CNS tissues (on the order of 1 kPa or less)[61,62] and from the optimal elasticity values for substrates for neural stem cell culture and their influence on proliferation and differentiation (on the order of 1 kPa)[36,64]. The obtained values are more appropriate for applications involving cartilage repair, where its usage has been extensively explored[35,171].

Further studies are needed to explore the relation between concentration and mechanical properties of hydrogels, as well as optical transmittance, wettability and hydrogel swelling. A special focus is needed at 75 wt% HBS, which had a peculiar transmittance spectrum and a very high contact angle when compared to other concentrations of HBs and to pure PEGDA.

The formation of domains upon UV-crosslinking within the polymer matrix can be studies with different techniques: AFM could be used to check the formation of aggregates in the hydrogels, while the size of domains can be studied by diffraction microscopy. The morphology can also be studied with SEM. Also, Differential Scanning Calorimetry could be used to measure the T_g of the hydrogels to assess the level of homogeneity of the hydrogel and the presence of domains: for example, a T_g that is the mean of the glass transition temperatures for PEGDA and Plasticizer indicates an homogeneous composition.

Studies with an integrating sphere could be used to assess the true absorption of these hydrogels. This data and data on the formation of domains can then be correlated with mechanical and optical properties of PEGDA.

Future studies with these PEGDA-plasticizer blends should take into account NSC viability and the flexibility limits of PEDOT:PSS films: the results of the previously suggested study of PEDOT:PSS flexibility should be correlated with data from mechanical properties. Also, NSC viability should be assessed and correlated with data from compressive moduli and strength in order to assess which plasticizer and which concentration are best suited to create platforms adequate for NSC culture.

IV. Enhancement of PEGDA Transparency

In this study, an attempt to enhance PEGDA transparency using different blends of PEGDA with plasticizers was made. This was mainly inspired by the study of Zhao *et al.*[96], where glycerol was used to increase transparency of PEGDA hydrogels made by gelling. Here, several concentrations of the polyalcohols glycerol, sorbitol and PEG with two molecular weights (400 and 600 Da) were used to create UV-crosslinked PEGDA hydrogels, whose transmittance was then assessed by UV-Vis absorption spectroscopy. The transmittance spectra obtained for the several solutions are shown in Figure 43.

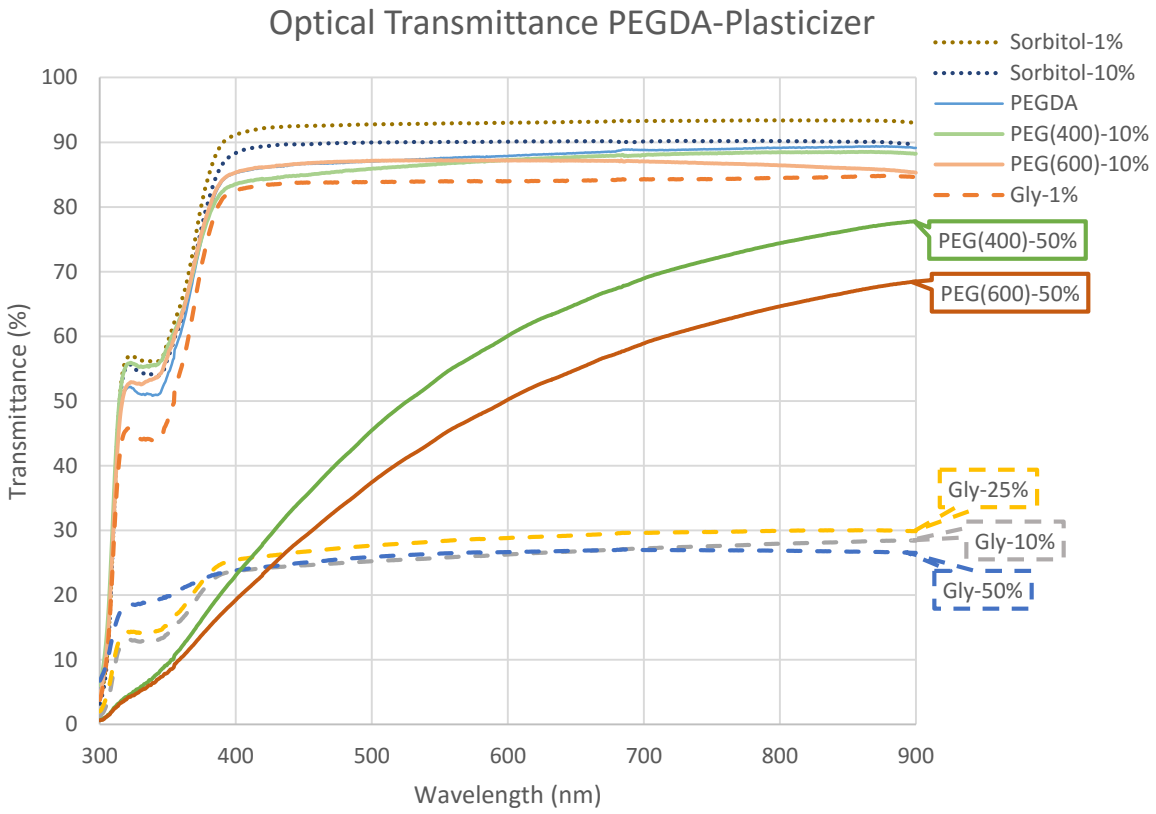

Figure 43. Optical transmittance of several PEGDA-plasticizer blends.

From the plasticizers studies, sorbitol was the only on that improved optical transmittance of pure PEGDA when used at low concentrations.

As shown in Figure 43, the only effective process to increase PEGDA transparency is the addition of sorbitol, where 1 wt% concentration is more effective than 10 wt%. For low concentrations of other plasticizers, such as 1% glycerol and 10% of hlycerol and PEG, the spectra shape is similar to the pure PEGDA one, but show slightly lower transmittance values than the one for pure PEGDA. For higher blends, such as the ones obtained with 25% glycerol and 50% glycerol and PEG, the transmittance spectra are not only lower, but differ in shape, which is attributed to scattering phenomena, caused by hydrogel inhomogeneity. In fact, when these hydrogels were observed to the naked view, it was possible to see they start to become more opaque, pale, blurring the light that traversed them.

The addition of 1 wt% Sorbitol greatly improves optical transmittance on the previously developed PEGDA-plasticizer hydrogels.

Based on the previous data, it was further tested if the transparency of the previously developed PEGDA-HBS and PEGDA-PEG hydrogels could be improved upon addition of sorbitol without considerably modifying mechanical properties, namely compressive modulus and ultimate strength. For this purpose, sorbitol was added at 1 wt% concentration to hydrogels with 75 wt% concentration of the different plasticizers – HBS, PEG(400) and PEG(600). Pure PEGDA hydrogels were also compared against PEGDA with 1 wt% Sorbitol. The referred mechanical properties, swelling behaviour and optical transmittance were assessed for these sorbitol-supplemented hydrogels.

Figure 44. Optical transmittance of pure PEGDA and PEGDA-plasticizer hydrogels with and without 1 wt% sorbitol.

As shown in Figure 44, Optical transmittance is significantly enhanced when 1% Sorbitol is added to the PEGDA-plasticizer blends. The increased transparency could be discernible to the naked eye when both hydrogels were observed. It is important to notice that these changes are solely due to a decrease in scattering across the whole spectra, as most spectra for the hydrogels supplemented with Sorbitol are similar to the spectra for unsupplemented hydrogels, with the exception of HBS.

The mechanism for improving transparency with plasticizers proposed by Zhao *et al.*[96] involves modifications on the conformation of the polymer network and crystallinity of the PEGDA network that reduce light scattering.

Regarding polymer conformation, the presence of a hydrophilic plasticizer within the polymer matrix, when compared to water alters the secondary polymer network conformation by reducing the entanglement of polymer chains (Figure 45, left). This is because plasticizer molecules normally have two or more hydroxyl groups,

which lead to the formation of more hydrogen bonds with the crosslinked PEGDA backbone than the ones formed between PEGDA and water, stretching the PEGDA molecule and reducing conglomeration of polymer chain. This reduced conglomeration and stretching with glycerol was observed by TEM[96].

Concerning PEGDA crystallinity, the conformation of the PEGDA network without plasticizer addition in dense and compact conglomerates lead to the formation of spherulites with dimensions on the order of the visible light wavelength, thus causing strong scattering. When plasticizer is added, the more stretched polymer chains tend to reduce crystallinity, packing in more amorphous cylindrical nanostructures (Figure 45, right).

In this work, it is further hypothesized that sorbitol, which has 6 hydroxyl groups, has a higher effect on the stretching of PEGDA network through the establishment of hydrogen bonds than glycerol or PEG, which have only 3 and 2 hydroxyl groups, respectively – this results in lowest scattering and highest transmittance for PEGDA-sorbitol blends. This would need, of course, to be confirmed by future studies with TEM.

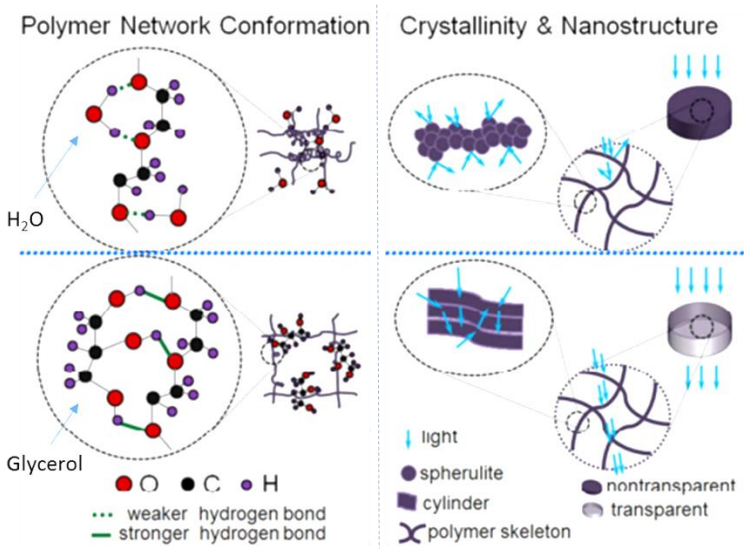

Figure 45. The increased transmittance and reduced scattering when a plasticizer (in the picture, glycerol) is added is a result of: changes in polymer network conformation from a densely packed structure to a more stretched one (as depicted on the left); and reduction of degree of crystallinity, changing from spherulites that cause strong light scattering to more amorphous cylindrical nanostructures that improve transmittance (as depicted on the right). Adapted from Zhao et al.[96].

Mechanical Properties, Swelling Degree and Wettability are virtually the same for hydrogels with or without sorbitol addition.

Looking at the compressive moduli and compressive strength (Figure 46), it is possible to infer that mechanical properties are not drastically changed with the addition of sorbitol. For PEGDA-plasticizer hydrogels, the addition of sorbitol led to a decrease in compressive modulus and an increase in ultimate strength, which could be related to the higher linear arrangement of the polymer chains, which increases mobility, decreases stiffness and thus decreases compressive modulus, while increasing ultimate strength, as deformation from higher loads can be supported.

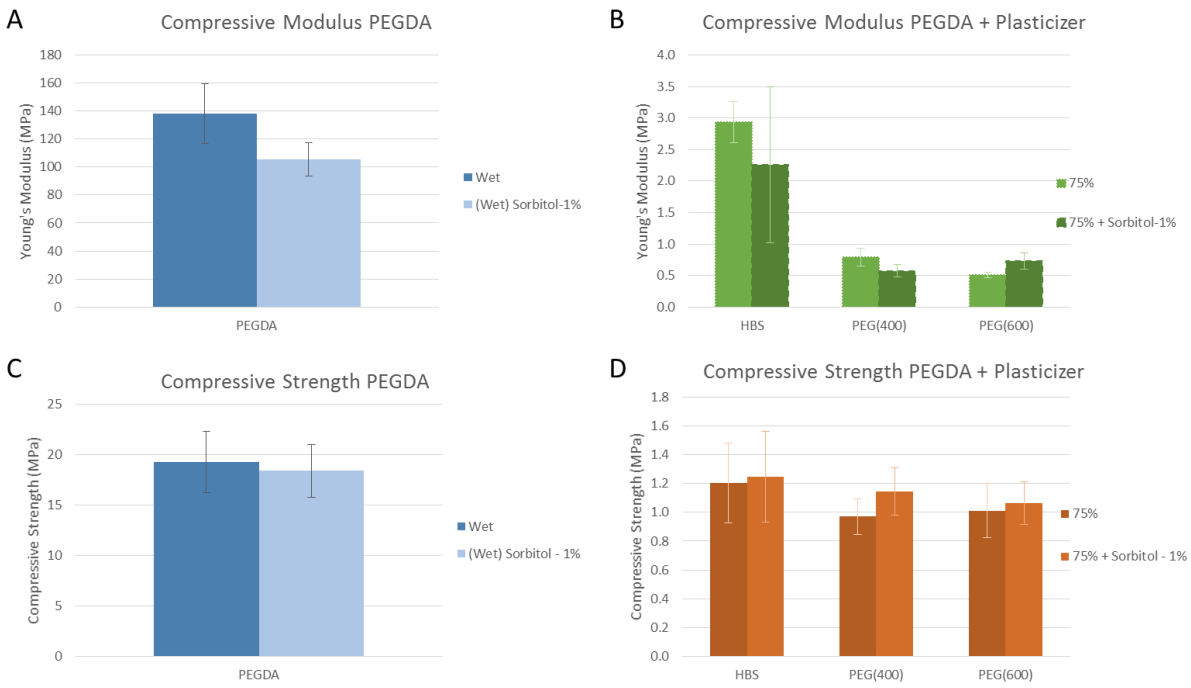

Figure 46. Variation of mechanical properties with the addition of sorbitol: compressive modulus of pure PEGDA (A) and PEGDA-plasticizer blends (B); compressive strength of PEGDA (C) and PEGDA-plasticizer blends (D).

No significant differences in the swelling degree are detected between hydrogels with and without 1% sorbitol, with the exception of HBS-containing hydrogels (Figure 47). This may be once again due to the presence of Sorbitol within the dried hydrogel matrix that leads to the decrease in the amount of water that is possible to be absorbed.

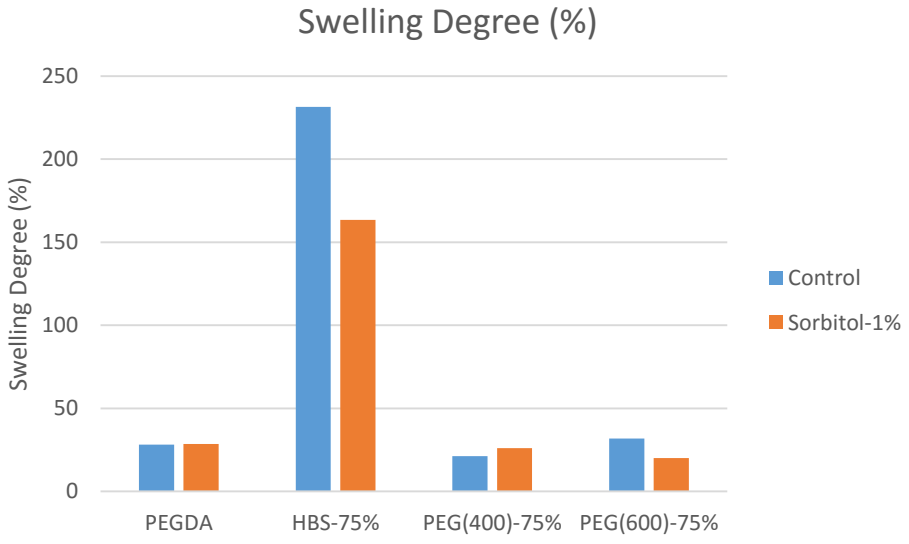

Figure 47. Swelling degree for pure PEGDA and hydrogels with plasticizers at 75 wt% with and without 1 wt% sorbitol.

Similarly to swelling degree, no significant differences in the contact angle are detected between hydrogels with and without 1% sorbitol, with the exception of HBS-containing hydrogels (Figure 48). This may due to the presence of the hydrophilic sorbitol within the dried hydrogel matrix that leads to the decrease in contact angle.

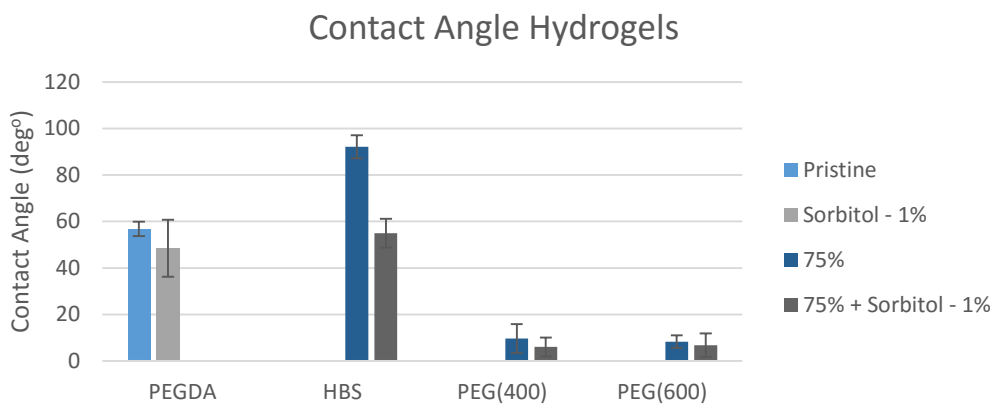

Figure 48. Contact angle for pure PEGDA and hydrogels with plasticizers at 75 wt% with and without 1 wt% sorbitol.

In sum, optical clearance is found to occur in PEGDA hydrogels upon addition of sorbitol. Lower concentration of different plasticizers should be explored to find alternative ways of taking advantage of this optical clearance mechanism, and it should be assessed if this is reproducible for different concentrations of PEGDA-plasticizer blends. This is of great value for applications where high transparency of hydrogels is needed, such as the one being developed on this work, for microfluidic platforms made with PEGDA substrates[177,178], or even for better cell visualization for strategies involving PEGDA-encapsulated cells[33,107].

.

.

Conclusions and Future Trends

The main goal of this work was the establishment of scaffold platforms to study the effect of electric field on NSC culture. The proposed platforms were developed and able to be used in proof-of-concept electric field effect studies, but several optimization steps are needed.

On the 3DP PET/cPLA scaffolds, the high conductivity provided by the cPLA filaments allows the application of a wide range of current values, but the transparency of the PET substrate is very limited due to its geometry, as cells could only be focused at specific areas– it could be addressed in the future if confocal microscopy would improve the overall visualization of cells. Besides limited visualization, the characteristic 3DP geometry may influence the orientation of cells, as assessed after expansion of NSCs; immediate future iterations of this scaffold could be tested using a simpler transparent substrate, such as glass or polystyrene substrate with the extruded cPLA filaments on top.

This scaffold was an attempt to establish a commercial 3DP system as viable tool for constructing user-designed platforms or scaffolds cell culture. The limitations in printing 3D motifs with size magnitude of 100 µm, related to cPLA gap size, severely impairs the viability of using this machine for this specific application. Nevertheless, there are systems being developed that allow to print features much smaller with higher resolution, namely FDM bioprinters with 10 µm resolution, with emerging use in the design and production of vascular grafts[46,179], or bioprinters using hydrogel and inkjet technology[48].

With the aim to explore the use of these materials for NSC culture and to study the effect of electric field on these cells, this work succeeded in further establishing PEGDA and PEDOT:PSS as biomaterials for the development of Tissue Engineering strategies, especially hinting its use for the CNS: both PEGDA transparency and electroconductivity and resolution of IJP PEDOT:PSS were satisfactory. Unfortunately, due to time constraints, only one study was possible on these scaffolds, so in the immediate future, expansion and differentiation studies with electric fields on this platform should be done.

Regarding proof-of-concept electric field effect on NSC studies performed, further work is needed to validate the developed platform for these studies, namely simulating with computational models the electric field on the scaffolds when an ionic liquid, such as the culture medium, is present. Also, future work should be done to fully understand, characterize and compare the effects of different electric field conditions on NSCs, such as current/voltage intensity, pulse duration and period of stimulation, as well as to elicit the mechanisms behind the effect of electric field on expansion and differentiation of NSCs.

In the optimization of PEDOT:PSS all procedures were effective in enhancing the electrical conductivity, and crosslinked PEDOT:PSS films formed by IJP are stable for as long as two weeks. There is the need to further assess by high-resolution TEM and spectroscopic analysis the morphological changes that occur on conductivity enhancement of PEDOT:PSS films with additives or upon film treatment. There is also a concern with the possible cytotoxicity of the additives used, especially with strong acids such as TCAA treatment, or the use of organic

solvent such as methanol – both cytotoxicity and release kinetics of these components during culture medium should be studied.

Regarding PEGDA mechanical properties and transparency, it was possible to obtain a large range of compressive moduli from 100 kPa to 100 MPa through modification by addition of plasticizers. However, as already said, these values are still 100 higher than the ones adequate for physiological brain or for promotion of NSC proliferation and neural differentiation.

Modification with plasticizers should be further studied, namely the variation of compressive modulus and ultimate strength with concentration of plasticizer and the formation of domains of different sizes within the crosslinked PEGDA matrix should be assessed through TEM and X-ray diffraction. In this work, PEG of different molecular weights was used due to their similarity to PEGDA and their established biocompatibility; nonetheless, cell proliferation on these PEGDA-PEG hydrogels should be assessed to optimize culture conditions for possible applications using these hydrogels, such as for cell encapsulation. Future work on physical and chemical characterization, biocompatibility and influence of the materials on cell culture is also needed.

References

1. Bredesen, D. E., Rao, R. V & Mehlen, P. Cell death in the nervous system. *Nature* **443,** 796–802 (2006).

2. Dickson, D. W. Parkinson's disease and parkinsonism: neuropathology. *Cold Spring Harb. Perspect. Med.* **2,** (2012).

3. Blurton-Jones, M. *et al.* Neural stem cells genetically-modified to express neprilysin reduce pathology in Alzheimer transgenic models. *Stem Cell Res. Ther.* **5,** 46 (2014).

4. Rubinsztein, D. C. The roles of intracellular protein-degradation pathways in neurodegeneration. *Nature* **443,** 780–6 (2006).

5. Prince, M. *et al. World Alzheimer Report 2015 - Alzheimer's Disease International*. (2015).

6. *Toxicity and Autophagy in Neurodegenerative Disorders*. (Springer, 2015).

7. Shields, D. Regenerative Medicines Market (Technology, Application and Geography) - Size, Global Trends, Company Profiles, Demand, Insights, Analysis, Research, Report, Opportunities, Segmentation and Forecast, 2013 - 2020. (2014). at <https://www.alliedmarketresearch.com/regenerative-medicines-market> (accessed November 18, 2015)

8. Lee, S., Kwon, T., Chung, E. K. & Lee, J. W. The market trend analysis and prospects of scaffolds for stem cells. *Biomater. Res.* **18,** 11 (2014).

9. Trounson, A. & McDonald, C. Stem Cell Therapies in Clinical Trials: Progress and Challenges. *Cell Stem Cell* **17,** 11–22 (2015).

10. Kim, S. U. & de Vellis, J. Stem cell-based cell therapy in neurological diseases: a review. *J. Neurosci. Res.* **87,** 2183–200 (2009).

11. Benedetti, S. *et al.* Gene therapy of experimental brain tumors using neural progenitor cells. *Nat. Med.* **6,** 447–50 (2000).

12. Müller, F.-J., Snyder, E. Y. & Loring, J. F. Gene therapy: can neural stem cells deliver? *Nat. Rev. Neurosci.* **7,** 75–84 (2006).

13. Gage, F. H. Mammalian Neural Stem Cells. *Science (80-.).* **287,** 1433–1438 (2000).

14. Lu, P., Jones, L. ., Snyder, E. . & Tuszynski, M. . Neural stem cells constitutively secrete neurotrophic factors and promote extensive host axonal growth after spinal cord injury. *Exp. Neurol.* **181,** 115–129 (2003).

15. Adami, R., Scesa, G. & Bottai, D. Stem cell transplantation in neurological diseases: improving effectiveness in animal models. *Front. cell Dev. Biol.* **2,** 17 (2014).

16. Alvarez-Buylla, A. & Garcia-Verdugo, J. M. Neurogenesis in Adult Subventricular Zone. *J. Neurosci.* **22,** 629–634 (2002).

17. Eriksson, P. S. *et al.* Neurogenesis in the adult human hippocampus. *Nat. Med.* **4,** 1313–7 (1998).

18. Kempermann, G., Wiskott, L. & Gage, F. H. Functional significance of adult neurogenesis. *Curr. Opin. Neurobiol.* **14,** 186–91 (2004).

19. Mammadov, B., Sever, M., Guler, M. O. & Tekinay, A. B. Neural differentiation on synthetic scaffold materials. *Biomater. Sci.* **1,** 1119 (2013).

20. Yu, X. & Bellamkonda, R. Tissue-engineered scaffolds are effective alternatives to autografts for bridging peripheral nerve gaps. *Tissue Eng.* **9,** 421–30 (2003).

21. Mahoney, M. & Anseth, K. Three-dimensional growth and function of neural tissue in degradable polyethylene glycol hydrogels. *Biomaterials* **27,** 2265–74 (2006).

22. Subramanian, A., Krishnan, U. & Sethuraman, S. Development of biomaterial scaffold for nerve tissue engineering: Biomaterial mediated neural regeneration. *J Biomed Sci* **16,** 108 (2009).

23. Bottai, D., Madaschi, L., Di Giulio, A. M. & Gorio, A. Viability-dependent promoting action of adult neural precursors in spinal cord injury. *Mol. Med.* **14,** 634–44 (2008).

24. Yang, S., Leong, K., Du, Z. & Chua, C. The design of scaffolds for use in tissue engineering. Part I. Traditional factors. *Tissue Eng.* **7,** 679–89 (2001).

25. Struzyna, L., Harris, J. & Katiyar, K. Restoring nervous system structure and function using tissue engineered living scaffolds. *Neural Regen. Res.* **10,** 679–85 (2015).

26. Bartis, D. & Pongrácz, J. *Three dimensional tissue cultures and tissue engineering*. (2011).

27. Yu, H. *et al.* Improvement of peripheral nerve regeneration in acellular nerve grafts with local release of nerve growth factor. *Microsurgery* **29,** 330–6 (2009).

28. Gao, S., Zheng, Y., Cai, Q., Deng, Z. & Yao, W. Combination of Acellular Nerve Graft and Schwann Cells-Like Cells for Rat Sciatic Nerve Regeneration. *Neural Plast.* **2014,** 139085–139085 (2014).

29. Hoshiba, T. & Chen, G. Decellularized Extracellular Matrix as an In Vitro Model to Study the Comprehensive Roles of the ECM in Stem Cell Differentiation. *Stem Cells Int.* **2015,** (2015).

30. Salih, V. Biodegradable scaffolds for tissue engineering. in *Cell. response to Biomater. CRC Press. Boca …* (2008).

31. Ahmed, E. M. Hydrogel: Preparation, characterization, and applications. *J. Adv. Res.* **6,** 105–121 (2013).

32. Discher, D. E., Janmey, P. & Wang, Y.-L. Tissue cells feel and respond to the stiffness of their substrate. *Science* **310,** 1139–43 (2005).

33. Chan, V., Zorlutuna, P., Jeong, J., Kong, H. & Bashir, R. Three-dimensional photopatterning of hydrogels using stereolithography for long-term cell encapsulation. *Lab Chip* **10,** 2062–70 (2010).

34. Gaharwar, A. K., Rivera, C. P., Wu, C.-J. & Schmidt, G. Transparent, elastomeric and tough hydrogels from poly(ethylene glycol) and silicate nanoparticles. *Acta Biomater.* **7,** 4139–48 (2011).

35. Buxton, A. N. *et al.* Design and characterization of poly(ethylene glycol) photopolymerizable semi-interpenetrating networks for chondrogenesis of human mesenchymal stem cells. *Tissue Eng.* **13,** 2549–60 (2007).

36. Banerjee, A. *et al.* The influence of hydrogel modulus on the proliferation and differentiation of encapsulated neural stem cells. *Biomaterials* **30,** 4695–9 (2009).

37. Cao, H., Liu, T. & Chew, S. Y. The application of nanofibrous scaffolds in neural tissue engineering. *Adv. Drug Deliv. Rev.* **61,** 1055–64 (2009).

38. Xie, J., MacEwan, M. R., Schwartz, A. G. & Xia, Y. Electrospun nanofibers for neural tissue engineering. *Nanoscale* **2,** 35–44 (2010).

39. Liang, D., Hsiao, B. S. & Chu, B. Functional electrospun nanofibrous scaffolds for biomedical applications. *Adv. Drug Deliv. Rev.* **59,** 1392–1412 (2007).

40. Yang, F., Xu, C. Y., Kotaki, M., Wang, S. & Ramakrishna, S. Characterization of neural stem cells on electrospun poly(L-lactic acid) nanofibrous scaffold. *J. Biomater. Sci. Polym. Ed.* **15,** 1483–1497 (2004).

41. Xiong, Y. *et al.* Coseeded Schwann cells myelinate neurites from differentiated neural stem cells in neurotrophin-3-loaded PLGA carriers. *Int. J. Nanomedicine* **7,** 1977–89 (2012).

42. Horne, M. K., Nisbet, D. R., Forsythe, J. S. & Parish, C. L. Three-dimensional nanofibrous scaffolds incorporating immobilized BDNF promote proliferation and differentiation of cortical neural stem cells. *Stem Cells Dev.* **19,** 843–52 (2010).

43. Blacher, S. *et al.* Image analysis of the axonal ingrowth into poly(D,L-lactide) porous scaffolds in relation

to the 3-D porous structure. *Biomaterials* **24,** 1033–40 (2003).

44. Graf, B. W. & Boppart, S. A. Imaging and analysis of three-dimensional cell culture models. *Methods Mol. Biol.* **591,** 211–27 (2010).

45. Abarrategi, A. *et al.* Label-free magnetic resonance imaging to locate live cells in three-dimensional porous scaffolds. *J. R. Soc. Interface* **9,** 2321–31 (2012).

46. Lee, V. K. *et al.* in *Bioprinting Regen. Med.* (Turksen, K.) (Springer International Publishing, 2015). doi:10.1007/978-3-319-21386-6

47. Ouyang, L., Yao, R., Chen, X., Na, J. & Sun, W. 3D printing of HEK 293FT cell-laden hydrogel into macroporous constructs with high cell viability and normal biological functions. *Biofabrication* **7,** 015010 (2015).

48. Nishiyama, Y. *et al.* Development of a three-dimensional bioprinter: construction of cell supporting structures using hydrogel and state-of-the-art inkjet technology. *J. Biomech. Eng.* **131,** 035001 (2009).

49. Hsieh, F.-Y., Lin, H.-H. & Hsu, S.-H. 3D bioprinting of neural stem cell-laden thermoresponsive biodegradable polyurethane hydrogel and potential in central nervous system repair. *Biomaterials* **71,** 48–57 (2015).

50. Lee, Y.-B. *et al.* Bio-printing of collagen and VEGF-releasing fibrin gel scaffolds for neural stem cell culture. *Exp. Neurol.* **223,** 645–52 (2010).

51. Jacobs, S. *et al.* Retinoic acid is required early during adult neurogenesis in the dentate gyrus. *Proc. Natl. Acad. Sci. U. S. A.* **103,** 3902–7 (2006).

52. Taupin, P. *et al.* FGF-2-Responsive Neural Stem Cell Proliferation Requires CCg, a Novel Autocrine/Paracrine Cofactor. *Neuron* **28,** 385–397 (2000).

53. Yu, L. M. Y., Leipzig, N. D. & Shoichet, M. S. Promoting neuron adhesion and growth. *Mater. Today* **11,** 36–43 (2008).

54. Flanagan, L. A., Rebaza, L. M., Derzic, S., Schwartz, P. H. & Monuki, E. S. Regulation of human neural precursor cells by laminin and integrins. *J. Neurosci. Res.* **83,** 845–56 (2006).

55. Hall, P. E., Lathia, J. D., Caldwell, M. A. & Ffrench-Constant, C. Laminin enhances the growth of human neural stem cells in defined culture media. *BMC Neurosci.* **9,** 71 (2008).

56. Li, X. *et al.* Short laminin peptide for improved neural stem cell growth. *Stem Cells Transl. Med.* **3,** 662–70 (2014).

57. Silva, G. A. *et al.* Selective differentiation of neural progenitor cells by high-epitope density nanofibers. *Science* **303,** 1352–5 (2004).

58. Tysseling, V. M. *et al.* Self-assembling peptide amphiphile promotes plasticity of serotonergic fibers following spinal cord injury. *J. Neurosci. Res.* **88,** 3161–70 (2010).

59. Ren, Y., Zhang, H., Huang, H. & Wang, X. In vitro behavior of neural stem cells in response to different chemical functional groups. *Biomaterials* **30,** 1036–44 (2009).

60. Nakajima, M. *et al.* Combinatorial protein display for the cell-based screening of biomaterials that direct neural stem cell differentiation. *Biomaterials* **28,** 1048–60 (2007).

61. Franceschini, G. The mechanics of human brain tissue. *Univ. Trento* (2006).

62. Engler, A., Sen, S., Sweeney, H. & Discher, D. Matrix elasticity directs stem cell lineage specification. *Cell* **126,** 677–89 (2006).

63. Green, M., Bilston, L. & Sinkus, R. In vivo brain viscoelastic properties measured by magnetic resonance elastography. *NMR Biomed.* **21,** 755–64 (2008).

64. Leipzig, N. D. & Shoichet, M. S. The effect of substrate stiffness on adult neural stem cell behavior.

Biomaterials **30,** 6867–78 (2009).

65. Saha, K. *et al.* Substrate modulus directs neural stem cell behavior. *Biophys. J.* **95,** 4426–38 (2008).

66. Toh, J. B. Synthesis and characterisation of PEGDA-based hydrogels crosslinked with pentaerythritol tetrakis (3-Mercaptopropionate). (2011).

67. Qi, L. *et al.* The effects of topographical patterns and sizes on neural stem cell behavior. *PLoS One* **8,** e59022 (2013).

68. Mahoney, M. J., Chen, R. R., Tan, J. & Saltzman, W. M. The influence of microchannels on neurite growth and architecture. *Biomaterials* **26,** 771–8 (2005).

69. Nomura, H. *et al.* Extramedullary chitosan channels promote survival of transplanted neural stem and progenitor cells and create a tissue bridge after complete spinal cord transection. *Tissue Eng. Part A* **14,** 649–65 (2008).

70. Sisken, B. F., Kanje, M., Lundborg, G., Herbst, E. & Kurtz, W. Stimulation of rat sciatic nerve regeneration with pulsed electromagnetic fields. *Brain Res.* **485,** 309–16 (1989).

71. Shi, G., Rouabhia, M., Meng, S. & Zhang, Z. Electrical stimulation enhances viability of human cutaneous fibroblasts on conductive biodegradable substrates. *J. Biomed. Mater. Res. A* **84,** 1026–37 (2008).

72. Chang, K.-A. *et al.* Biphasic electrical currents stimulation promotes both proliferation and differentiation of fetal neural stem cells. *PLoS One* **6,** e18738 (2011).

73. Kam, N. W. S., Jan, E. & Kotov, N. A. Electrical stimulation of neural stem cells mediated by humanized carbon nanotube composite made with extracellular matrix protein. *Nano Lett.* **9,** 273–8 (2009).

74. Pires, F., Ferreira, Q., Rodrigues, C. A. V., Morgado, J. & Ferreira, F. C. Neural stem cell differentiation by electrical stimulation using a cross-linked PEDOT substrate: Expanding the use of biocompatible conjugated conductive polymers for neural tissue engineering. *Biochim. Biophys. Acta - Gen. Subj.* **1850,** 1158–68 (2015).

75. Ghasemi-Mobarakeh, L., Prabhakaran, M. P., Morshed, M., Nasr-Esfahani, M. H. & Ramakrishna, S. Electrical Stimulation of Nerve Cells Using Conductive Nanofibrous Scaffolds for Nerve Tissue Engineering. *Tissue Eng. Part A* **15,** 3605–19 (2009).

76. Ghasemi-Mobarakeh, L. *et al.* Application of conductive polymers, scaffolds and electrical stimulation for nerve tissue engineering. *J. Tissue Eng. Regen. Med.* **5,** e17–35 (2011).

77. Lynn, A. D., Kyriakides, T. R. & Bryant, S. J. Characterization of the in vitro macrophage response and in vivo host response to poly(ethylene glycol)-based hydrogels. *J. Biomed. Mater. Res. A* **93,** 941–53 (2010).

78. Chung, K. *et al.* Structural and molecular interrogation of intact biological systems. *Nature* **497,** 332–7 (2013).

79. Castro, D. *et al.* Characterization of solid UV cross-linked PEGDA for biological applications. in *2013 IEEE 26th Int. Conf. Micro Electro Mech. Syst.* 457–460 (IEEE, 2013). doi:10.1109/MEMSYS.2013.6474277

80. Yang, F., Williams, C., Wang, D. & Lee, H. The effect of incorporating RGD adhesive peptide in polyethylene glycol diacrylate hydrogel on osteogenesis of bone marrow stromal cells. *Biomaterials* **26**, 5991-98 (2005).

81. Kadakia, A. & Keskar, V. Hybrid superporous scaffolds: an application for cornea tissue engineering. *Critical Reviews in Biomedical Engineering.* **36**, 441-71 *(*2008).

82. Bryant, S. J. & Anseth, K. S. Hydrogel properties influence ECM production by chondrocytes photoencapsulated in poly(ethylene glycol) hydrogels. *J. Biomed. Mater. Res.* **59,** 63–72 (2002).

83. Gabler, S., Stampfl, J. & Koch, T. Determination of the viscoelastic properties of hydrogels based on polyethylene glycol diacrylate (PEG-DA) and human articular cartilage. *Int. J. Mater. Eng. Innov.* **1,** 3–20 (2009).

84. Roberts, J. J. & Bryant, S. J. Comparison of photopolymerizable thiol-ene PEG and acrylate-based PEG hydrogels for cartilage development. *Biomaterials* **34,** 9969–9979 (2013).

85. Li, X., Liu, X., Zhang, N. & Wen, X. Engineering in situ cross-linkable and neurocompatible hydrogels. *J. Neurotrauma* **31,** 1431–8 (2014).

86. O'shea, T. M. Injectable hydrogels for the improved delivery of treatments in spinal cord injury. (2014).

87. Stukel, J., Thompson, S., Simon, L. & Willits, R. Polyethlyene glycol microgels to deliver bioactive nerve growth factor. *J. Biomed. Mater. Res. A* **103,** 604–13 (2015).

88. Rogers, C. Optimization of Nonadsorptive Polymerized Polyethylene Glycol Diacrylate as a Material for Microfluidics and Sensor Integration. (2015).

89. Hahn, M. S. *et al.* Photolithographic patterning of polyethylene glycol hydrogels. *Biomaterials* **27,** 2519–24 (2006).

90. Beamish, J. A., Zhu, J., Kottke-Marchant, K. & Marchant, R. E. The effects of monoacrylated poly(ethylene glycol) on the properties of poly(ethylene glycol) diacrylate hydrogels used for tissue engineering. *J. Biomed. Mater. Res. A* **92,** 441–50 (2010).

91. Lo, Y., Lai, Y. & Fan, S. Hydrogel Patterning Using Electro-Microfluidic Techniques. *elite.newhopetek.com.tw* (20155).

92. Koskela, J. E., Turunen, S., Ylä-Outinen, L., Narkilahti, S. & Kellomäki, M. Two-photon microfabrication of poly(ethylene glycol) diacrylate and a novel biodegradable photopolymer-comparison of processability for biomedical applications. *Polym. Adv. Technol.* **23,** 992–1001 (2012).

93. Browning, M. B. & Cosgriff-Hernandez, E. Development of a biostable replacement for PEGDA hydrogels. *Biomacromolecules* **13,** 779–86 (2012).

94. Ali, S., Saik, J. E., Gould, D. J., Dickinson, M. E. & West, J. L. Immobilization of Cell-Adhesive Laminin Peptides in Degradable PEGDA Hydrogels Influences Endothelial Cell Tubulogenesis. *BioResearch open access*. **2**, 241-49 (2013).

95. Fujioka, H. & Dairyo, Y. Neural functions of matrix metalloproteinases: plasticity, neurogenesis, and disease. *Biochemistry Research International* (2012).

96. Zhao, S. *et al.* Glycerol-mediated nanostructure modification leading to improved transparency of porous polymeric scaffolds for high performance 3D cell imaging. *Biomacromolecules* **15,** 2521–31 (2014).

97. Nemir, S., Hayenga, H. N. & West, J. L. PEGDA hydrogels with patterned elasticity: Novel tools for the study of cell response to substrate rigidity. *Biotechnol. Bioeng.* **105,** 636–44 (2010).

98. McHale, M. K. A Tunable Hydrogel System and Pulsatile Flow Bioreactor for the Development of Tissue Engineered Vascular Grafts. (2009).

99. Santobianco, J. G., Nguyen, Ch. K. & Brady, C. A. Class of amine coinitiators in photoinitiated polymerizations. (2007).

100. Maitra, J. & Shukla, V. Cross-linking in Hydrogels-A Review. *Am. J. Polym. Sci.* **4,** 25–31 (2014).

101. Poly(ethylene glycol) diacrylate average Mn 575 | Sigma-Aldrich. at <http://www.sigmaaldrich.com/catalog/product/aldrich/437441?lang=pt&region=PT> (accessed November 5, 2015).

102. Vieira, M. G. A., da Silva, M. A., dos Santos, L. O. & Beppu, M. M. Natural-based plasticizers and biopolymer films: A review. *Eur. Polym. J.* **47,** 254–263 (2011).

103. Gil, N., Saska, M. & Negulescu, I. Evaluation of the effects of biobased plasticizers on the thermal and mechanical properties of poly(vinyl chloride). *J. Appl. Polym. Sci.* **102,** 1366–1373 (2006).

104. Wojciechowska, P. The Effect of Concentration and Type of Plasticizer on the Mechanical Properties of Cellulose Acetate Butyrate Organic-Inorganic Hybrids. *INTECH Open Access Publ.* 141–164 (2012).

105. Shipman, C. Evaluation of 4-(2-Hydroxyethyl)-1-piperazineethanesulfonic Acid (HEPES) as a Tissue Culture Buffer. *Exp. Biol. Med.* **130,** 305–310 (1969).

106. Moon, J. J., Hahn, M. S., Kim, I., Nsiah, B. A. & West, J. L. Micropatterning of poly(ethylene glycol) diacrylate hydrogels with biomolecules to regulate and guide endothelial morphogenesis. *Tissue Eng. Part A* **15,** 579–85 (2009).

107. Olabisi, R. & Lazard, Z. Hydrogel microsphere encapsulation of a cell-based gene therapy system increases cell survival of injected cells, transgene expression, and bone volume in a model. *Tissue Eng. Part A* **16,** 3727–36 (2010).

108. Wen, X., Mao, Z., Han, Z., Tuchin, V. V & Zhu, D. In vivo skin optical clearing by glycerol solutions: mechanism. *J. Biophotonics* **3,** 44–52 (2010).

109. Kiess, H. G. *Conjugated Conducting Polymers*. **102,** (Springer Berlin Heidelberg, 1992).

110. Harun, M., Saion, E. & Kassim, A. Conjugated conducting polymers: A brief overview. *J. J. Adv. Sci. Arts* **2,** 63–68 (2007).

111. Balint, R., Cassidy, N. & Cartmell, S. Conductive polymers: towards a smart biomaterial for tissue engineering. *Acta Biomater.* **10,** 2341–53 (2014).

112. Louwet, F., Groenendaal, L. & Dhaen, J. PEDOT/PSS: synthesis, characterization, properties and applications. *Synth. Met.* **135,** 115–117 (2003).

113. Ouyang, J., Chu, C.-W., Chen, F.-C., Xu, Q. & Yang, Y. High-Conductivity Poly(3,4-ethylenedioxythiophene):Poly(styrene sulfonate) Film and Its Application in Polymer Optoelectronic Devices. *Adv. Funct. Mater.* **15,** 203–208 (2005).

114. Wang, G., Tao, X. & Wang, R. Fabrication and characterization of OLEDs using PEDOT:PSS and MWCNT nanocomposites. *Compos. Sci. Technol.* **68,** 2837–2841 (2008).

115. Ely, F. *et al.* Patterning quality control of inkjet printed PEDOT:PSS films by wetting properties. *Synth. Met.* **161,** 2129–2134 (2011).

116. Farinhas, J. *et al.* Nanostructured donor/acceptor interfaces in photovoltaic cells using columnar-grain films of a cross-linked poly(fluorene-alt-bithiophene). *J. Mater. Chem.* **21,** 12511 (2011).

117. Ouyang, J. Solution-processed PEDOT:PSS films with conductivities as indium tin oxide through a treatment with mild and weak organic acids. *ACS Appl. Mater. Interfaces* **5,** 13082–8 (2013).

118. Villers, D., Jobin, D. & Soucy, C. The influence of the range of electroactivity and capacitance of conducting polymers on the performance of carbon conducting polymer hybrid supercapacitor. *J. Electrochem. Soc.* **150,** A747–A752 (2003).

119. Sun, K. *et al.* Review on application of PEDOTs and PEDOT:PSS in energy conversion and storage devices. *J. Mater. Sci. Mater. Electron.* **26,** 4438–4462 (2015).

120. Lefebvre, M., Qi, Z. & Pickup, P. Electronically conducting proton exchange polymers as catalyst supports for proton exchange membrane fuel cells. Electrocatalysis of oxygen reduction, hydrogen. *J. Electrochem. Soc.* **146,** 2054–58 (1999).

121. Lipomi, D. & Tee, B. Stretchable organic solar cells. *Adv. Mater.* **23,** 1771–75 (2011).

122. Vosgueritchian, M. Highly conductive and transparent PEDOT: PSS films with a fluorosurfactant for stretchable and flexible transparent electrodes. *Adv. Funct. Mater.* **22,** 421–428 (2012).

123. Luo, S.-C. *et al.* Poly(3,4-ethylenedioxythiophene) (PEDOT) nanobiointerfaces: thin, ultrasmooth, and functionalized PEDOT films with in vitro and in vivo biocompatibility. *Langmuir* **24,** 8071–7 (2008).

124. Berezhetska, O., Liberelle, B., De Crescenzo, G. & Cicoira, F. A simple approach for protein covalent grafting on conducting polymer films. *J. Mater. Chem. B* **3,** 5087–5094 (2015).

125. Kim, D.-H., Abidian, M. & Martin, D. C. Conducting polymers grown in hydrogel scaffolds coated on neural

prosthetic devices. *J. Biomed. Mater. Res. A* **71,** 577–85 (2004).

126. Aregueta-Robles, U. A., Woolley, A. J., Poole-Warren, L. A., Lovell, N. H. & Green, R. A. Organic electrode coatings for next-generation neural interfaces. *Front. Neuroeng.* **7,** 15 (2014).

127. Green, R., Lovell, N., Wallace, G. & Poole-Warren, L. Conducting polymers for neural interfaces: challenges in developing an effective long-term implant. *Biomaterials* **29,** 3393–99 (2008).

128. Green, R. A. *et al.* Living electrodes: tissue engineering the neural interface. *Conf. Proc. ... Annu. Int. Conf. IEEE Eng. Med. Biol. Soc. IEEE Eng. Med. Biol. Soc. Annu. Conf.* **2013,** 6957–60 (2013).

129. Shi, H., Liu, C., Jiang, Q. & Xu, J. Effective Approaches to Improve the Electrical Conductivity of PEDOT:PSS: A Review. *Adv. Electron. Mater.* **1,** (2015).

130. Kirchmeyer, S. & Reuter, K. Scientific importance, properties and growing applications of poly(3,4-ethylenedioxythiophene). *J. Mater. Chem.* **15,** 2077 (2005).

131. Wiederrecht, G. *Handbook of Nanoscale Optics and Electronics*. (2010).

132. Elschner, A. & Lövenich, W. Solution-deposited PEDOT for transparent conductive applications. *MRS Bull.* **36,** 794–798 (2011).

133. Law, K.-Y., Zhang, Y. & Kanungo, M. Direct digital marking systems. (2012).

134. Lefebvre, M., Qi, Z., Rana, D. & Pickup, P. G. Chemical Synthesis, Characterization, and Electrochemical Studies of Poly(3,4-ethylenedioxythiophene)/Poly(styrene-4-sulfonate) Composites. *Chem. Mater.* **11,** 262–268 (1999).

135. Suchand Sangeeth, C. S., Jaiswal, M. & Menon, R. Correlation of morphology and charge transport in poly(3,4-ethylenedioxythiophene)-polystyrenesulfonic acid (PEDOT-PSS) films. *J. Phys. Condens. Matter* **21,** 072101 (2009).

136. Ouyang, J. *et al.* On the mechanism of conductivity enhancement in poly (3, 4-ethylenedioxythiophene): poly (styrene sulfonate) film through solvent treatment. *Polymer (Guildf).* **45,** 8443–50 (2004).

137. Yoo, J. E. *et al.* Directly patternable, highly conducting polymers for broad applications in organic electronics. *Proc. Natl. Acad. Sci. U. S. A.* **107,** 5712–7 (2010).

138. Mengistie, D., Wang, P. & Chu, C. Highly Conductive PEDOT: PSS Electrode Treated With Polyethylene Glycol for ITO-Free Polymer Solar Cells. *ECS Trans.* **58,** 49–56 (2013).

139. Cruz-Cruz, I., Reyes-Reyes, M. & López-Sandoval, R. Formation of polystyrene sulfonic acid surface structures on poly(3,4-ethylenedioxythiophene): Poly(styrenesulfonate) thin films and the enhancement of its conductivity by using sulfuric acid. *Thin Solid Films* **531,** 385–390 (2013).

140. Stavrinidou, E. *et al.* Direct measurement of ion mobility in a conducting polymer. *Adv. Mater.* **25,** 4488–93 (2013).

141. Zhang, S. *et al.* Solvent-induced changes in PEDOT:PSS films for organic electrochemical transistors. *APL Mater.* **3,** 014911 (2015).

142. Tung, V. C., Kim, J., Cote, L. J. & Huang, J. Sticky Interconnect for Solution-Processed Tandem Solar Cells. *J. Am. Chem. Soc.* **133,** 9262–9265 (2011).

143. Gesser, H. D. *Applied Chemistry: A Textbook for Engineers and Technologists*. (Springer Science & Business Media, 2002).

144. Batista, U., Miklavčič, D. & Serša, G. Low level direct current — cell culture fibroblast model. *Bioelectrochemistry Bioenerg.* **35,** 99–101 (1994).

145. Liu, C. *et al.* Highly conducting free-standing poly(3,4-ethylenedioxythiophene)/poly(styrenesulfonate) films with improved thermoelectric performances. *Synth. Met.* **160,** 2481–2485 (2010).

146. Alemu, D., Wei, H., Ho, K. & Chu, C. Highly conductive PEDOT: PSS electrode by simple film treatment

with methanol for ITO-free polymer solar cells. *Energy Environ. Sci.* **5,** 9662–71 (2012).

147. Kim, N. *et al.* Highly conductive PEDOT:PSS nanofibrils induced by solution-processed crystallization. *Adv. Mater.* **26,** 2268–72, 2109 (2014).

148. t-glase Features - taulman 3D. at <http://www.taulman3d.com/t-glase-features.html> (accessed October 28, 2015).

149. Conductive PLA – ProtoPlant, Makers of Proto-pasta. at <http://www.proto-pasta.com/pages/conductive-pla> (accessed October 28, 2015).

150. Falcon® Product Selection Guide. at <http://csmedia2.corning.com/LifeSciences/Media/eFlip/Falcon-Product-Selection-Guide/edition1/FC3744C25A31A341BB9DEEFC48A72CA3/CLS-F-PSG-001.pdf> (accessed October 28, 2015).

151. Nemir, S., Hayenga, H. N. & West, J. L. PEGDA hydrogels with patterned elasticity: Novel tools for the study of cell response to substrate rigidity. *Biotechnol. Bioeng.* **105,** 636–644 (2010).

152. ReNcell VM Human Neural Progenitor Cell Line. at <https://www.merckmillipore.com/PT/en/product/ReNcell-VM-Human-Neural-Progenitor-Cell-LIne,MM_NF-SCC008?bd=1> (accessed October 28, 2015).

153. Baust, J. G. & Baust, J. M. *Advances in Biopreservation*. (CRC Press, 2006).

154. Baust, J. M., Buskirk, R. Van & Baust, J. G. Cell Viability improves following inhibition of Cryopreservation-induced Apoptosis. *Vitr. Cell. Dev. Biol. - Anim.* **36,** 262 (2000).

155. Hunt, C. J. Cryopreservation of Human Stem Cells for Clinical Application: A Review. *Transfus. Med. Hemother.* **38,** 107–123 (2011).

156. Donato, R. *et al.* Differential development of neuronal physiological responsiveness in two human neural stem cell lines. *BMC Neurosci.* **8,** 36 (2007).

157. DAPI for nucleic acid staining | Sigma-Aldrich. at <http://www.sigmaaldrich.com/catalog/product/sigma/d9542?lang=pt&region=PT> (accessed October 4, 2015).

158. Phalloidin–Tetramethylrhodamine B isothiocyanate Phalloidin from Amanita phalloides | Sigma-Aldrich. at <http://www.sigmaaldrich.com/catalog/product/sigma/p1951?lang=pt&region=PT> (accessed October 4, 2015).

159. Alexa Fluor® 546 dye. at <https://www.thermofisher.com/pt/en/home/life-science/cell-analysis/fluorophores/alexa-fluor-546.html> (accessed October 4, 2015).

160. Alexa Fluor® 488 dye. at <https://www.thermofisher.com/pt/en/home/life-science/cell-analysis/fluorophores/alexa-fluor-488.html?icid=fr-af488-main> (accessed October 4, 2015).

161. Filament Tolerances and Print Quality. at <http://www.protoparadigm.com/news-updates/filament-tolerances-and-print-quality/> (accessed October 4, 2015).

162. Mohanty, A., Misra, M. & Drzal, L. *Natural fibers, biopolymers, and biocomposites*. (CRC Press, 2005).

163. Cho, C.-K. *et al.* Mechanical flexibility of transparent PEDOT:PSS electrodes prepared by gravure printing for flexible organic solar cells. *Sol. Energy Mater. Sol. Cells* **95,** 3269–3275 (2011).

164. Savagatrup, S. *et al.* Plasticization of PEDOT:PSS by Common Additives for Mechanically Robust Organic Solar Cells and Wearable Sensors. *Adv. Funct. Mater.* **25,** 427–436 (2015).

165. Rodríguez Hernández, J. C., Salmerón Sánchez, M., Soria, J. M., Gómez Ribelles, J. L. & Monleón Pradas, M. Substrate chemistry-dependent conformations of single laminin molecules on polymer surfaces are revealed by the phase signal of atomic force microscopy. *Biophys. J.* **93,** 202–7 (2007).

166. LIVE/DEAD Viability/Cytotoxicity Kit, for mammalian cells - Thermo Fisher Scientific. at <https://www.thermofisher.com/order/catalog/product/L3224> (accessed November 13, 2015).

167. Dráberová, E. *et al.* Class III beta-tubulin is constitutively coexpressed with glial fibrillary acidic protein and nestin in midgestational human fetal astrocytes: implications for phenotypic identity. *J. Neuropathol. Exp. Neurol.* **67,** 341–54 (2008).

168. Mazzoccoli, J. P., Feke, D. L., Baskaran, H. & Pintauro, P. N. Mechanical and cell viability properties of crosslinked low- and high-molecular weight poly(ethylene glycol) diacrylate blends. *J. Biomed. Mater. Res. A* **93,** 558–66 (2010).

169. Liao, H. *et al.* Influence of hydrogel mechanical properties and mesh size on vocal fold fibroblast extracellular matrix production and phenotype. *Acta Biomater.* **4,** 1161–71 (2008).

170. Hongbin, Z., Guoguang, N., Li, S., YangHuai & Siquan, Z. Preparation,hydrophilicity, swelling behaviors and mechanical properties of crosslinked poly(ethylene glycol) diacrylate hydrogels with different molecular weights. (2009).

171. Nguyen, Q. T., Hwang, Y., Chen, A. C., Varghese, S. & Sah, R. L. Cartilage-like mechanical properties of poly (ethylene glycol)-diacrylate hydrogels. *Biomaterials* **33,** 6682–90 (2012).

172. Kalakkunnath, S., Kalika, D. S., Lin, H. & Freeman, B. D. Viscoelastic characteristics of UV polymerized poly(ethylene glycol) diacrylate networks with varying extents of crosslinking. *J. Polym. Sci. Part B Polym. Phys.* **44,** 2058–2070 (2006).

173. Okay, O. in *Hydrogel sensors and actuators* 1–14 (Springer Berlin Heidelberg, 2009).

174. Tran-Cong-Miyata, Q. The roles of reaction inhomogeneity in phase separation kinetics and morphology of reactive polymer blends. *Chinese J. Polym. Sci.* **27,** 23–36 (2009).

175. Fleischer, S. & Tonomura, Y. *Structure and Function of Sarcoplasmic Reticulum*. (Elsevier Science, 2013).

176. Ciba® IRGACURE® 651. at <http://people.rit.edu/deeemc/reference_13/Imprint/irgacure_651.pdf> (accessed November 13, 2015).

177. Cuchiara, M. P., Allen, A. C. B., Chen, T. M., Miller, J. S. & West, J. L. Multilayer microfluidic PEGDA hydrogels. *Biomaterials* **31,** 5491–7 (2010).

178. Castro, D. *et al.* Characterization of solid UV cross-linked PEGDA for biological applications. *Proc. IEEE Int. Conf. Micro Electro Mech. Syst.* 457–460 (2013). doi:10.1109/MEMSYS.2013.6474277

179. Chia, H. & Wu, B. Recent advances in 3D printing of biomaterials. *J. Biol. Eng.* **9,** 4 (2014).

Annex A – Prototypes for 3D Transparent and Electroconductive Scaffolds

As already mentioned in the Research Strategy, in an early stage of the project it was intended to create 3D transparent, electroconductive scaffolds that could overcome the cell visualization problems of common 3D scaffolding systems, while being able to provide electrical cues for NSC growth and differentiation. Three attempts were made as described below.

Prototype 1

A first attempt was made at creating 3D scaffolds with a woodpile design using a common cell culture polymer substrate (Polystyrene, PS) by perfusing solutions of these polymers on 3D-printed molds, which were made from common commercial filaments of PLA. First, 3DP PLA molds were created using a woodpile design, with 0.5 mm for the filament size (thus creating 0.5 mm in the PS scaffold) and either 0.5 or 1 mm pore size (thus creating filaments of PS with those sizes); second, viscous solutions of PS were created by dissolution in toluene or chloroform, and used to perfuse the mold; third, the solvent in PS would evaporate, forming the scaffold structure, and the mold would then be removed by dissolution in aqueous sodium hydroxide (NaOH). This attempt failed due to inability of PS to perfuse the mold, as shown in Figure S49, even when various solutions of different viscosities were used, vacuum was used to force the entrance of PS, or mold pore size was increased from 0.5 to 1 mm (Figure S49 , on the left).

Another way of creating such prototype was by direct thermal or photopolymerization of the corresponding monomers (styrene and methyl methacrylate) on these 3D molds. However, quick dissolution of the mold when in contact with the styrene and methyl methacrylate monomers occurred, even when the filament of co-polymer of acrylonitrile butadiene styrene (ABS) was used as the mold material alternative to PLA. Given these limitations, no scaffold was produced with these procedures (Figure S49, on the right).

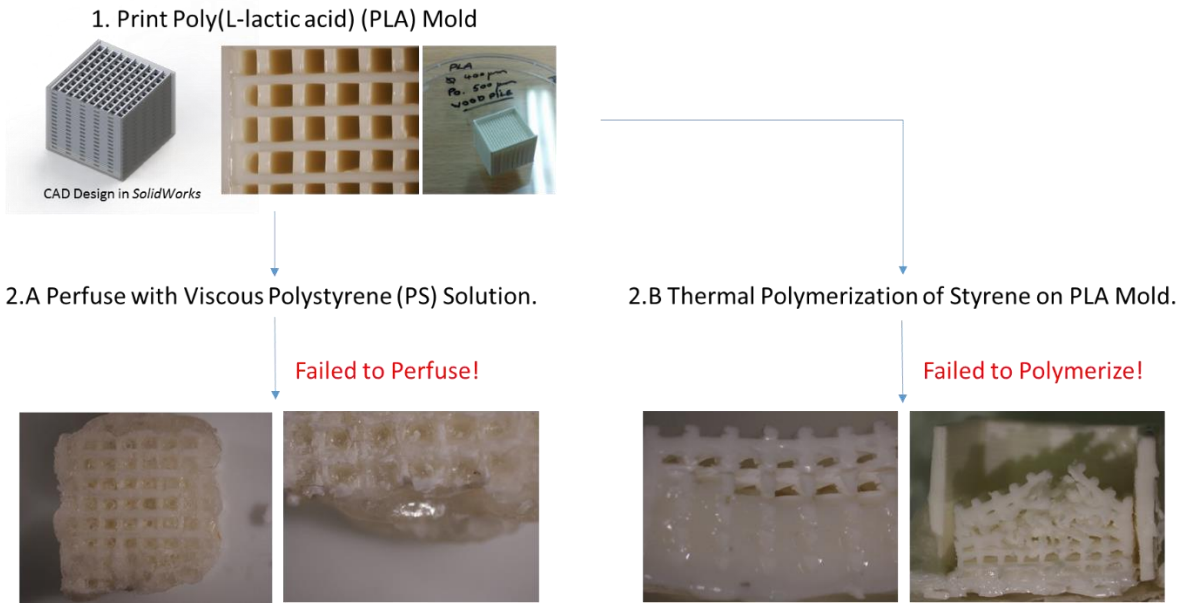

Figure S49. Fabrication of Prototype 1, with emphasis to the failures occurred during production of the scaffold.

Prototype 2

A second attempt at creating 3D scaffolds was made by fabricating a 2D mesh of PEGDA by UV-crosslinking using a PDMS mold (Figure S50). This PDMS mold was fabricated by creating a wafer, that is, an anti-mold on the 3D printer, and then crosslinking the PDMS on this anti-mold to replicate the structure by soft lithography. Several 2D PEGDA meshes could be stacked to create porous transparent scaffolds with an organized structure, and some layers could be electroconductive by forming a homogeneous PEDOT:PSS film through dip-coating technique. This scaffold was successfully constructed, but it was not further characterized or used in biological studies, as it was decided to focus on 2D scaffold platforms.

This prototype had good transparency from PEGDA and good conductivity properties from dip-coated PEDOT:PSS, serving as a 3D analogous to the PEGDA/PEDOT:PSS scaffold described before. After characterization and studying the electric field effect on the 2D platforms, the transition to 3D could be done through this prototype.

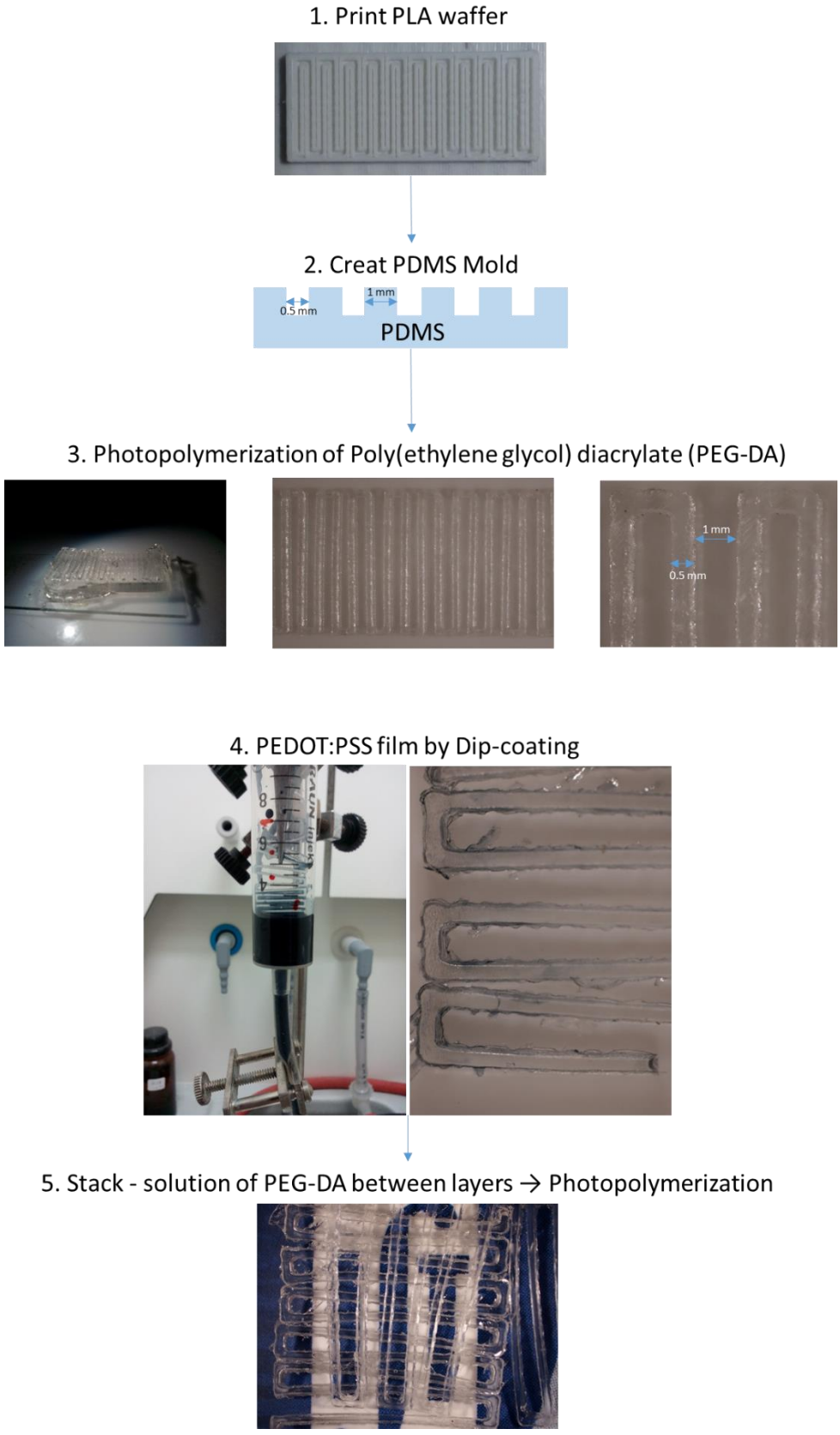

Figure S50. Fabrication of Prototype 2. It is noteworthy the high transparency of the resulting 3D scaffold from the stacking of several PEGDA layers.

Prototype 3

A third prototype was made by directly printing a woodpile scaffold design with PET filament. A conductive layer of cPLA can be added, as shown in Figure S51, or specified filaments in the scaffold matrix can be chosen to be conductive by tweaking the design.

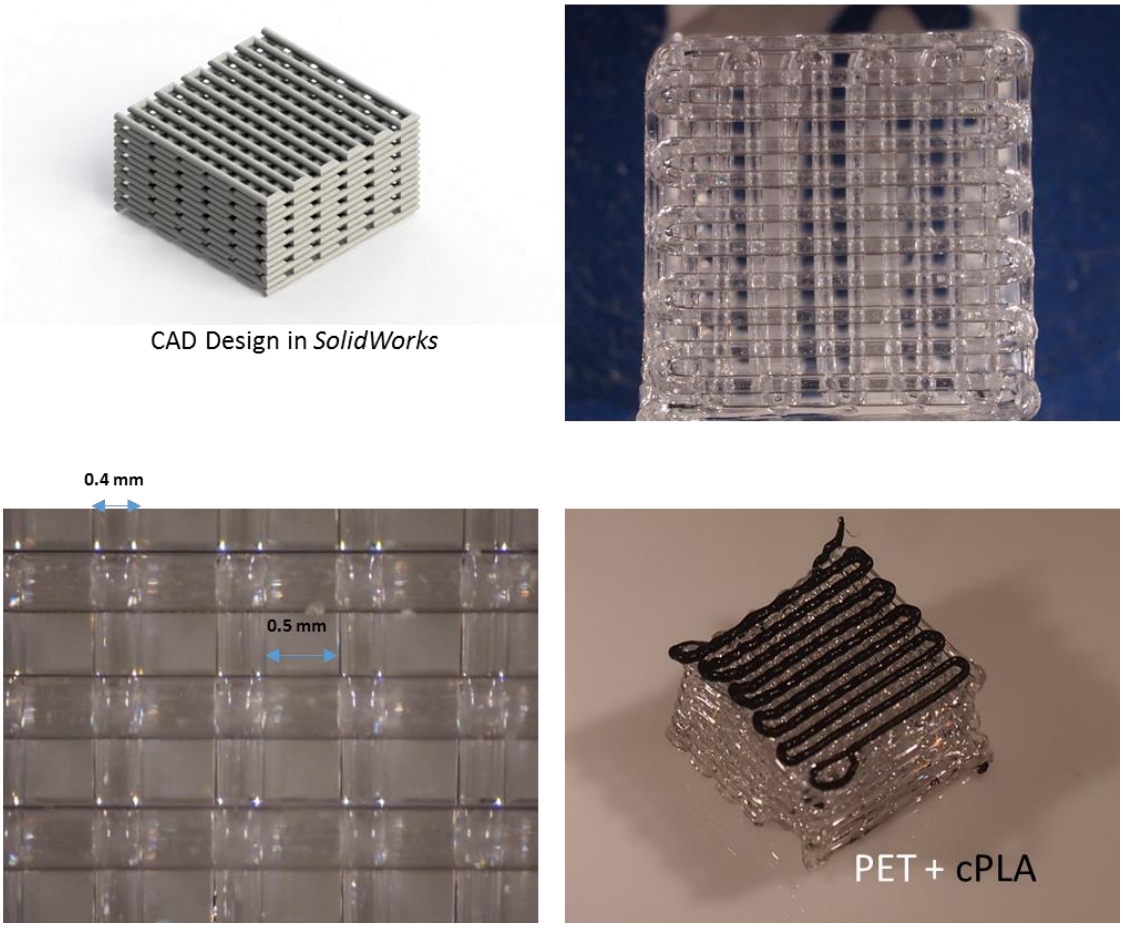

Figure S51. Fabrication of Prototype 3, showing the PET woodpile structure and a possible conjugation of PET and cPLA to provide electrical conductivity to the scaffold.

This prototype had satisfactory transparency from PET, but confocal microscopy or other enhanced microscopy techniques like multiphoton microscopy may be needed to access inner regions of the scaffold. Importantly, the 3DP system could print with good detail at the dimensions specified (0.4 mm filament size and 0.5 mm pore size). The conductivity of cPLA is also adequate. This prototype serves as 3D analogous to the PET/cPLA scaffold previously described in this work, and could be used in the future if transition to 3D scaffolds with these materials and 3DP system is desired.

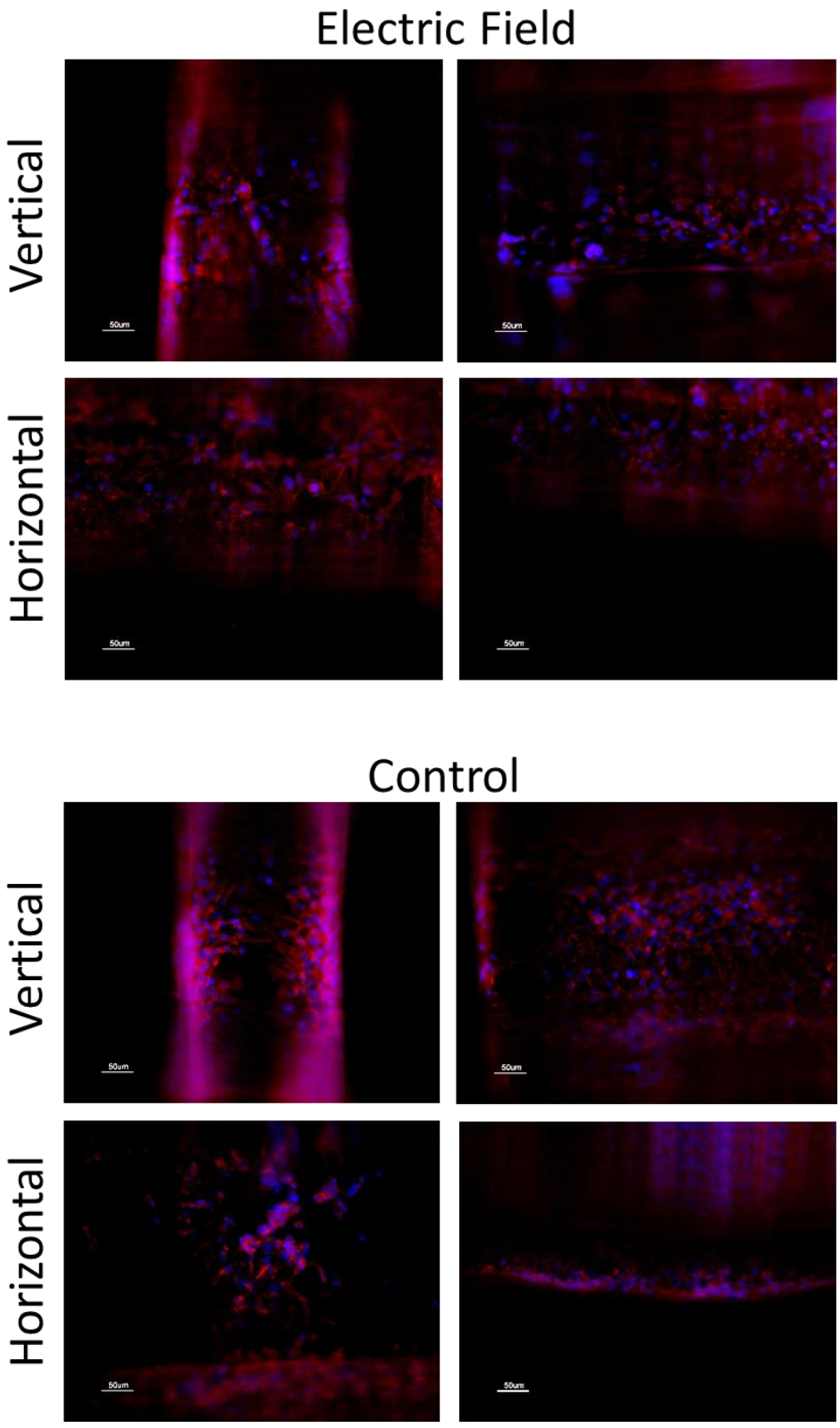

Figure S52. FM Images of overlaid DAPI Phalloidin after 4 days of expansion on the PET/cPLA scaffolds with curves, with and without electric field (scale bar at 50 µm). Although it is possible to focus on cells, the staining quality is not good enough to perform cell morphology and alignment studies.

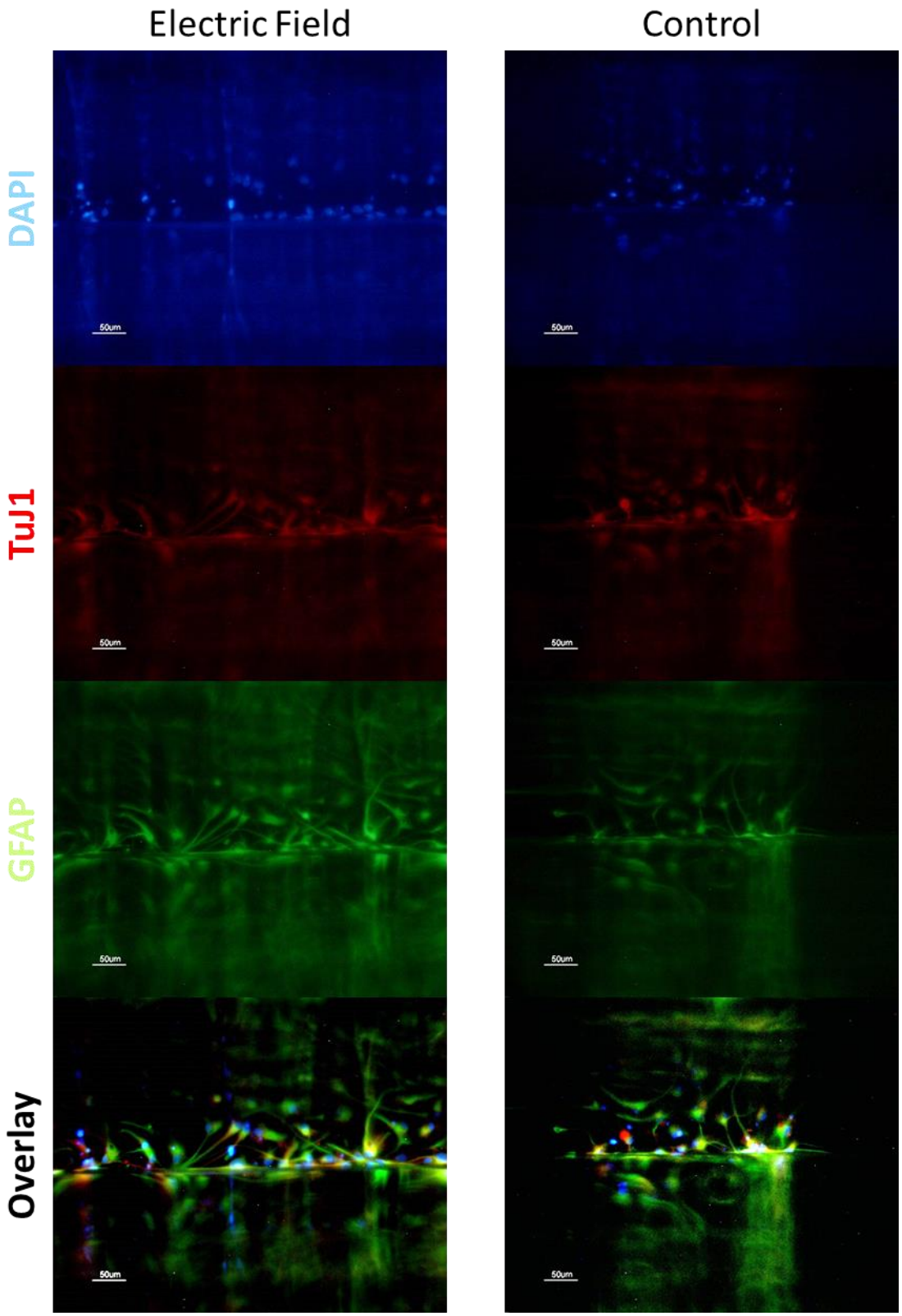

Figure S53. FM Images of DAPI, TuJ1 and GFAP staining, and their overlay after differentiation on the PET/cPLA scaffolds, with and without electric field (scale bar at 50 µm). It is possible to note the overlay between TuJ1 and GFAP signal by the yellowish colour on the bottom images.

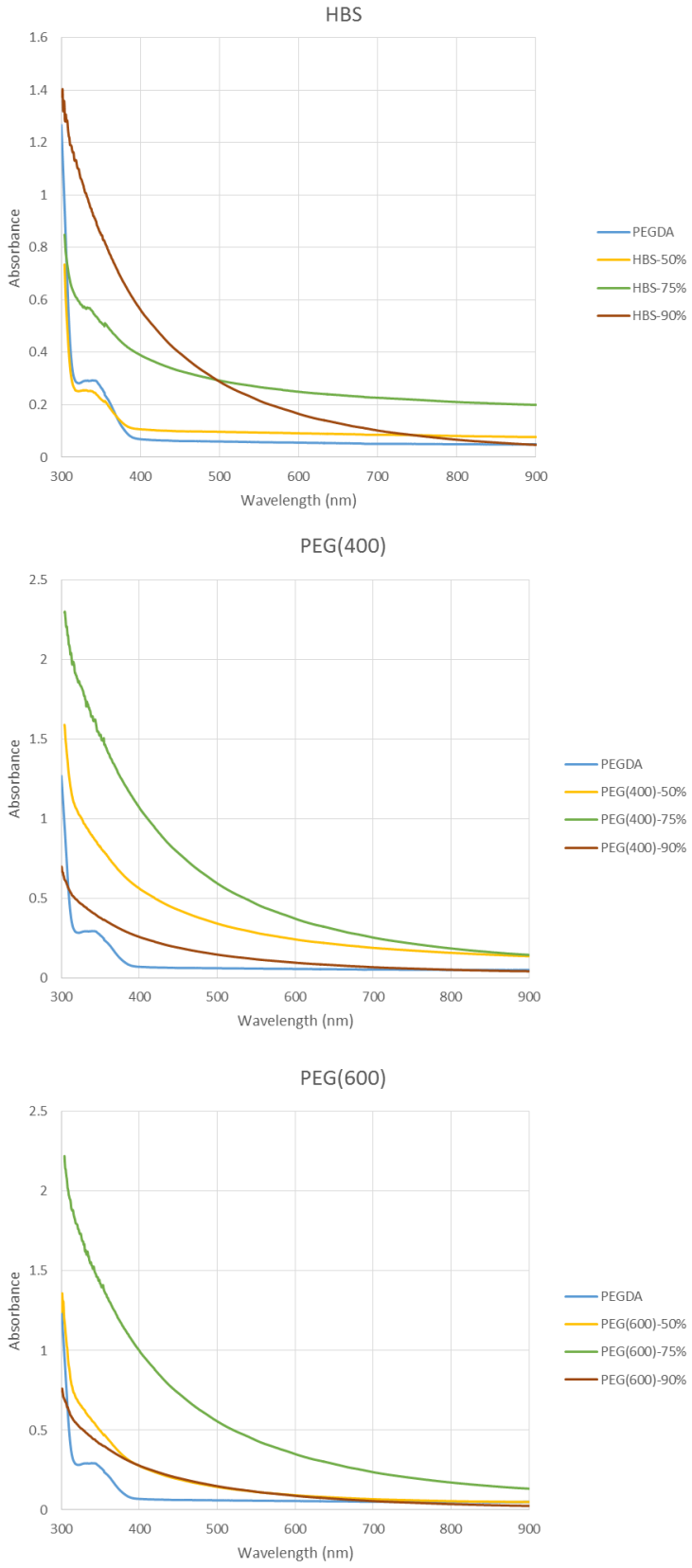

Figure S54. Absorption spectra for HBS (top), PEG(400) (centre) and PEG(600) (bottom) at different concentrations.